USE OF SATELLITE-BASED DATA AND REAL-TIME RAINFALL DATA TO IMPROVE FLOOD PREDICTIONS IN THE LOWER KELANI RIVER BASIN

Dissanayaka Mudiyanselage Pavithra Sudeshika

208043B

Degree of Master of Science

Department of Civil Engineering

University of Moratuwa

Sri Lanka

September 2021

USE OF SATELLITE-BASED DATA AND REAL-TIME RAINFALL DATA TO IMPROVE FLOOD PREDICTIONS IN THE LOWER KELANI RIVER BASIN

Dissanayaka Mudiyanselage Pavithra Sudeshika

208043B

Thesis submitted in partial fulfillment of the requirements for the degree Master of Science in Civil Engineering

Department of Civil Engineering

University of Moratuwa

Sri Lanka

September 2021

DECLARATION

I declare that this is my own work and this thesis does not incorporate without acknowledgment any material previously submitted for a Degree or Diploma in any other University or institute of higher learning and to the best of my knowledge and belief it does not contain any material previously published or written by another person except where the acknowledgment is made in the text.

Also, I hereby grant to the University of Moratuwa the non-exclusive right to reproduce and distribute my thesis, in whole or in part in print electronic, or another medium. I retain the right to use this content in whole or part in future works (such as articles or books)

Signature: Date: 2021-09-06

The above candidate has carried out research for the Masters under my supervision.

Name of the supervisor: Prof. R. L. H. L. Rajapakse

Signature of the supervisor: Date: 2021-09-06

ACKNOWLEDGEMENT

I would like to take this opportunity to express my gratitude to the individuals who have supported me throughout the research to complete the Master's Degree.

I would like to express my sincere gratitude to my research supervisor Prof. R. L. H. L. Rajapakse, Professor, Department of Civil Engineering, University of Moratuwa for his immense support, guidance, and motivation throughout the MSc. Program.

I wish to convey my sincere gratitude to Prof. S. A. S. Kulathilaka, Head of Department of Civil Engineering, University of Moratuwa, and Prof N. T. S. Wijesekera for their support to achieve success in the MSc. Program. I would like to appreciate the valuable suggestions and comments given by Prof. (Mrs.) J. C. P. H. Gamage and Dr. T. M. N. Wijerathna.

I would also like to express my gratitude to South Asia Foundation (SAF) and UNESCO Madanjeet Singh Centre for South Asia Water Management (UMCSAWM) for financially supporting me to undertake this Master Degree at UNESCO Madanjeet Singh Centre for South Asia Water Management (UMCSAWM), Department of Civil Engineering, University of Moratuwa.

I am obliged to give my special thanks to the Department of Meteorology, Irrigation Department, and Center for Urban Water (CUrW) for acquiring necessary meteorological and hydrological data for this research. I would like to appreciate the free software access for the RRI model provided by International Centre for Water Hazard and Risk Management (ICHARM).

Furthermore, sincere thanks to the staff of the Department of Civil Engineering, University of Moratuwa for their massive support towards this research.

Finally, I would like to express my heartfelt gratitude to my parents and my friends for their support and constant encouragement throughout this research work.

Use of Satellite-based Data and Real-time Rainfall Data to Improve Flood Predictions in the Lower Kelani River Basin

ABSTRACT

The downstream of the Kelani river with relatively flat terrain is extremely important as a region with high population density and semi/highly built-up areas. However, this part of the basin is highly flood-prone and frequently affected. Therefore, simulation of rainfall-runoff-inundation processes using hydrological modelling plays a vital role in flood management. However traditional distributed hydrological models are unsuitable due to higher computational time, uncertainties, and no link to accommodate actual and real-time data. The distributed hydrological models such as MIKE-SHE, LISFLOOD, and Rainfall-Runoff-Inundation model are considered to be informative and efficient models. Those have been applied to several event-based flood simulations and inundation analyses.

The research aims to develop a Rainfall-Runoff-Inundation model to improve model accuracy by using available real-time precipitation and satellite-based data for the Lower Kelani River Basin to enhance flood prediction and risk mitigation. It includes three major components named study on impacts of DEM products on RRI model, impacts of land-use change on RRI model, and improvement of RRI model using real-time data such as AWS rainfall data, and satellite-based data such as MODIS yearly global land cover data, and SMAP/ Sentinel-1 soil moisture data.

The RRI model using surveyed cross-sections and satellite-based land-use and soil moisture data shows the best performance with the lowest RMSE of 0.69 m and lowest ME of 0.18 m. The weakest performance indices were shown in the RRI model using AWS with the lowest R^2 of 0.65, and the highest RMSE of 2.4 m. The RRI models using 3-arc resolution SRTM and ALOS PALSAR DEMs performed well for flood modelling in the Lower Kelani River Basin compared to ASTER, and HydroSHEDS 3-arc resolution DEMs. The upstream flood shows an increasing trend while the downstream water depths and flood inundation show a decreasing trend for the 10 and 50 years return period floods of the Lower Kelani River Basin from 2001 to 2019. However, total flood inundation is in an increasing trend. This study concluded that the RRI performs well for the Lower Kelani River Basin when using SRTM 90-m DEM, surveyed cross-section data, and satellite-based data such as MODIS yearly global land cover and SMAP/Sentinel-1 soil moisture data.

Keywords: AWS, DEM, Event-based Flood Modelling, MODIS, Rainfall-Runoff-Inundation Modelling

TABLE OF CONTENTS

LIST OF FIGURES

LIST OF TABLES

LIST OF ABBREVIATIONS

ANN	Artificial Neural Network
AWS	Automated Weather Station
CK	Co-Kriging
CMORPH	CPC Morphing Technique
CUrW	Center for Urban Water
DEM	Digital Elevation Model
GAM	Generalized Additive Model
GPM	Global Precipitation Measurement
GSMap	Global Satellite Mapping of Precipitation
GWR	Geographically Weighted Regression
HASM	High Accuracy Surface Modelling
IDW	Inverse Distance Weighting
KED	Kriging with External Trend
ME	Mean Error
OK	Ordinary Kriging
R^2	Coefficient of Correlation
RK	Regression-Kriging
RKNNRK	Regression Kriging and Neural Network Residual Kriging
RMSE	Root Mean Square Error
RRFA	Regional Frequency Analysis
SiB2	Simple Biosphere Model-2
STRFA	at-site frequency analysis
TRMM	Tropical Rainfall Measuring Mission
UK	Universal Kriging
WEB-DHM	Water and Energy Budget Distributed Hydrological Model
WEB-RRI	Water, and Energy Budget based Rainfall-Runoff-Inundation

1. INTRODUCTION

1.1 Background

Kelani river basin is the seventh-largest basin in Sri Lanka concerning the extent of the basin (Hettiarachchi, 2020). This basin is residence to more than one-quarter of the Sri Lankan population, approximately four million people (2011 census). It receives significant rainfall yearly annual average rainfall of 3,450 mm since the basin is in the wet zone of Sri Lanka (Dissanayaka & Rajapakse, 2019). The severe rainstorms cause floods in the Kelani river basin, and Lower Kelani River Basin is highly vulnerable to floods. The Lower Kelani River Basin is a significant region due to urbanization and commercial activities (*Strategic Environmental Assessment*, 2018).

Flooding often occurs in the Lower Kelani River Basin due to the steep terrain in upstream and heavy rainfall (Hettiarachchi, 2020). The floods above 1.524 m MSL water level at Nagalagam street hydrometric station had recorded in 1837, 1872, 1891, 1904, 1906, 1913, 1922, 1925, July 1928, May/ October 1930, May 1933, May 1936, May 1937, May 1939, May 1940, July 1942, August 1947, October 1952, September 1966, October 1966, October 1967, September 1971, June 1989, May 2011 and May 2016 (*Strategic Environmental Assessment*, 2018).

The flood in 2016 was the most severe in the recent past. On 14th May 2016, the Department of Meteorology had issued a weather warning regarding heavy storms (>150 mm) and predicted to affect the North-Western and the Western regions of Sri Lanka (Rogers et al., 2016). The Hydrology Division of the Irrigation Department had monitored rainfalls and water levels at the hydrometric stations (Rogers et al., 2016).

Before experiencing torrential rainfall, rainfall greater than 100 mm was recorded only at the Deraniyagala station (Rogers et al., 2016). On 14th May 2016, the Lower Kelani River Basin received intense rainfall around 80 mm even though, no considerable rainfall in the upper Kelani river basin (Rogers et al., 2016). However, the entire basin was saturated before experiencing torrential rainfall on 15th May

2016. On 15th May 2016, the highest one-day rainfall of 355.5 mm had been recorded at Deraniyagala station (Rogers et al., 2016). The entire basin received intense and long-duration precipitation during the flood period (Rogers et al., 2016).

The flood in 2016 affected approximately half a million people. The Colombo and Gampaha Districts were severely affected by the flood in 2016. This flood affected 228,871 and 74,003 persons in Colombo and Gampaha, respectively as per the Ministry of National Policies and Economic Affairs and the Ministry of Disaster Management in 2016 (*Strategic Environmental Assessment*, 2018).

The structural and non-structural countermeasures are necessary to prevent and mitigate flood damages (Nastiti et al., 2015). Non-structural countermeasures are significant in flood management along with flood predictions and alerts. That would improve the competency of other countermeasures (Nastiti et al., 2015).

Simulation of rainfall-runoff-inundation processes plays a vital role in developing flood alert systems and flood hazard maps (Nastiti et al., 2015). The distributed hydraulic models such as MIKE-SHE, LISFLOOD, and Rainfall-Runoff-Inundation (RRI) model can simulate rainfall-runoff-inundation processes and have been used for various event-based flood modelling and analyses (Rasmy et al., 2019).

Flood modelling for flood forecasting would provide early warning in dangerous situations to minimize flood damages, and its accuracy will depend on temporal and spatial resolutions of the rainfall data (Nastiti et al., 2015).

The institutions such as the Department of Meteorology, Disaster Management Center, National Building Research Organization, and the Irrigation Department are responsible for providing precise and beneficial forecasts and disaster warnings timely (Rogers et al., 2016).

Several rain gauges have been installed throughout the Kelani river basin, mainly by the Department of Meteorology, Irrigation Department, and Center for Urban Water (CUrW) (Rogers et al., 2016).

The Automatic Weather Station (AWS) network has been introduced recently and functioning in Sri Lanka with the support of agro-meteorology, river gauging, and dam monitoring. The Department of Meteorology has installed 38 AWSs as a part of the Japanese International Cooperation Agency (JICA) funded project (Rogers et al., 2016).

Under Dam Safety and Water Resources Planning Project, a new AWS network has been deployed by the Irrigation Department and the Mahaweli Authority of Sri Lanka with the support of the World Bank (Rogers et al., 2016). In total, 122 automatic hydro-meteorological monitoring stations have been installed under Phase 1, and the installation of another 40 automatic hydro-meteorological monitoring stations has been proposed under Phase 2 of this project (Rogers et al., 2016). Installation of additional AWSs in the Kelani river basin would be costly.

1.2 Study Region

The Kelani river basin is one of the main river basins in Sri Lanka. It comes to be seventh related to basin extent and third related to water resources in Sri Lanka (Hettiarachchi, 2020). It is located entirely in the wet zone of Sri Lanka (Dissanayaka & Rajapakse, 2019), which is bounded by latitudes 6° 47' to 7° 05' and longitudes 79° 52' to 80° 13' (De Silva, et al., 2012). The basin area is about 2,230 km^2 with an upstream watershed in steep terrain and the downstream watershed below Hanwella in flat terrain (De Silva, et al., 2012). It receives an average yearly precipitation of 3,450 mm and a corresponding volume of 7,860 MCM (Dissanayaka & Rajapakse, 2019). The major portion of precipitation is received during the southwest monsoon from April to June (Dissanayaka & Rajapakse, 2019).

The study will be carried out for the Lower Kelani River Basin (about 500 km^2) (Silva et al., 2012). The Lower Kelani River Basin lies covering most parts of the Colombo District, which are the heavily populated regions and the commercial center of Sri Lanka. The study region, the Lower Kelani River Basin below Hanwella is illustrated in Figure 1.1.

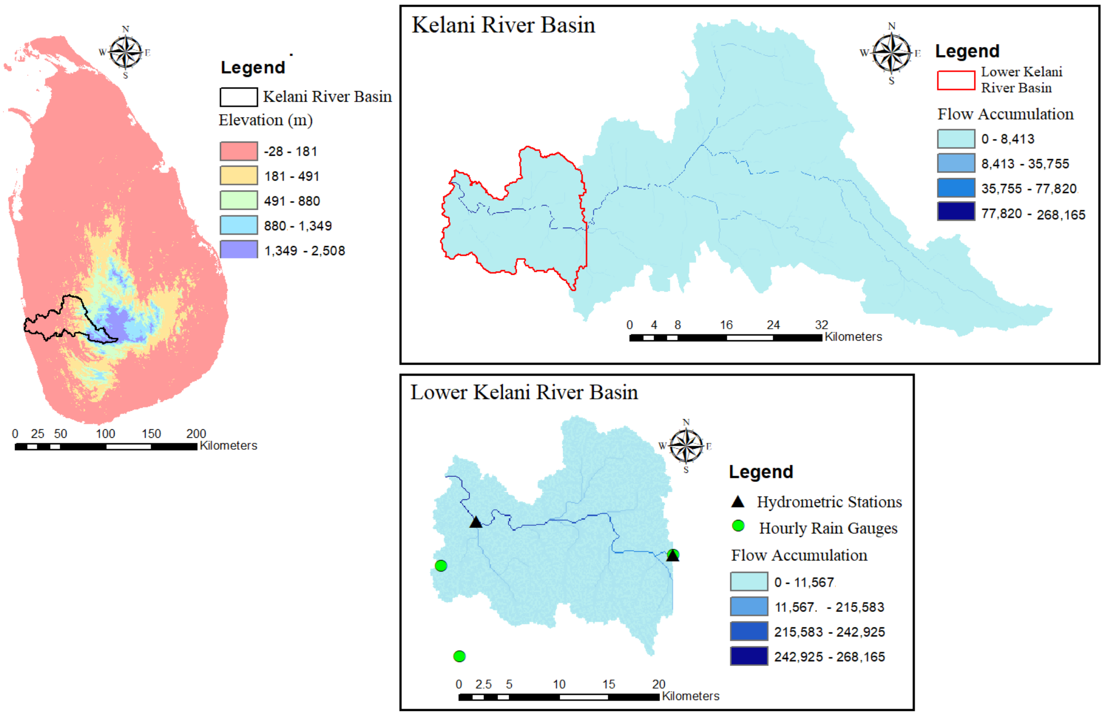

Figure 1.1: Site Map of the study region

1.3 Problem statement

The traditional distributed models are unsuitable for modelling flash flood conditions in semi/highly urbanized watersheds due to higher run time, no link to accommodate actual/ real-time data, inaccuracies, and uncertainties as a result of not updating state variables data in real-time.

1.4 Objectives

The main objective is to develop a hydrological model to improve model accuracy using available real-time precipitation and satellite-based data of the Lower Kelani River Basin for enhanced flood prediction and risk mitigation.

Specific objectives are,

- Evaluate the impact of different Digital Elevation Model products on flood modelling
- Evaluate the effects of land use and climate change on RRI modeling for 10- and 50-year return period flood from 2001 to 2019.

- Identify flood-affected areas and flood extents in the Lower Kelani River Basin
- To verify whether the available number of rain gauges is enough or not in the Lower Kelani River Basin
- Investigate the possibilities of improving the hydrological model results by using real-time and satellite data

1.5 Methodology

The following steps were adapted to achieve the objectives of the research.

- A literature review was carried out to identify a suitable model for modelling rainfall-runoff-inundation processes and, available real-time data and satellite data for improving traditional models.
- The Rainfall-Runoff-Inundation (RRI) model was selected for this study and developed for the 2016 flood event in Lower Kelani River Basin. The model was validated for 2017, and 2018 flood events.
- The effect of the Digital Elevation Model (DEM) on the RRI model was studied using Hydrological data and maps based on SHuttle Elevation Derivatives at multiple Scales (HydroSHEDs) 3-arc (90 m gridded), Shuttle Radar Topography Mission (SRTM) 3-arc (90 m gridded), Advanced Spaceborne Thermal Emission and Reflection Radiometer (ASTER) 1-arc and 3-arc (30 m, 90 m gridded), and Advanced Land Observing Satellite - Phased Array type L-band Synthetic Aperture Radar (ALOS PALSAR) 12.5 m and 90 m gridded data. Among the aforementioned DEM, the SRTM 3-arc (90 m) DEM performed well for the Lower Kelani River Basin. Therefore, the model developed from SRTM 3-arc (90 m) DEM was used for further model improvements.
- The impacts of land-use change on the RRI model were studied for 2001, 2006, 2011, 2016, and 2019 years using MODIS yearly global land cover datasets.
- The RRI model was improved for using real-time data such as AWS rainfall data, and satellite data such as SRTM 3-arc DEM, MODIS yearly global land

cover data version 6, and SMAP/ Sentinel-1 Radiometer/ Radar 30-second Scene 3 km EASE-Grid soil moisture version 2 data of the 2019 flood event in the Lower Kelani River Basin.

- The adequacy or inadequacy of the number of rain gauges in the Lower Kelani River Basin was evaluated through model performance.

1.6 Arrangement of the Thesis

- Chapter 1 includes the research background, study region, statement of problem, objectives, and methodology.
- Chapter 2 presents the literature review on rain-gauge networks, Kelani river basin, RR models, RRI models, and the effect of various parameters on hydrological models.
- Chapter 3 provides the methodology flow chart and describes followed each step of the methodology for the research.
- Chapter 4 presents and discusses the results of the research.
- Chapter 5 provides the conclusions and recommendations.

2. LITERATURE REVIEW

2.1 Water Cycle

The hydrological cycle that involves water on the earth continuously circulates in the hydrosphere which continues up to almost 15 km into the atmosphere and nearly 1 km downwards the lithosphere (the earth crust) (Chow et al., 1988).

Since hydrological phenomena are extremely complex, the hydrological cycle may be simplified as a system whose elements can be emphasized as precipitation, evaporation, runoff, and other stages of the hydrologic cycle (Chow et al., 1988).

2.2 Precipitation

2.2.1 Introduction

Precipitation in all forms of water that reaches surfaces of the earth from the atmosphere and rainfall is the predominant form of precipitation in Sri Lanka (Subramanya, 2008). Variations in the amount of precipitation in various regions of the country with time and space cause various disasters such as floods and drought. In Sri Lanka, it can be considered to have four rainfall seasons annually. These are,

1. The southwest monsoon from May to September
2. The inter-monsoon from October to November
3. The north-east monsoon from December to February
4. The inter-monsoon from March to April

Among the three types of rainfalls, monsoon rainfall (southwest and northeast monsoon) is sharing approximately 55% of the rainfall each year, and convectional and depression rain occur during the inter-monsoon season (*Area and Climate - Department of Census and Statistic- Sri Lanka*, n.d.).

2.2.2 Measurements of Precipitation

Ground observation of precipitation has been conducted by using rain gauges, disdrometer, and radars. Rain gauges are given a direct spot measurement of precipitation in a particular position while the disdrometer is used to estimate total precipitation as well as the influence of the size classification of the drop. Both instruments respond to individual drops and a quite small sampling area, but the radar sample is large and provides an estimation of precipitation based on indirect observations (Tapiador et al., 2012).

- Rain gauges

Precipitation can be defined as the vertical depth of water accumulated in an area concerned if all the rainwater was collected on it (Subramanya, 2008). There are two types of rain gauges for the measurement of precipitation namely non-recording and recording gauges. Recording gauges such as tipping-bucket type rain gauges, capacitance rain gauges, weighing type rain gauges, optical rain gauges, natural-siphon type rain gauges, and telemetered rain gauges produce automatically records the depth of rainfall against time intervals of one minute in duration (Subramanya, 2008). The two types of non-recording gauges; standard gauges and storage gauges are read manually at longer time intervals (Chow et al., 1988). Among those rain gauges, the most common rain gauges are tipping-bucket type rain gauges that are subject to many potential errors and are known to underestimate heavy precipitation (Tapiador et al., 2012). Other than the instrument errors, intrinsic errors such as effects of wind flow and turbulence induced by gauges may possible (Tapiador et al., 2012).

- Disdrometer gauge

The most popular disdrometer gauge is Joss-Woldvogel impact sensors among two types of disdrometer namely optical and impact sensors. Weaknesses of Joss-Woldvogel disdrometer are the impact on drop size distribution measurements on the small drop less than 0.7 mm diameter end of the spectrum due to sensitivity to acoustic noise, inability to resolve the drop larger than 5 mm diameter end of the spectrum, and recovery dead time during a heavy rainfall event (Tapiador et al., 2012).

- Ground radar

Radar estimation of precipitation has been developed to fill sampling voids where rain gauge density is insufficient to measure precipitation accurately (Tapiador et al., 2012). Further combined radar-gauges approach with relatively high quality has been introduced in the recent past and used in validating precipitation estimates from tropical rainfall measuring mission (TRMM) satellite (Wolff et al., 2005).

- Satellite estimates

Satellites are the only instrument that is the ability to retrieve global and relatively homogeneous precipitation estimation. Different methods such as visible, infrared-based, active, and passive microwave techniques, and merged infrared-based and microwave techniques are available to obtain precipitation from the radiations measured by satellites (Tapiador et al., 2012).

The recent infrared-based method is providing high temporal sampling, high spatial resolution (lower than 3km), and broad coverage of the geostationary platform. The logic behind the infrared-based method is the relationship between the top of the cloud and surface rainfall. The problem is that the relationship is indirect and complicated by blocking the view of the actual precipitating cloud layer by multi-layers of the cloud system (Tapiador et al., 2012).

The microwave technique is a straight mode to assess the precipitation from the satellite. There are two types of microwave techniques namely passive microwave technique (emission estimate) and active microwave technique (scattering estimate) (Huffman et al., 1997).

In many cases, the estimation of the merger of two microwaves has been conducted simply by estimating histogram-based emission over water and scattering index-based scattering overland (Huffman et al., 1997).

The rain gauges are still the most commonly used precipitation measuring instrument even though the weather radar-based and satellite-based precipitation assessing techniques have been introduced recently (Zeng et al., 2018). Those alternative precipitation estimation techniques have their advantages and limitations where precipitation-based remote sensing has better spatial coverage, however, limiting the temporal sampling. Rain gauge network is a more efficient direct measurement of precipitation even though the spatial coverage is considered a weak aspect (Paula et al., 2018).

2.3 Optimize rain gauge network

Multiple gauge positioning will be helpful to alleviate the errors engaged individual gauge quality control procedures (Tapiador et al., 2012).

The required rain gauge density depends on the purposes such as expected degree of accuracy, the variation of the precipitation over the watershed, and the aspects of the watershed (Tilford et al., 2003). A dense gauge network is required to measure total water yield or the spatial variability of precipitation amount from convective systems with a high degree of accuracy (Rainbird, 2007). In the mountainous area, spatial variability would be higher compared to flat terrain. Therefore, these results might have led to a conclusion on the requirement of a dense gauge network to obtain the desired degree of accuracy in spatial precipitation. Uncertainties may be involved in estimated rainfalls by using rain gauge data with proper variation in time and space at the basin scale (Andiego et al., 2018).

The mean percentage error in spatial precipitation depth would be lower for heavy shower type rain compared to lower shower type rain because spatial variability of precipitation depth tends to decrease with an increase in average spatial precipitation amount (Rainbird, 2007). The requirement for the accuracy of spatial precipitation should be modified in inverse relation to the size and importance of the storm (Rainbird, 2007). The quantitative criteria for the establishment of the densities of rain gauge networks depend on the number of storms occurring (Amorocho et al., 1968).

To design a precipitation network, minimum and optimum spatial gauge densities and operating periods for each gauge shall be considered. The systematic errors in spatial precipitation estimates often may be no relative significance when precipitation data are correlated with other parameters, as the errors may be absorbed in empirical constants (Rainbird, 2007). However, the same errors could be of greater significance in water balance studies (Rainbird, 2007).

Estimation of real-time rainfall is very important to forecast groundwater recharge assessment under the various hydrological cases and makes a significant contribution to agriculture water management too. To identify the variation of rainfall in space, a well-defined rain gauge network is essential even if rain gauges are equipped with real-time rainfall data from automatic rainfall recording instruments (Andiego et al., 2018).

The spatial averaging/ interpolation of rainfall data is required when estimating precipitation to a large extent since rain gauges are given a measurement of precipitation at a point. Various mathematical statistical theories or methods are available and shall be selected an appropriate method based on the objective of the study, state of topography and gauges of the region, and temporal and spatial resolution of the rainfall data (Hu et al., 2019). The accuracy of spatial averaging of rainfall data often depends on the study area, temporal resolution and, precipitation type (Hu et al., 2019).

The interpolation methods such as multiple regression, geostatistics, high-accuracy surface modelling, machine learning, hybrid interpolation, Theissen Polygen method, and Inverse Distance Weighting (IDW) are mostly used for spatial averaging/ interpolation of rainfall data and are consisting of different attributes (Hu et al., 2019).

2.3.1 Multiple regression method

Multiple regression methods such as Geographically Weighted Regression (GWR) and the Generalized Additive Model (GAM) are used to determine spatial averaging rainfall based on a linear or non-linear relationship between rainfall and predictor. The main principle of GWR is that the dependant variable and predictor has a non-stationary relationship among them and the regression coefficient differs spatially while the GAM has been developed based on the numerical relationship among the expected dependent variable and the predictor through the link function and can be analyzed the nonlinear relationship between them. GWR can analyze spatiotemporal aspects of precipitation as well as estimate precipitation (Brunsdon et al., 2001).

2.3.2 Geostatic method

Geostatic methods such as Ordinary Kriging (OK), Universal Kriging (UK), Kriging with External Trend (KED), and Co-Kriging (CK) are applied in different areas such as mineralogy, hydrology, environment, and climate (Goovaerts, 1997). The OK captures the autocorrelations of predictors and assumes structural elements locally fixed spatially while, UK, KED, and CK capture the impacts of auxiliary factors on predictors by following their modelling and calculation procedure. Theoretically, CK and KED methods are more accurate compared to the OK method due to capture impacts of explanatory variables and are still based on factors of each method (Hu et al., 2019).

2.3.3 High Accuracy Surface Modelling

High Accuracy Surface Modelling (HASM) is a comparatively new method and not wide-ranging as multiple regression and geostatic methods (Yue, 2011). The numerical experiment has revealed that the accuracy of HASM is high compared to OK and other traditional techniques (Hu et al., 2019). The main problem in HASM is difficulty in proceeding with interpolation of the spatial component directly with obvious trend components (Hu et al., 2019).

2.3.4 Machine Learning Algorithm

The machine learning algorithm namely Artificial Neural Network (ANN) is conducted by using data-driven analysis and does not require definite mathematical equations to use for this method. Since the machine learning algorithm deals with nonlinear relationships well, this method is very appropriate for the estimation of spatial averaging precipitation with its complicated factors and indefinite physical mechanism (Rigol et al., 2001).

Hybrid interpolation algorithms such as Regression-Kriging (RK) and Regression Kriging and Neural Network Residual Kriging (RKNNRK) coupled algorithms develop by integrating different algorithm varieties. The previous studies have revealed that RK is more flexible compared to KED and CK. Moreover, RKNNRK is more accurate than RK, UK, common Neural Network, and Residual Kriging coupled algorithm (NNRK) (Hu et al., 2019).

2.3.5 Thiessen Polygon method

Thiessen Polygon method is mainly used for estimating average spatial precipitation (Schumann, 1998). In this method, weights are assigned to each gauge station relative to its polygon area which is bounded by the perpendicular bisectors of links between nearby gauge stations (Lee et al., 2018). The main disadvantage of the method is that neglects orographic features of rainfall distribution (Schumann, 1998).

2.3.6 Inverse Distance Weight

The inverse distance method is one of the popular spatial interpolation methods that is used in many GIS packages (Maleika, 2020). The sampling point's values are estimated based on the weighted mean of near points. The weight of this technique is inversely proportional to the distance between two points (Pakoksung, 2016). The disadvantage of the IDW method is the computational time taken to process a huge set of data (Maleika, 2020).

2.4 Effects of real-time data and soil moisture data on hydrological models

Various real-time weather data sources such as AWS, Wireless Sensor Network (WSN), Satellite data (MODIS, EarthNow, NOAA Satellite Maps), and Radar systems (XRAD3D) are currently available. An AWS has been recently introduced in Sri Lanka. The measurements of AWS are temperature, relative humidity, air pressure, wind speed and direction, soil temperature and moisture, rainfall, and solar radiation, and probably other factors (Hema & Kant, 2016). The objective of inventing AWS is to provide a transmitter adapted to work under inoperative conditions, automatically transfer meteorological information by pulse signals and provide improve meteorological factor responsive devices to control the factor indicating signals (Diamond et al., 1942). The data of AWS will directly affect the accuracy and effectiveness of weather forecasting.

The consideration of soil moisture in flood modelling is very important since soil moisture represents the main role in the hydrological characteristics of the watershed (Shahrban et al., 2018). The formation of rainfall into the infiltration of surface runoff depends on the soil moisture store condition of the watershed and better initialization of soil moisture variable causes to improve the accuracy of flood simulation by better segregating the infiltration and surface runoff components of rainfall (Brocca et al., 2012). Soil Moisture Data mainly rely on soil type, land gradient, vegetation, and air temperature (Hema & Kant, 2016).

The study related to the significance of soil moisture in the RR model calibration has been conducted for two Australian sub-watershed under two conditions; calibrate only streamflow, and calibrate both streamflow and soil moisture in both two sub-watersheds (Shahrban et al., 2018). According to the results of this study, the simulation results of the joint-calibrated model show much more compatibility with the actual condition of the sub-watersheds (Shahrban et al., 2018). The study concluded that the joint-calibrated model produces a better streamflow prediction when the observations of streamflow are not better fit by only calibrating streamflow due to uncertainty in rainfall or streamflow data (Shahrban et al., 2018).

The various satellite-based soil moisture products such as Soil Moisture Active Passive (SMAP), Metop ASCAT, Windsat, and SMOS are available. The coarse resolution soil moisture data from these products provide well-captured soil moisture data at a daily or sub-daily scale. However, these products are not suitable for local hydrological analysis due to a lack of spatial details.

The SMAP satellite was initiated in 2015 by the National Aeronautics and Space Administration (NASA) to acquire surface soil moisture of top 5 cm soil using brightness temperature via its active and passive sensors. Active sensors such as synthetic aperture radar provide high-resolution data compared to passive sensors such as radiometers. However, they tend to have higher uncertainty because of the swath width and sensitivity to thin vegetation cover. In 2016, NASA issued a data product namely enhanced SMAP radiometer which is developed by interpolating the original 36 km gridded SMAP data into 9 km gridded data using the Backus-Gilbert optimal interpolation algorithm. Later in 2018, Sentinel 1A and Sentinel 1B data have been used to produce high-resolution soil moisture data of 3 km. This product has shown a reasonable precision of around 0.05 m^3/m^3.

2.5 Effects of precipitation data on hydrological modelling

Ground observations and precipitation estimation are necessary to represent components of hydrological components. However, they are not possible to use in forecasting at temporal and spatial scales for many applications (Tapiador et al., 2012).

Even if an average estimation is enough for some of the applications, spatial and temporal variation of precipitation are important for hydrological modelling (Lopez et al., 2015). Therefore, different models are used to predict precipitation and typically deals with sets of 3D initial and boundary conditions such as temperature, horizontal wind, humidity, and geopotential (Tapiador et al., 2012).

spatial rainfall estimates for a week or 10 days are sufficient for the identification of periods of low rainfall, but the estimation of daily rainfall or rainfall at small-time intervals is needed to rainfall-runoff models applied for flood prediction and river management (Grimes et al., 1999).

Spatial average precipitation data are used for most of the lumped hydrological models as model input (Zeng et al., 2018). Those models are broadly utilized for flood prediction and assessment, water resource assessment, and impact evaluation on water resources due to climate changes (Zeng et al., 2018). The reliability of precipitation data is one of the key inputs of hydrological modelling (Paula et al., 2018).

A study extended on the effects of the number of rain gauges and their distribution on the uncertainty of lumped hydrological modelling with various watershed extents has been investigated previously. According to this study, seven criteria for rain gauge density have been defined and different rain gauge distribution has been selected randomly for sub-basins. The spatial average precipitation has been estimated for each sample and used as input of the lumped hydrology model of densely gauged main watershed, Xiangjiang River basin. Further, the calibration of model and evaluation of model uncertainty has been conducted using shuffled complex evolution algorithm, and Bayesian method, respectively. The research revealed that an irregular gauge network will result in significant uncertainties in factor prediction and flood modelling. The imperfect precipitation assessments cause the reduction of model efficiency. The model uncertainty will be reduced when optimizing rain gauge density or distribution pattern but show no significant improvement in the efficiency of the lumped model beyond a certain threshold. Therefore the major conclusion of the study was the optimum selection of the number of rain gauges and locations will enhance the correctness of spatial average precipitation estimation with cost-effective (Zeng et al., 2018).

Several studies have been carried out on the influence of the rain gauge network and how it will affect the efficiency of lumped model performed for various watershed extents where it reveals that the spatial distribution of the rain gauge network is critical in the rainfall representation. Moreover, satellite-based precipitation estimate has given better results in the lumped rainfall-runoff modelling in contrast to sparse or irregular rain gauge networks. According to this study, flow simulation performance has been improved as a result of disregarding some of the rain gauges in spatial average precipitation estimation. Characteristics of high local spatial variation of the precipitation had been the major reason for that (Paula et al., 2018).

A study, the impacts of density and distribution of rain gauges on runoff simulation using a lumped hydrological modelling approach has revealed that for large-scale flood, density and spatial distribution of rain gauge affect highly on runoff simulation and this problem can be overcome by increasing the number of gauges (Zeng et al., 2018).

The regional frequency analysis (RRFA) and the at-site frequency analysis (STRFA) methods are used to optimize rainfall networks in the past based on the rainfall depth at a high return period. According to the results, a less number of gauge stations are requiring in the RRFA method compared to the STRFA method. And also RRFA applies to the homogeneous region. Further, research revealed that it is possible to reduce errors by increasing the number of stations and installing selected rain gauges at relatively high rainfall zones and high altitude sites (Abdelkhalek et al., 2018).

The impacts of rain gauge network configuration on the spatial interpolation have been quantitatively investigated by using an operational hydro-meteorological sensor network in the Thur river basin. The combination of radar and rain gauge data has been used as real data against the rainfall data from the sensor network. According to the results, the sensor network has shown significant improvement in the performance for every error indicator with an increase in the rain gauge density. This sensor network is more suited for the average precipitation intensities values up to 10 mmh^{-1} (Lopez et al., 2015).

The use of interpolation is unreliable where precipitation varies highly in short distances due to sparse or irregular rain gauge networks. Therefore, the research has been conducted on the Nett River watershed to measure the performance of interpolation as a purpose of alleviating the problem of using gauge data. Radar precipitation data have been used in the position of 53 rain gauge stations. The mean Field Bias method has been used to apply corrections in temporal errors of radar data by the use of rain gauge data. Moreover, the influences of rain gauge density on the HBV-IWW model have been evaluated by the use of Inverse Distance Weighting and OK interpolation methods and simulated discharge corresponding densities. Obtained results for winter are much better compared to the results of summer and further performance will increase with an increase in rain gauge density for these two interpolation approaches (Andiego et al., 2018).

RRI model is a newly developed two-dimensional model which is the ability to simulate rainfall-runoff and flood inundation as well as slopes and river channels can be separately dealt (Pakoksung & Takagi, 2016). The study on evaluation of runoff accuracy has been carried out by input five different satellite-based data products namely Global Precipitation Measurement (GPM), Global Satellite Mapping of Precipitation (GSMap), Tropical Rainfall Measuring Mission (TRMM), CPC Morphing Technique (CMORPH), and Precipitation Estimation from Remotely Sensed Information using Artificial Neural Networks at daily to the RRI model. As one of the major conclusions which have been converged that TRMM showed overestimated peak rainfall while the GPM was the best among the underestimation products. Moreover, all satellite-based data products revealed low accuracies by showing a discrepancy in contrast to rain gauges based on the performance statistical (Pakoksung & Takagi, 2016).

2.6 Effect of DEM on flood modelling

Digital Elevation Model (DEM) is a gridded regular matrix representation of topography (Lakshmi & Yarrakula, 2019) and the elevation of each pixel is defined respected to a datum (Hawker, Bates, et al., 2018). DEM has been generated different techniques such as create from ground surveys, digitization of existing terrain maps, and airborne laser scanning (LIDAR and RADAR) (Hawker, Bates, et al., 2018). Among these methods, airborne and space-borne Interferometric Synthetic Aperture Radar (InSAR) is popular due to its economic, efficiency, and providing of wide coverage of DEM generation (Lakshmi & Yarrakula, 2019). The optical satellite systems such as IKONOS, ASTER, and GeoEye-1 are not functioning properly when the earth's surface is covered. Therefore, high-resolution satellites such as SRTM, CARTOSAT, etc. are used widely due to the accuracy of data, time-saving, economic, and easiness (Lakshmi & Yarrakula, 2019).

The digital elevation is represented by grid cells. The size of the grid cell namely resolution is related to the scale and details of DEM. Small grid cell sizes produce high-resolution DEM with great spatial details. The accuracy of the DEM is greater in the high-resolution DEM compared to coarse-gridded DEM (Mesa-Mingorance & Ariza-López, 2020).

High accuracy in DEM influences better flood estimation. However, errors can occur in a DEM for both vertical and horizontal directions due to errors propagation in input data during estimation of surface derivatives and use for complex applications (Hawker, Bates, et al., 2018).

The details of widely used high-resolution DEM are given in Table 2.1.

Table 2.1: Details of DEM (Source: (Lakshmi & Yarrakula, 2019), (METI/ERSDAC et al., 2009))

Satellite Sensor	**Country/ Company**	**Date of launch**	**Resolution**	**Vertical Accuracy**
SRTM	USA/ NASA	11th February 2000	1 arc-second	10 m and 16 m
ASTER	USA	18th December 1999	15 to 90 m	Aproximately 25 m
ASTER GDEM	USA	29th June 2009	1 arc-second	Approximately 20 m

The resolution of DEM is more important when modelling urban/ built-up areas for capturing buildings (Fewtrell et al., 2008) while it may not as much important for rural areas (Savage et al., 2016) due to unnecessary computational cost rising with fine grids. The use of only one DEM for flood modelling would raise difficulty in the identification of uncertainty of terrain profile (Fewtrell et al., 2008). The SRTM DEM has been long used for flood modelling specially in data-sparse regions (Hawker, Rougier, et al., 2018).

Various studies have been conducted on the effect of DEM on flood modelling. The water levels of the stream and flood inundation have shown a linear relationship between the DEM resolution and accuracy for the studied five streams. Through this linear relationship, the accuracy of the flood model has been improved by extrapolating the coarse resolution DEM to a finer resolution DEM (Saksena & Merwade, 2015).

The study on vertical accuracy assessment for North-Eastern Mindanao, Philippines revealed that ALOS World-30 m is more accurate than SRTM-30m and ASTER Global DEM Version 2. However, all these DEMs have shown an overestimation of true ground elevations in the Philippines (Santillan & Makinano-Santillan, 2016).

2.7 Effect of Land-use data on flood modelling

The rainfall-runoff-erosion responses in the catchment predominantly depend on its soil characteristics, land-use, and terrain. The soil characteristics and terrain do not change significantly with time. Therefore, changes in land-use and land cover causes variation of hydrological response in the catchment (Miller et al., 2002). The hydrologic impacts of land-use and land cover changes are manifest in different ways such as water yield, soil moisture, low or high flow, and evapotranspiration (Sikka et al., 2003).

The land-use and land cover of the watershed directly link to the spatially distributed properties and processes (Miller et al., 2002). Various researches have been conducted related to the impacts of land-use on hydrological responses. The research on the evaluation of effects of land-use change in upstream on the downstream flood pattern using HEC1 and GIS revealed that higher runoff occurs in every sub-catchment and at the outlet when decreasing forestry areas and the upstream land-use change has an influence on the downstream flood levels (Suwanwerakamtorn, 1994). The simulation results of hydrological responses for San Pedro catchment using SWAT and CN method shows a higher annual and event runoff, and poor water quality due to increasing urban and cultivation areas, invasion of wood plants and decrease grasslands (Miller et al., 2002). The prediction of daily/ hourly hydrograph for reforestation scenarios using the WetSpa model revealed that peak discharge decreases by 12% when increasing the forest areas by 50% and time to peak runoff increases by 14 hours compared to present land-use (Bahremand et al., 2006).

Moreover, the impacts of land-use on floods strongly depend on the storm and antecedent soil moisture (Bahremand et al., 2006).

The study on the impacts of land-use/ land cover changes on flood runoff and inundation in the Pampanga river basin using the RRI model has been conducted for 50 year and 100 year return period floods by considering a constant impact due to climate variability (Shrestha, 2019). In the period from 1996 to 2016, the cultivation land has decreased by 3.36% (48.14% of the catchment) and the urban area has increased by 3.5% (5.64% of the catchment). The flood inundation and extents have shown an increasing trend in the middle and lower regions of catchment due to urbanization (Shrestha, 2019).

2.8 Resampling Techniques

The resampling techniques are often required to make the raster data compatible with the hydrological models. The generalization of satellite data arise several problems such as uncontrolled loss of information in the up-scaled raster, and spectral variation within classes of categorical data (Gann, 2019). Various resampling techniques are available, and the suitability of the resampling method depends on data types such as continuous data and categorical data.

The common resampling methods for rasters in GIS are the majority, nearest-neighbor, bilinear, and cubic convolution rule (Gann, 2019). The majority rule and nearest-neighbor rules are mainly used for discrete data such as land-use and slope classification. The nearest-neighbor method is the fastest method among all these resampling techniques. It assigns a new pixel value with the nearest pixel value to the new cell. The majority method lean to produce smoother raster values compared to the nearest-neighbor method. It determines pixel values based on the majority pixel value of the sub-sample. Bilinear and cubic convolution techniques perform well for continuous data such as elevation and raw slope data. The bilinear method assigns value based on the weighted distance average of the nearest four-pixel values to the new pixel location (Baboo & Devi, 2010). This method also causes certain smoothing effects on the new raster. The cubic convolution method is not acceptable in some cases due to containing values outside the input pixel values and higher computational time about 10 times by the required computational time for the nearest-neighbor method. This method assigns a new pixel value by fitting a smooth curve through the 16 closest pixel value centers to the new pixel (Baboo & Devi, 2010).

Various studies have been done about the impacts of resampling techniques on satellite data. The research on evaluating the effect of aggregating SRTM DEM from 0.09 to 10 km using 6 resampling techniques namely mean, median, mode, nearest-neighbor, maximum, and minimum methods with the aim of the modelling water balance of Lake Chard Basin. The study revealed that mean and median techniques create smoother terrain data including removal of depressions in the flood plain. By contrast, the upscaled terrain data using maximum and nearest resampling techniques have shown a rough representation including depressions (Coz et al., 2009). (Wu et al., 2008) had studied the impacts of overall terrain gradient and bias from 3 resampling techniques namely nearest-neighbor, bilinear interpolation, and cubic convolution for the Back Creek Watershed, Southwest Virginia. It was discovered that slope angles reduce and corresponding area increase regularly when resampling DEMs gradually to the coarser spatial resolutions. However, a systemic trend has not been shown for the alteration of the flow path and catchment area with the resampling of DEM. The study on effects of resampling techniques on SWAT simulated streamflow Johor River Basin, Malaysia using majority, nearest-neighbor, bilinear, and cubic convolution resampling techniques was found that majority and nearest techniques produced the best DEM with the lowest relative error of 6% (Tan et al., 2015). The resampling 30-m gridded land cover data to 1 km resolution using majority rule has a substantial effect on minor land cover types due to replace them with surrounding major land cover types (Zandbergen, 2010). The same land classification in both original and resampled data has shown in 63% of all positions (Zandbergen, 2010). The resampling of 30 m land cover data to 60, 120, 210, 240, 480, 960, and 1920 m resolutions using the nearest-neighbor method has demonstrated that reduces accuracy when upscaling the raster (Usery et al., 2004).

2.9 Progress and future directions in Hydrological modelling

In the 1960s, the birth of the computer revolution causes massive development in hydrological modelling. New hydrology branches such as digital or numerical hydrology and statistical or stochastic hydrology were born as a result of the ability to perform computations using computers. First, the entire hydrological process has been simulated using hydrological models. Stanford Watershed model is one of the first hydrological models that was evaluated over the 40 years and transformed into modern embodiments such as HSPF (Hydrological Simulation Program FORTRAN) (Donigian & Imhoff, 2006). Then, optimization of operation techniques has been developed for simulating river basins, reservoir management, and operation and used for hydrological model calibration. Two and three-dimensional models such as groundwater, infiltration, and soil water flow models were invented with development in numerical mathematics (Remson et al., 1971). Then, modelling of large rivers such as Missippi at high temporal resolution data such as seconds or minutes has been attempted (Sorooshian et al., 2008). The integration of Hydrology with related sciences such as climatology, geomorphology, hydraulics, soil physics, and geology ecosystems has been begun for better modelling the hydrological processes (Singh, 2018). The drastic improvement in computation causes the creation of user-friendly software and tools for acquiring, storing, restoring, processing, and diffusing data as well as remote sensing tools (Hoggan, 1989).

The main disadvantages of traditional distributed models can be listed as follows,

- Higher computational time
- No link to accommodate actual/ real-time data
- Uncertainty due to not updating state variables in real-time data

2.10 Kelani River Basin

2.10.1 Introduction

The Kelani river basin is one of the main river basins in Sri Lanka, which is seventh related to the watershed extent and third related to water resources (Hettiarachchi, 2020). The entire watershed is located in the wet zone of Sri Lanka at Northern latitudes 6° 47' to 7° 05' and Eastern longitudes 79° 52' to 80° 13'. The watershed extends about 2,230 km^2 (Dissanayaka & Rajapakse, 2019) with a mountainous upstream watershed and flat downstream watershed below Hanwella (De Silva, et al., 2012). The map of the Kelani river watershed is illustrated in Figure 2.1.

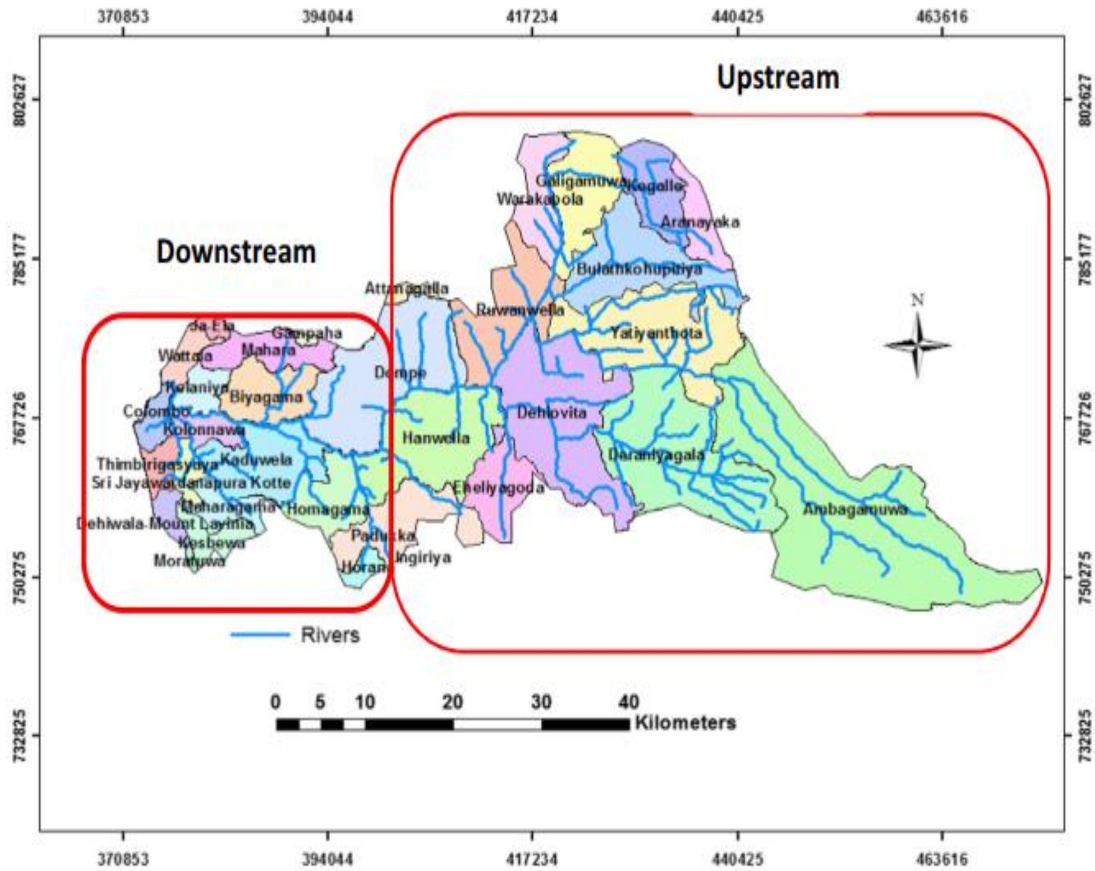

Figure 2.1: Kelani river basin

Source: (Komolafe et al., 2017)

It receives an average annual rainfall of 3,718 mm and a corresponding volume of 8,521 MCM (*Strategic Environmental Assessment*, 2018). The major portion of rainfall is received during the southwest monsoon from April to June and a considerable amount of rainfall is received during the North-East monsoon and inter-monsoonal periods too (Hettiarachchi, 2018). The streamflow of the river varies between 600 – 1,800 m^{3}s^{-1} during the monsoon season (Dissanayaka & Rajapakse, 2019).

The Kelani river basin is exposed to floods heavily (e.g. 2016 and 2017) due to its position, topography, and orientations (Dissanayaka & Rajapakse, 2019). The lower basin of the river is subjected to heavy floods as a result of receiving heavy rainfall and steep terrain of the upper watershed. The flood plain is formed below the Glencourse river gauge and becomes wider below Hanwella (Hettiarachchi, 2018). The Flood level of the Kelani river basin based on the water level in the Nagalagam street, Hanwella, and Glencourse hydrometric stations are classified as shown in Table 2.2.

Table 2.2: Flood level classification of the Kelani River

Station Name	**Flood Level Classification (m MSL)**			
	Alert	***Minor***	***Major***	***Danger***
Nagalagam street	1.22	1.52	2.13	2.74
Hanwella	7	8	10	11
Glencourse	15	16.5	19	22

Source: (Rogers et al., 2016)

Floods in the Kelani river basin have occurred in the following years and recorded water levels in each flood event at Nagalagam street hydrometric station are shown in Table 2.3.

Table 2.3: Historical flood data in the Kelani river basin

Year and Month	**Water Level (Max. ft) MSL**	**Year and Month**	**Water Level (Max. ft) MSL**
1837	13.50	1937 May	10.33
1872	11.90	1939 May	9.35
1891	9.80	1940 May	11.00
1904	9.90	1942 July	8.17

1906	10.80		1947 August	12.85
1913	11.00		1952 May	8.25
1922	12.60		1955 October	8.00
1925	11.50		1966 September	8.67
1928 July	9.08		1966 October	9.00
1930 May	10.91		1967 October	9.17
1930 October	9.83		1971 September	7.33
1933 May	9.95		1989 June	9.20
1936 May	9.43		2016 May	7.65

Source: (Hettiarachchi, 2018)

Note: Floods above 7 ft. MSL at Nagalagam Street has been considered a major flood.

2.10.2 Flood in 2016

The flood in 2016 was the latest and extreme flood event in the recent past. On 14th May 2016, the Department of Meteorology has issued a bad weather warning of torrential rainfall above 150 mm and was supposed to covering North-Western and the Western regions of the country. Following Table 2.4 shows recorded hourly water levels and rainfalls of each hydrometric station in the Kelani river basin by the Hydrology Division (Rogers et al., 2016).

Table 2.4: Daily rainfall throughout the flood period

Station	**Rainfall (mm)**								**Total Rainfall (mm)**
	13th May	***14th May***	***15th May***	***16th May***	***17th May***	***18th May***	***19th May***	***20th May***	
Castlereigh	6.2	15.6	137.5	116.3	72.0	15.8	68.2	11.6	443.2
Norton	20.9	11.7	201.5	200.5	109.4	12.1	77.0	47.0	680.1

Maussakelle	6.0	14.5	155.0	82.0	84.5	19.5	62.3	7.0	430.8
Canyon	30.5	13.0	179.2	187.5	87.1	22.9	64.0	12.1	596.3
Laxapana	20.6	12.0	158.5	167.9	129.1	12.7	78.5	20.2	599.5
Norwood	11.8	37.7	86.0	35.4	68.6	17.1	45.0	2.7	304.3
Kitulgala	23.1	32.9	336.9	70.0	66.9	51.6	138.7	21.9	742.0
Deraniyagala	142.6	22.8	355.5	91.7	69.4	58.2	144.3	14.3	898.8
Holombuwa	37.8	16.6	201.6	88.7	101.3	10.3	40.3	11.1	507.7
Glencourse	60.4	16.1	225.8	78.0	73.7	26.6	108.9	1.4	590.9
Hanwella	7.0	11.6	160.7	17.9	48.7	9.3	108.3	1.3	364.8
Colombo (ID)	2.6	82.6	217.4	7.6	13.4	1.7	10.1	0.0	335.4
Colombo (MET)	2.8	76.4	256.9	26.0	19.5	0.9	9.8	0.8	393.1

Source: (Rogers et al., 2016)

According to Table 2.4, before torrential rainfall (on 13th May 2016) only rainfall of Deraniyagala station was greater than 100 mm. On 14th May, the Lower Kelani River Basin received heavy rainfall around 80 mm even though no considerable rain in the upper Kelani river basin. However, the watershed was saturated totally before getting torrential rainfall on 15th May 2016. The greatest one-day rainfall recorded in Deraniyagala station was about 355.5 mm on 15th May 2016. The heavy and long duration of rain was received throughout the watershed during the torrential rainfall event (Rogers et al., 2016).

Around half a million people have been experienced adverse weather conditions during the flood in 2016. Colombo and Gampaha districts are subjected to heavy floods, as a result of increasing the water level of the Kelani River. According to the Ministry of National Policies and Economic Affairs and the Ministry of Disaster Management in 2016, floods in Colombo and Gampaha Districts affected 228,871 persons in 54,248 families and 74,003 persons in 17,485 families, respectively (*Strategic Environmental Assessment*, 2018).

2.10.3 Climate change trends in the Kelani river basin

The identification of climate variation in the catchment should be conducted on both climatic variables such as temperature and precipitation and hydrological parameters such as streamflow (Jayasekara et al., 2020). The various statistical methods such as Mann-Kendal, modified Mann-Kendal, regression analysis, and Innovative trend approach are available for trend analysis of hydro-meteorological time series data.

The study on runoff trend analysis has been conducted over the period from 1975 to 2005 at a daily scale for 39 river basins in Sri Lanka using the rank-based non-parametric Mann-Kendall method (Patabendige et al., 2019). The results have shown an increasing trend in the annual runoff of the main river basins which originate from central hills and are situated in the west and east of the central highland. It occurred as a result of increasing rainfall in this region. Seasonal runoff has fluctuated highly during the southwest monsoon (Patabendige et al., 2019). The highest monthly average runoff has been generated during the second inter-monsoon for the selected river basin (Patabendige et al., 2019).

The streamflow, rainfall, and temperature trends in the Kelani river basin have been analyzed for the period from 1983 to 2013 using the Innovative trend approach, Mann-Kendal, and Sen's slope (Jayasekara et al., 2020). The annual average streamflow trends of six stations in the Kelani river basin are given in Table 2.5 (Jayasekara et al., 2020).

Table 2.5: Annual average streamflow trends of six stations in Kelani river basin

Station	**Innovative trend approach (D)**	**Mann-Kendal (Z)**	**Sen's Slope ($m^3s^{-1}year^{-1}$)**
Deraniyagala	-3.13	-2.43	-139.91
Glencourse	-3.96	-3.93	-1204.48

Hanwella	-2.64	-2.39	-766.07
Holombuwa	-4.37	-2.31	-94.50
Kithulgala	-2.83	-2.17	-176.07
Norwood	-0.44	-1.49	-20.45

The annual streamflow at each station in the Kelani river basin has shown a decreasing trend for the period from 1983 to 2013. The annual average rainfall trends of eight stations in the Kelani river basin are given in Table 2.6 (Jayasekara et al., 2020).

Table 2.6: Annual average rainfall trends of eight stations in Kelani river basin

Station	**Innovative trend approach (D)**	**Mann-Kendal (Z)**	**Sen's Slope ($m^3s^{-1}year^{-1}$)**
Avissawella	-0.41	-0.82	-10.65
Chesterford	1.32	2.53	30.59
Colombo	0.39	1.32	9.73
Hanwella	-0.94	-0.89	-15.03
Henarathgoda	0.31	0.21	3.38
Maliboda	0.14	0.93	25.39
Nuwara Eliya	-1.02	-1.46	-11.43
Pasyala	0.82	0.86	11.62

The annual average temperature trends of two stations in the Kelani river basin are given in Table 2.7 (Jayasekara et al., 2020).

Table 2.7: Annual average temperature of Colombo and Nuwara Eliya stations

Station	**Innovative trend approach (D)**	**Mann-Kendal (Z)**	**Sen's Slope (^{0}C year^{-1})**
Colombo	0.007	1.003	0.005
Nuwara Eliya	0.071	0.935	0.004

The tendency of drying Kelani river basin during south-west monsoon and second intermonsoon periods have been identified for the studied period from 1983-2013 due to decreasing trend of streamflow and rainfall, and increasing trend of downstream temperature (Jayasekara et al., 2020).

2.10.4 Locations of rain gauges in Lower Kelani River Basin

Department of Meteorology, Disaster Management Center, National building Research Organization, and the Hydrology Division of Irrigation Department are responsible institutions regarding provide precise and beneficial forecasts, and warnings of hydrological and meteorological disasters timely (Rogers et al., 2016).

The Department of Meteorology asserts twenty meteorological stations that are operated by well-trained meteorological observers. Further, 38 AWSs have been installed by the Japanese International Cooperation Agency and Data from AWSs has been received every 10 minutes from the national forecasting center of the Department of Meteorology via VSAT communication network. Data from other available AWSs that are operated by agro-meteorology, river gauging, and dam operating have not been used by the Department of Meteorology due to uncertainty in observations, expenditure, lack of knowledge on the extent of the network, and difficulties in access the network. Currently, the 521 daily rainfall stations are operated by the Department of Meteorology, and external users cannot access this daily rainfall data (Rogers et al., 2016).

Before 2016, the hydro-meteorological network of the Irrigation Department had been operated manually with 35 principal station records at 1-hour intervals and 40 peripheral station record daily. Through the World Bank dam safety and water resources planning project, 122 automatic hydro-meteorological monitoring stations have been installed under phase 1, and the installation of another 40 automatic hydro-meteorological monitoring stations has been proposed under phase 2 of this project (Rogers et al., 2016).

Several rain gauges have been installed throughout the Kelani river basin, mainly by the Department of Meteorology, Irrigation Department, and CUrW.

Locations of Meteorological stations, Agromet stations, and rain gauge stations by the Department of Meteorology are shown in Figure 2.2.

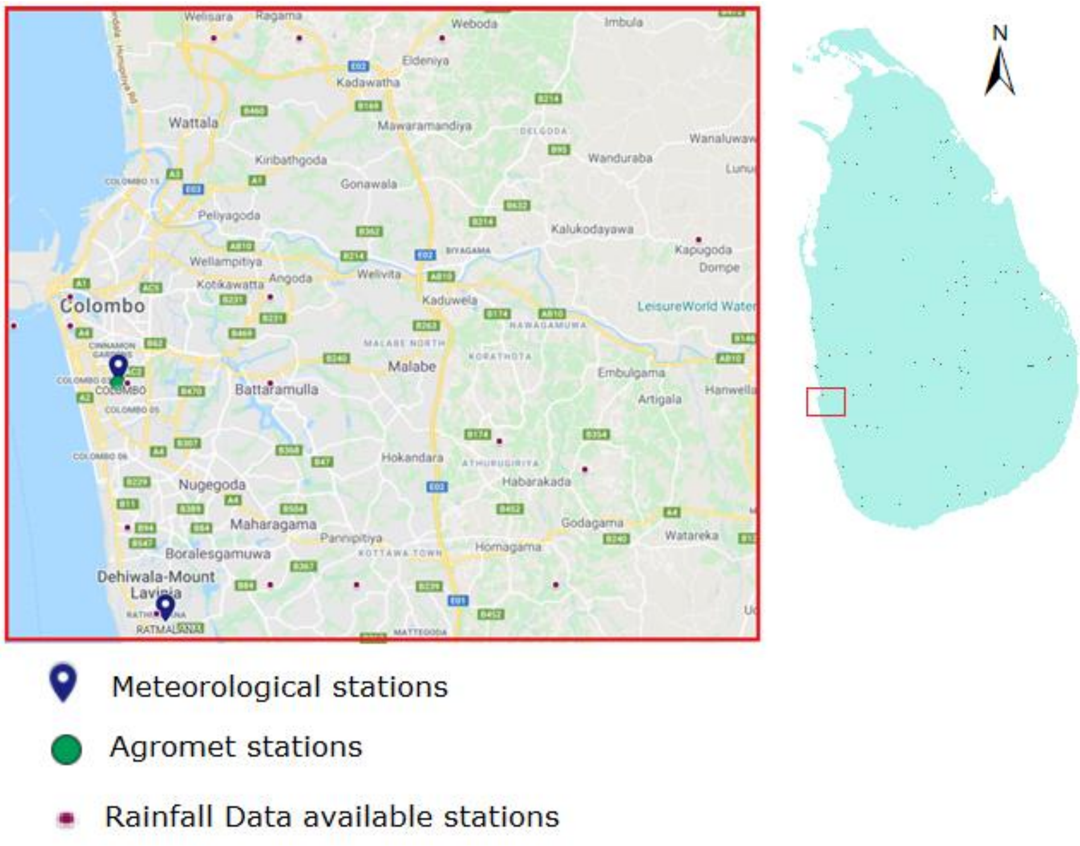

Figure 2.2: Location of Meteorological stations, Agromet stations, and Rain gauges by the Met Department in the study region

Source: (*Watersheds of Sri Lanka*, 2011)

The locations of the station by the Department of Meteorology in the study region are listed in Table 2.8.

Table 2.8: Meteorological stations, Agromet stations, and Rain gauges by the Department of Meteorology in the study region

Station	Locations
Meteorological stations	Colombo, Rathmalana
Agromet stations	Colombo
Rain gauges	Boralesgamuwa, Pannipitiya, Nayabedde, Homagama, Meegoda-Nawalamulla, Oruwala, Dehiwala Zoo, Colombo, Rathmalana, Colombo Maradana, Colombo Fort, Battaramulla, Angoda, Dompe, Kirillawala, Kadawatha, Ragama Camp, Welisara-Navy

The locations of Centre for Urban Water (CUrW) weather stations inside the Kelani river basin are shown in Figure 2.3.

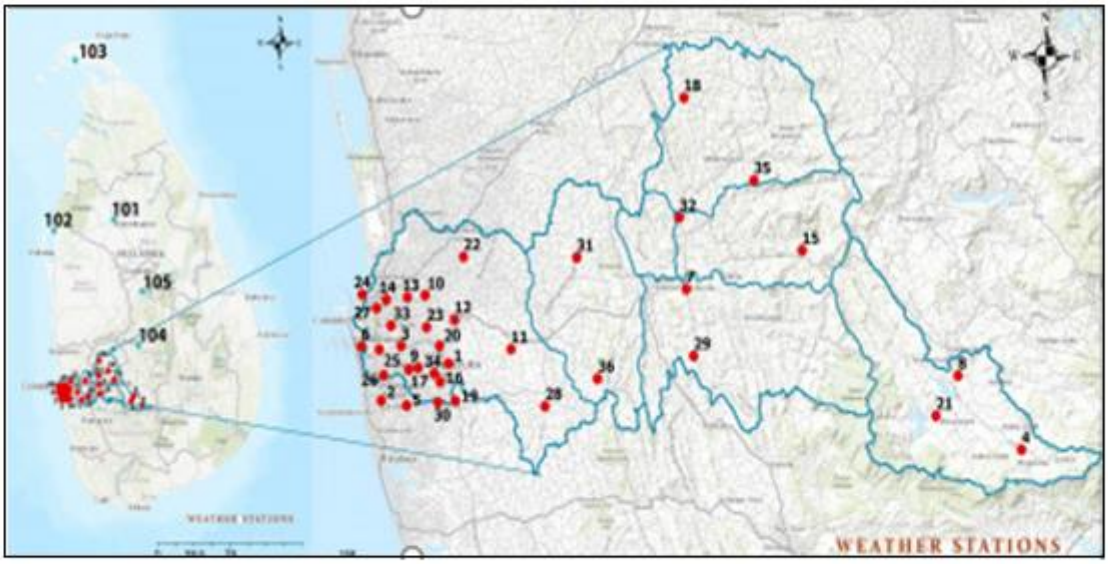

Figure 2.3: Locations of CUrW weather station inside Kelani Catchment

Source: (*CUrW Center for Urban Water*, 2019)

01	Arangala Station	20	Malabe Station
02	Attidiya Station	21	Maskeliya Station

03	Battaramulla Station	22	Mawaramandiya Station
04	Bogawantalawa station	23	Mulleriyawa Station
05	Boralasgamuwa station	24	Mutwal Station
06	Colombo 07 Station	25	Narahenpita Station
07	Dehiowita station	26	Nugegoda Station
08	Dickoya Station	27	Orugodawatta Station
09	Diyasaru Uyana Station	28	Padukka Station
10	Gonawala Station	29	Panawela Station
11	Jaltara Station	30	Pannipitiya Station
12	Kaduwela Station	31	Papiliyawela Station
13	Kelaniya Station	32	Ruwanwella Station
14	Kittampahuwa Station	33	Salamulla Station
15	Kitulgala Station	34	Thalawathugoda Station
16	Kottawa Station	35	Urumewella Station
17	Madiwela Station	36	Waga Station
18	Mahapallegama Station	37	Hingurana Station
19	Makumbura Station		

Arangala, Malmawaramandiya, Mulleriyawa, Boralasgamuwa, Mutwal, Colombo 07, Narahenpita, Nugegoda Station, Orugodawatta, Diyasaru Uyana, Padukka, Gonawala, Jaltara, Pannipitiya, Kaduwela, Kelaniya, Kittampahuwa, Salamulla, Thalawathugoda, Kottawa, Madiwela and Makumbura weather stations are located in the Lower Kelani River Basin.

The locations of Centre for Urban Water (CUrW) water level gauges in the Lower Kelani River Basin are shown in Figure 2.4.

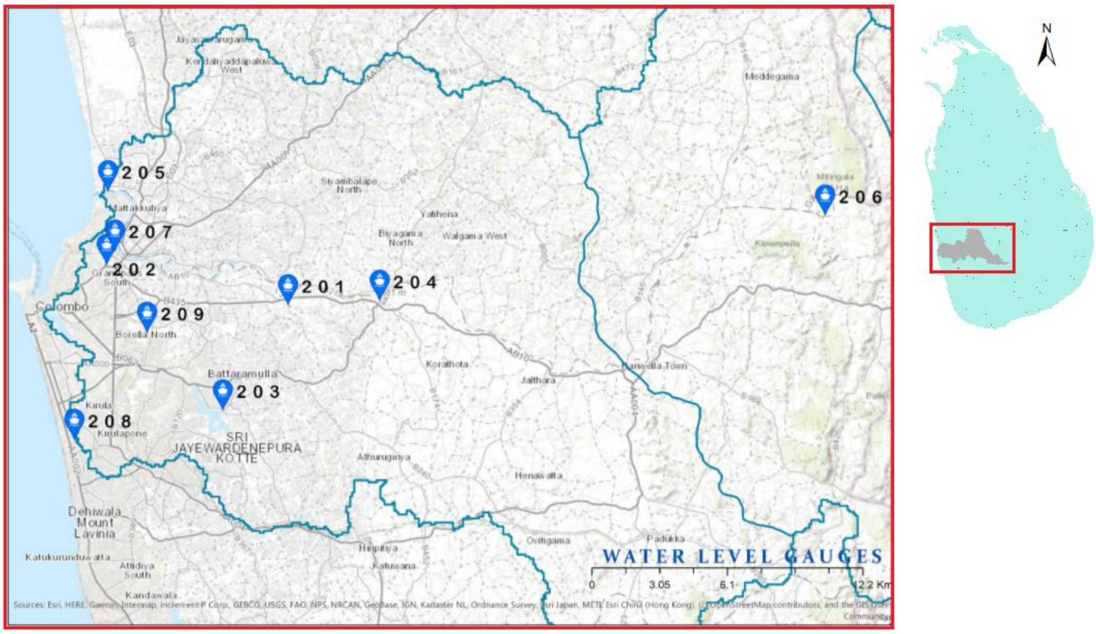

Figure 2.4: Location of CUrW water level gauges

Source: (*CUrW Center for Urban Water*, 2019)

The number of CUrW water level gauge stations in the Grama Niladhari divisions of the Lower Kelani River Basin is shown in Table 2.9.

Table 2.9: Locations of CUrW water level gauges in the Lower Kelani River Basin

Location	**Number of water level gauges**
Mattakkuliya	1
Grandpass South	2
Borella North	1
Kirulapana	1
Battaramulla	1

Mitirigala	1
Kaduwela	2

Seven hydrometric stations; Nagalagam Street, Hanwella, Glencourse, Kitulgala Norwood, Deraniyagala, and Holombuwa are maintained on the Kelani River to record hourly water levels and rainfalls (Hettiarachchi, 2018). The locations of hydrometric stations in the Kelani river basin are shown in Figure 2.5.

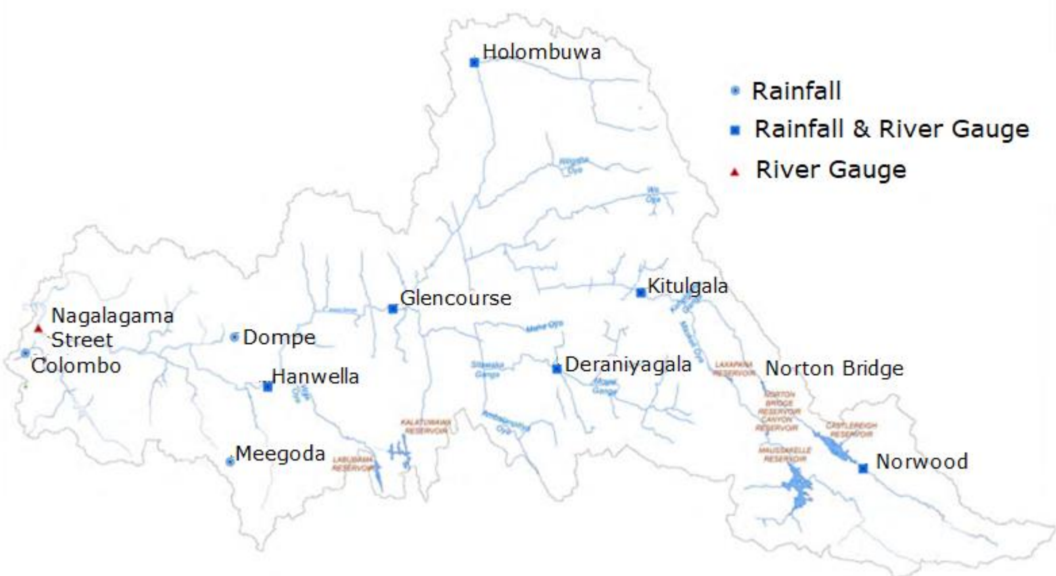

Figure 2.5: Locations of Hydrometric Stations on the Kelani River Basin

Source: (Rogers et al., 2016)

Note: All hydrometric stations are equipped with manual rain gauges that record rainfall at 1-hour intervals.

The hydrometric stations in the Kelani river basin by different agencies such as the Irrigation Department, Department of Meteorology, and Ceylon Electricity Board with the available data of each hydrometric station are shown in Table 2.10.

Table 2.10: Rainfall stations functioned in Kelani Catchment

Station Name	Agency	Type of data collected
Norwood	Irrigation Department	Record water levels and rainfall at 1-hour intervals
Holombuwa	Irrigation Department	
Kitulgala	Irrigation Department	
Deraniyagala	Irrigation Department	
Glencourse	Irrigation Department	
Hanwella	Irrigation Department	
Nortonbridge	Ceylon Electricity Board	Record 1-day rainfalls
Castelreigh	Ceylon Electricity Board	
Maussakele	Ceylon Electricity Board	
Canyon	Ceylon Electricity Board	
Laxapana	Ceylon Electricity Board	
Nagalagam Street	Irrigation Department	The record water level at 1-hour intervals. No rainfall data collected
Colombo	Department of Meteorology	Record continuous rainfall

Source: (Rogers et al., 2016)

2.11 Rainfall-Runoff (RR) models

2.11.1 Introduction

Since hydraulic measurement techniques are not capable of a measure of everything on the hydraulic system as well as limited range of measurement in both space and time (Beven, 2012), Rainfall-Runoff models are standard tools that have been introduced to improve decision making on hydraulic problems in water resource planning, flood protection or other areas and applied to real-time flood forecasting, design calculation of flood, evaluate management strategies and/or watershed respond to climate and/or land-use variability (Wagener et al., 2003). Runoff models visualize how changes in the previous surface, vegetation, and meteorological events affect the water systems, give a better understanding of hydrologic phenomena (Devia et al., 2015).

2.11.2 Modelling process

The modelling process includes five steps such as perceptual model, conceptual model, procedural model, model calibration, and model validation, and is shown in Figure 2.6.

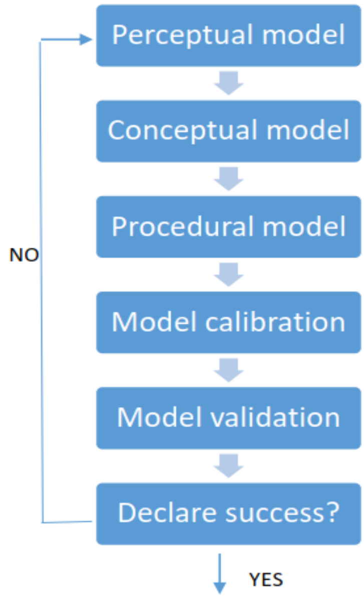

Figure 2.6: Modelling Process

Source: (Beven, 2012)

- Perceptual model

The perception model is deciding on the processes based on perceptions of the rainfall-runoff model in what way the watershed reacts to rainfall under various states or, rather, perceptions of the owner. These models are different from that of another due to the effects of referred books and articles, analyzed data sets, field sites, and experience (Beven, 2012).

The mathematical descriptions of predictions will be inevitably simplified or grossly simplified the perception model and in some cases still possible to provide predictions (Beven, 2012).

- Conceptual model

The conceptual model is deciding on the equations that will make quantitative predictions and simplify the descriptions and processes by made hypotheses and assumptions. Evaluation of the model relative to the perceptual model shall be started where the background for the equation is known (Beven, 2012).

- Procedural model

The procedural model is defined by using the technique of numerical analysis to get the code to run on the computer specially if the equations cannot be solved analytically under boundary conditions are given for the real system (Beven, 2012).

- Model calibration

Before the code is run on the computer, quantitative forecasts for a specific watershed shall be made by calibrating parameters. Different inputs that are related to the shape of the watershed are usually deliberated as constants throughout the particular simulation, a variable namely precipitation and other meteorological variables that are defined in time boundary conditions and state variables namely water table depth or soil water storage have been compromised in all hydrological models. In model calibration, values of the parameters have been adjusted to not deviate from the model predictions from the actual watershed response (Beven, 2012).

Different calibration techniques such as the manual trial-and-error method, automatic optimization algorithms, and goodness-of-fit calibration techniques are available to calibrate parameters of rainfall-runoff models. In the manual trial-and-error method, model parameters are adjusted by using observed historic data and then compared visually to check the weather requirement of another trial execution (Singh, 1995). This method takes high computational time, requires experience for proper calibration, and is difficult to identify the "best" fit (Pechlivanidis et al., 2011). Automatic-optimization algorithms are a computer-based approach that quickens the calibration and reduces differences between simulation outputs and observed data by confidence intervals (Sitterson et al., 2017). Goodness-of-fit calibration techniques such as Least-squares methods and maximum likelihood methods generate an arithmetical relationship among observations and outputs of simulation to calibrate parameters (Sitterson et al., 2017).

- Model evaluation

One or more indicators of the model efficiency will be calculated referring to the available observations such as runoff response (Beven, 2012).

2.11.3 Types of models

Rainfall-runoff models can be categorized as lumped versus distributed modelling approach, deterministic versus stochastic models, black box versus conceptual versus physical-based models, event-based and continuous simulation models, and other types as well as sometimes models cannot be unambiguously assigned to one category (Montanari, 2016).

- Model structures

Model structure determines how runoff is calculated and varies simplicity or complexity based on governing equations (Sitterson et al., 2017). Basic structures for rainfall-runoff models are empirical, conceptual, and physical-based models in order of increasing complexity (Sitterson et al., 2017).

a. Empirical models

Empirical models such as Curve Number and Artificial Neural Networks[a] (Sitterson et al., 2017) have developed a nonlinear relationship between inputs and outputs (Kokkonen et al., 2001) by the use of a fewer number of parameters which may be high accuracy and fast run time. The principal of the model is a function of runoff, Q = f (X, Y) where X and Y are inputs of precipitation and historic runoff (Sitterson et al., 2017).

However, the model has no connection with physical watershed and input data distortion by the way the best use of these models is that in ungauged watersheds and when requiring only runoff as the output of the model (Pechlivanidis et al., 2011).

b. Conceptual models

The basic equations of the model denote water storage in the watershed. Especially the water balance equation with components of rainfall, runoff, evapotranspiration, and groundwater are used to developed conceptual models (Vaze et al., 2012) such as HSPF[b], TOPMODEL[a], HBV[a], and Stanford[a] with easiness in calibration and simple model structure (Sitterson et al., 2017). The common governing equations of the conceptual model are versions of the water balance equation. The components in the water balance equation are determined by numerical equations (Sitterson et al., 2017).

The most popular version of the water balance equation which controls surface water and storage variations is $\frac{ds}{dt} = P - ET - Q_s \pm GW$; where $\frac{ds}{dt}$ is a change in reservoir storage, P is precipitation, ET is evaporation, Q_s is surface runoff and GW is groundwater (Sitterson et al., 2017).

The main weakness of this model structure is that it does not consider spatial variability within the watershed (Sitterson et al., 2017).

c. Physical models

Physically-based models have been created based on physical rules and equations include water balance equations, conservation of mass and energy, momentum, and kinematics. St. Venant, Boussinesq’s, Darcy, and Richard’s equations based on real hydrologic responses (Pechlivanidis et al., 2011) with the advantages of incorporate spatial and temporal variability and very fine-scale as well as disadvantages of a large number of parameters required for calibration and site-specific (Sitterson et al., 2017). The physical models such as MIKE-SHE[a], KINEROS[c], VIC[a], and PRMS[d] (Singh, 1995) are most suitable to use where available considerable data on a fine-scale (Sitterson et al., 2017).

Moreover, most of these models can be used to provide a three-dimensional illustration of water exchange with the soil, surface, and air, and also simulate movements of groundwater, and interactions of the watershed with sediments, nutrients, and chemicals (Singh, 1995).

- Spatial structures

According to the spatial structure of rainfall-runoff models, there are 3-categories namely lumped, semi-distributed, and distribution models that represent the particular watershed depend on input data set, runoff generation, and routine throughout the watershed.

a. Lumped models

Lumped models disregard the spatial variability of the watershed and consider as one unit (Moradkhani & Sorooshian, 2009). All average data by watershed are input to these models (Beven, 2012) with the advantages of less time consuming for computation and being good at simulating average conditions (Sitterson et al., 2017). However, lumped models are not ideal for large areas due to the use of many assumptions for modelling and the loss of spatial resolution (Moradkhani & Sorooshian, 2009). Some examples of lumped models are empirical and conceptual models and machine learning (Sitterson et al., 2017). The spatial structure in a lumped model is shown in Figure 2.7.

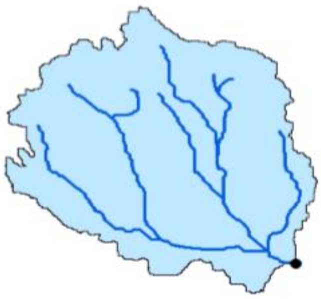

Figure 2.7: Spatial structure of a lumped model

b. Semi-distributed models

The semi-distributed model consists of a series of lumped and distributed parameters that are different for each sub-watershed area that is divided (Rinsema, 2014) based on slope, soil group, vegetation zone, or hydraulic response units (HRUs) in the model process (Beven, 2012). Since both average and specific data by sub-watershed are used as inputs for these models, it represents important features in the watershed as well as fewer data and fewer parameters compared to distributed models (Pechlivanidis et al., 2011). The main weakness of the model is the loss of spatial resolution due to assigning average data into sub-watershed areas (Sitterson et al., 2017). It is possible to run conceptual and physical models in semi-distributed matter based on the input data set. TOPMODEL[a] and SWAT[b] models are semi-distributed models that are divided into sub-watershed areas based on a land surface slope & soil characteristics and hydraulic response spectrum, respectively (Sitterson et al., 2017). The spatial structure in a semi-distributed model is illustrated in Figure 2.8.

Figure 2.8: Spatial structure of a semi-distributed model

c. Distributed models

The fully distributed model is more complex and provides an improved hydrograph (Smith et al., 2012) compared to lumped and semi-distributed models due to accounts of spatial heterogeneity in inputs and parameters by dividing the watershed into small elements or grid cells as shown in Figure 2.9 (Sitterson et al., 2017).

Figure 2.9: Spatial structure of a distributed model

Here, hydrological responses of each element or grid cell are estimated individually but, with interactions of neighboring cells (Rinsema, 2014). Therefore, these models are data-intensive and if calculate the runoff of each grid cell, the model can provide comprehensive information of runoff at many points within the watershed. The structure of distributed models is similar to physical-based models which makes it related to the actual hydrological process (Sitterson et al., 2017). Some examples of distributed models are MIKESHE[c] and VELMA[d].

The main weakness of these models is the long computational time depend on the input data set, watershed extent, and computational restraints (Vaze et al., 2012), and also distributed models require distributed data and calibrated parameters for each grid cell. Weighted averages are used to extrapolate data where data are not fully distributed. Therefore, distributed models are also restricted in space by model resolution or input grid size (Sitterson et al., 2017).

2.12 RRI model

2.12.1 Introduction

The flood is a frequently experienced harmful natural hazard that is experienced due to the impacts of extreme changes in the climate. The structural and non-structural countermeasures are necessary to prevent and mitigate flood damages. Non-structural countermeasures are important in flood management including flood prediction that would improve the competency of other countermeasures. Flood modelling for flood forecasting would provide early warning in dangerous situations to minimize flood damages and its accuracy will depend on rainfall data referring to time and space scale (Nastiti et al., 2015).

Non-structural countermeasures can be carried out with rainfall-runoff modelling, and inundation simulation. The inundation is simulated using a conventional separate modelling approach with two models namely the rainfall-runoff model, and the hydraulic model for forecasting river discharge, and propagation of water, respectively. Since interactions between the river and floodwater are significant in flat terrain and large flooded area, this approach cannot be applied under these conditions. Moreover, the determination of parameters for both two models apart is quite hard. Therefore, the rainfall-runoff-inundation (RRI) model has been introduced with a completely combined model of the rainfall-runoff model and hydraulic inundation model (Nastiti et al., 2015).

The RRI model is a two-dimensional model that is the ability to simulate both rainfall-runoff and inundation simultaneously. The flows on the slopes are derived by 2D diffusive wave equations disregarding the topography (Sayama et al., 2017) while the channel flows are determined by 1D diffusive wave equations (Nastiti et al., 2015). The flood extent can be simulated for different conditions of surface and subsurface flow. The RRI model structure is shown in Figure 2.10.

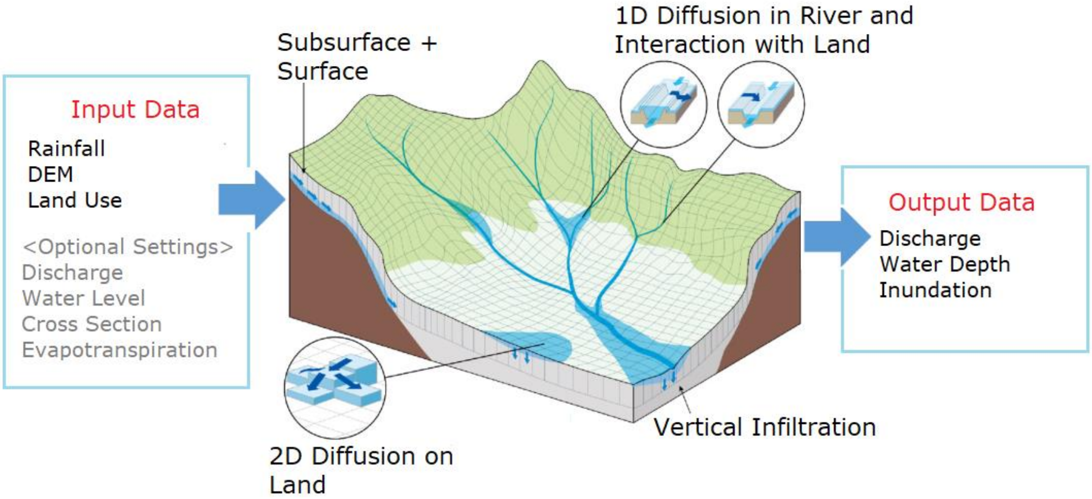

Figure 2.10: RRI model structure

Source: (Sayama et al., 2017)

In RRI models, the lateral subsurface flow in mountainous areas and infiltration in flat areas are considered separately. Further, lateral subsurface flow, vertical infiltration flow, and surface flow are simulated for representing the RRI process well. Moreover, flow interactions between the river and channels are determined by using various formulae of overflowing, based on the level of water and height of the dam conditions (Nastiti et al., 2015).

The performance of RRI models mainly relies on inputs of rainfall intensity and distribution and is enhanced by the use of more and accurate precipitation data, higher-resolution elevation data, and concern on dam operations in implementing models. The main advantage of the RRI model is applicable for flat river basins also. In a flat river basin, since floodwater retains much longer to drain out the water, the inundated area will be larger and retain for a longer period. The previous study on the RRI model for flood mapping in a deltaic area of Myanmar shows the deviation between simulated results and observed satellite-based data due to the neglected effect of the energy budget component. The RRI modelling answers well for shortening periods modelling. However, it does contain a drawback related to the accuracy of long-term events. Therefore, the energy budget component should be essentially taken into consideration when estimating the inundation area to high precision on the condition of long-term events. Further, well-calibrated models are required for flood prediction, flood alert systems, and flood inundation maps (Bhagabati & Kawasaki, 2017).

The dynamics of a flood shall be considered for large-scale floods on a real-time basis. The study, RRI modelling to the Chao Phraya River basin totally for large scale based on Thailand flood in 2011 has been conducted on an approximately real-time simulation for emergency responses by use of satellite-based rainfall and topography data and post-flood simulation rely on more local data. For both two simulations, parameters and concerns are different from each as an example for emergency response type simulation, satellite and predicted data for precipitation without concern on the effect of evapotranspiration and dam, and cross-sectional data such as river depth (D) and width (W) estimated by equations $D = C_D A^{SD}$ and $W=C_W A^{SW}$ (A – contributing upstream area in km^2), respectively while for post-flooding simulation corrected satellite-based rainfall with gauged rainfall for precipitation, measured cross-sectional data, consideration on dam model and the effect of evapotranspiration have been used. This study shows a higher recession rate compared to the actual rate due to not a detailed representation of the effects of artificial structures such as roads and paddy fields in RRI models as a result of it floodwater in the model flows back to the river fast and smoothing the flow when begin to drop the water level of the nearby river. The sensitive analysis with different updated inputs regarding more concerns on evapotranspiration, dams, and cross-section of the river as well as inundation effects may be useful for improving the accuracy of the model (Sayama et al., 2017).

Some degree of uncertainty remains in models due to parameters that are not possible to calibrate. Various methods are available to evaluate uncertainty in RRI models and the Monte Carlo method is the popular method among them. However, this method is not practical for large-scale rainfall-runoff inundation simulation due to computationally expensive. Therefore, it is better for doing a sensitive analysis by changing parameters rather than do a complete uncertainty analysis (Sayama et al., 2012).

2.12.2 Model Formulation

- Two-dimensional surface and subsurface flow model - Lateral flows on slope grid cells are calculated by the mass balance equation (2.1) and momentum equation (2.2) and (2.3) for regularly varied unsteady flow and the terms $\frac{\tau_x}{\rho_w}$ and $\frac{\tau_y}{\rho_w}$ are calculated with Manning's equations (2.4) and (2.5) as follows.

$$\frac{\partial h}{\partial t} + \frac{\partial q_x}{\partial x} + \frac{\partial q_y}{\partial y} = r \tag{2.1}$$

$$\frac{\partial q_x}{\partial t} + \frac{\partial u q_x}{\partial x} + \frac{\partial v q_x}{\partial y} = -gh\frac{\partial H}{\partial x} - \frac{\tau_x}{\rho_w} \tag{2.2}$$

$$\frac{\partial q_y}{\partial t} + \frac{\partial u q_y}{\partial x} + \frac{\partial v q_y}{\partial y} = -gh\frac{\partial H}{\partial y} - \frac{\tau_y}{\rho_w} \tag{2.3}$$

$$\frac{\tau_x}{\rho_w} = \frac{g n^2 u \sqrt{u^2 + v^2}}{h^{1/3}} \tag{2.4}$$

$$\frac{\tau_y}{\rho_w} = \frac{g n^2 v \sqrt{u^2 + v^2}}{h^{1/3}} \tag{2.5}$$

where h is the water height from the local surface, q_x and q_y are the unit breadth discharges in x and y directions, u and v are the flow velocities in x and y directions, r is the rainfall intensity, H is the water height from the datum, ρ_w is the water density, g is the gravitational acceleration, τ_x and τ_y are the shear stress in x and y directions and n is Manning's roughness.

Under diffusion wave approximation, inertia components are unconcerned in equations (2.2) and (2.3). Equations (2.6) and (2.7) are derived in x and y directions, respectively.

$$q_x = -\frac{1}{n} h^{5/3} \sqrt{\left|\frac{\partial H}{\partial x}\right|} \operatorname{sgn}\left(\frac{\partial H}{\partial x}\right) \tag{2.6}$$

$$q_y = -\frac{1}{n} h^{5/3} \sqrt{\left|\frac{\partial H}{\partial y}\right|} \operatorname{sgn}\left(\frac{\partial H}{\partial y}\right) \tag{2.7}$$

where sgn is the signum function.

The RRI model spatially discretizes mass balance equation (2.1) as the following equation (2.8).

$$\frac{dh^{i,j}}{dt} + \frac{q_x^{i,j-1} - q_x^{i,j}}{\Delta x} + \frac{q_y^{i-1,j} - q_y^{i,j}}{\Delta y} = r^{i,j} \tag{2.8}$$

where $q_x^{i,j}$, $q_x^{i,j}$ are discharges from a grid cell at (i, j) in the x and y-direction.

The equations for saturated subsurface flow by Darcy's law and the combination of the saturated subsurface flow and the surface flow are shown by the following equations (2.9) and (2.10).

$$q_x = -kh\frac{\partial H}{\partial x} \qquad (h \leq d) \tag{2.9}$$

$$\frac{1}{n}(h-d)^{5/3}\sqrt{\left|\frac{\partial H}{\partial x}\right|}\ \mathrm{sgn}\left(\frac{\partial H}{\partial x}\right) - k(h-d)\frac{\partial H}{\partial x} \qquad (d < h)$$

$$q_y = -kh\frac{\partial H}{\partial y} \qquad (h \leq d) \tag{2.10}$$

$$\frac{1}{n}(h-d)^{5/3}\sqrt{\left|\frac{\partial H}{\partial y}\right|}\ \mathrm{sgn}\left(\frac{\partial H}{\partial y}\right) - k(h-d)\frac{\partial H}{\partial y} \qquad (d < h)$$

where k is the lateral saturated hydraulic conductivity and d is the soil depth times the effective porosity.

- Infiltration model – The vertical infiltration component is defined based on the Green-Ampt infiltration model.

$$f = k_v \left[1 + \frac{(\emptyset - \theta_i)S_f}{F}\right] \tag{2.11}$$

where f is the infiltration rate, k_v is the vertical saturated hydraulic conductivity, $\emptyset$ is the soil porosity, θ_i is the initial water volume content, S_f is the suction at the vertical wetting front and F is the cumulative infiltration depth.

- Interactions of water among slope and river – Under the flow from slope to the river under the normal condition, the discharge from the slope into the river is estimated by using equation (2.12).

$$q_{sr} = \mu_1 h_s \sqrt{g h_s} \tag{2.12}$$

where, μ_1 is the constant coefficient (=0.544) and h_s is the water depth on a slope cell.

No water exchange will be taken when the water level of the river is above the water level of the slope and below the dam height.

Overtopping flow from the river to the slope is estimated using an over-bank flow formula.

$$q_{rs} = \mu_2 h_1 \sqrt{2 g h_1} \tag{2.13}$$

where, μ_2 is the constant coefficient (=0.35) and h_1 is the difference between the river water level and the levee crown.

Overtopping flow from slope to the river is calculated by using over-bank flow formulae (2.13) and q_{rs} is replaced with q_{sr} (Sayama et al., 2012).

2.12.3 Selection of flood events for RRI simulation

The flood hydrographs of the known storm in a specific watershed delineate the duration of the flood event namely the base time of the flood hydrographs. There are several methods to develop flood hydrographs resulting from a known storm event. However, the most widely utilized and popular method is the unit hydrograph method which was introduced by Sharman in 1932 (Chow et al., 1988).

Unit hydrographs have been developed based on the following basic assumptions.

- The intensity of the excess rainfall is constant during the considered period.
- The excess rainfall is uniformly distributed throughout the watershed.

- The base time is constant for the resultant unit hydrograph for excess rainfall of a given duration.
- Every ordinate of the hydrograph of a mutual base time is directly proportional to the total direct runoff of each hydrograph.

Since the unit hydrograph concept is developed based on aforementioned assumptions that are not perfectly matched with actual conditions.

Different methods such as Snyder's method, Soil Conservation Service (SCS) method, and Gray's method are popular for synthesizing the peak runoff. In Snyder's method, mainly five determinants such as peak discharge per unit area of catchment lag time, base time, and width of unit hydrographs at 50%, and 75% of peak discharge. The Soil Conservation Service method in 1971 has been developed for dimensionless hydrographs and applied under different drainage areas and geographical regions. The peak discharge and the time to the peak can be calculated from this method. From Gray's method, peak discharge can be determined by dimensionalizing the partial Gamma function.

2.13 Water and Energy-Based Rainfall-Runoff-Inundation (WEB-RRI)

RRI model is important in flood forecasting, mapping flood and flood hazards, and damage valuation. However, the RRI model is applicable only for post-flood simulation due to neglect of the effects of energy budget components and interactions between soil, vegetation, and atmosphere during the flood (Sayama et al., 2012). The major drawback of not estimating the effects of the temperature could be observed in these models for drought assessment and water resource management. This may lead to the deficiency to apply the water budget modelling (Rasmy et al., 2019).

The Water and Energy Budget Distributed Hydrological Model (WEB-DHM) is a semi-distributed and kinematic wave model that has been introduced as a new model consisting of the Simple Biosphere Model-2 (SiB2) with a hydrological model. However, this model has not a successful as expecting due unable to simulate the runoff inundation process (Rasmy et al., 2019).

A new distributed hydraulic model, the Water, and Energy Budget-based Rainfall-Runoff-Inundation (WEB-RRI) model has been introduced by coupling SiB2 and RRI models. SiB2 model with RRI model has been developed to determine processes of water and energy budget and initial soil storage, flood forecasting, and also long term flood simulation by incorporating diffusive wave equations of RRI for a land surface model (hydro - SiB2) (Rasmy et al., 2019).

The model structure of WEB-RRI consists of four components as illustrated in Figure 2.11.

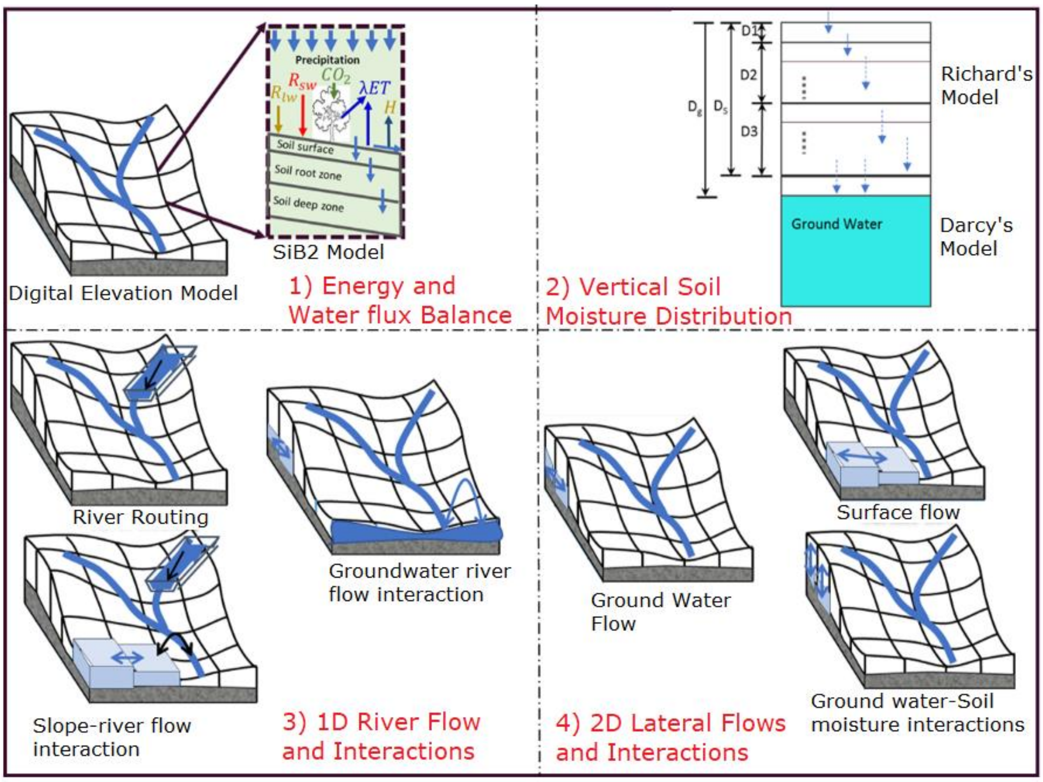

Figure 2.11: Model structure of WEB-RRI

Source: (Rasmy et al., 2016)

1) Energy and Water Flux Balance - estimation of energy and water transfer between land and atmosphere using SiB2 model

2) Vertical Soil Moisture and Profile - estimation of vertical soil moisture distribution using Richard's formula and Darcy's law,

3) Lateral Flow - estimation of lateral flow for surface flow and groundwater flow using the 2D diffusive wave equation

4) River Routing - estimation of river routing and discharge using the 1D diffusion wave equations.

3. METHODOLOGY

3.1 Methodology Flow chart

The overall methodology of the research includes the main seven steps as shown in Figure 3.1 and can be divided into two as traditional RRI model and improved RRI model.

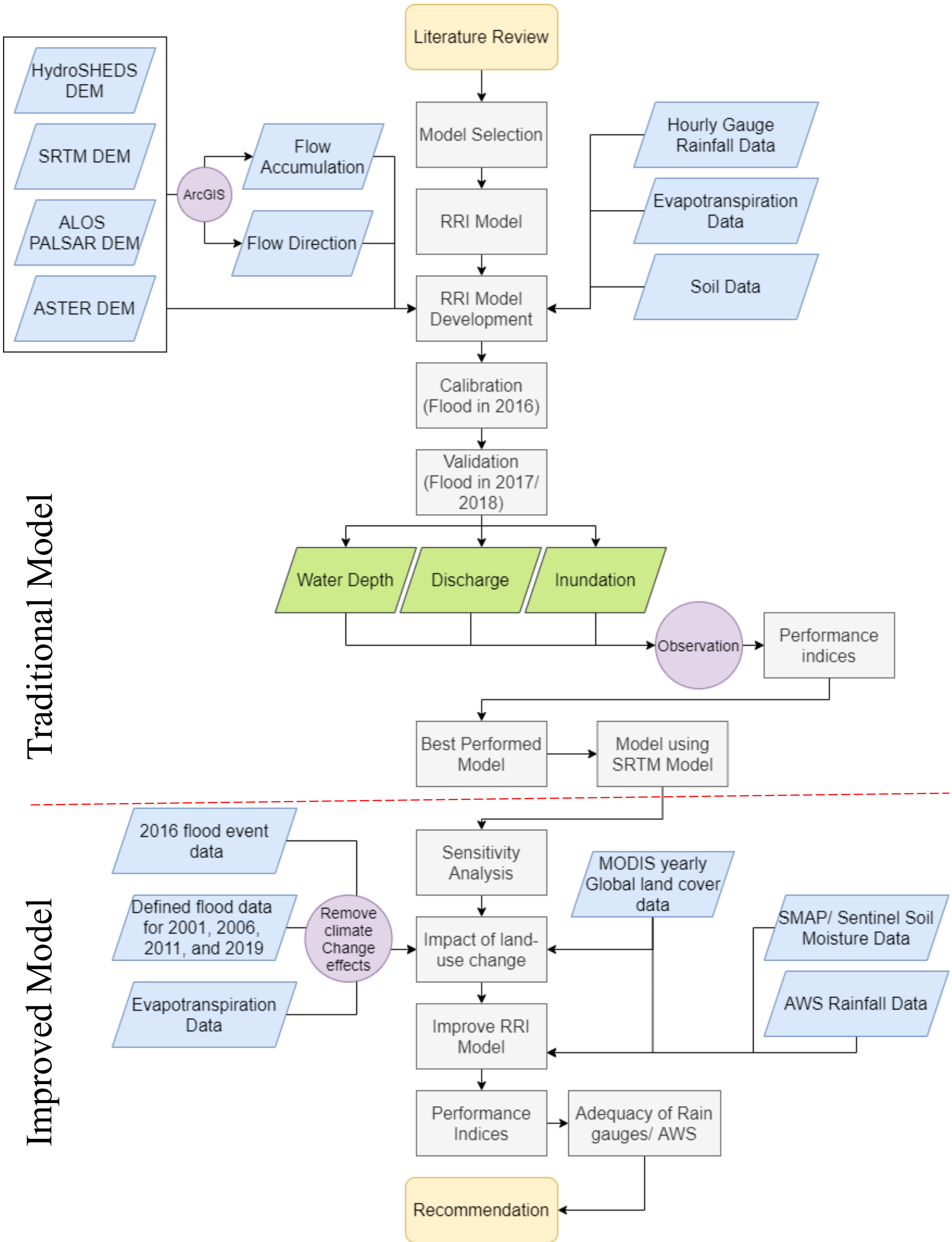

Figure 3.1: Methodology Flow Chart

3.2 Model Selection

Various hydrological models that are capable of flood modelling are available and the Table 3.1 shows selected few flood models and their capabilities.

Table 3.1: Capabilities of Hydrological models

Model	Characteristics	Reference
LISFLOOD-FP	• Capable of simulating the hydrological processes that occur in a watershed specially use for large-scale and multinational watersheds. • It has been used for various applications including flood prediction, assessment of impacts of river regulation measures, land-use, and climate changes. • It considers the equivalent distribution of water across all raster grid cells. It may lead to a miscalculation of the flood inundation. • The water propagation in four directions shall be considered at every cell face when the topography of the watershed is complex.	(Shustikova et al., 2019)
HEC-RAS	• It has been developed as a 2D computational model and uses both the 2D St Venant equation and 2D diffusion wave equations. • The main disadvantage of the model is that is not capable of estimating flood inundation and water depth distribution in some cases due to leakage effects of the model.	(Shustikova et al., 2019)

RRI	• It is capable of Simulating both rainfall-runoff and inundation synchronously. • Applicable for flat river basin • Perform well for the short-term modelling. • Less accuracy for long term events due to neglect effect of the energy budget component	(Bhagabati & Kawasaki, 2017)
WEB-DHM	• A semi-distributed and kinematic wave model • Not successful as expected due to unable to simulate the runoff inundation process.	(Rasmy et al., 2019)
WEB-RRI	• It is capable to determine processes of water and energy budget and initial soil storage, flood forecasting, and also long-term flood simulation by incorporating diffusive wave equations of RRI for a land surface model (hydro -SiB2). • Not available public domain software	(Rasmy et al., 2019)

Since RRI is the most suitable hydrological model for simulating rainfall-runoff-inundation processes according to the aforementioned capabilities of each hydrological model, the RRI model was selected as the hydrological model for this research.

3.3 Data Acquisition

The data listed in Table 3.2 are required to develop the RRI model, model calibration, and validation.

Table 3.2: Required data for model

Data	Resolution	Source
Topography data • DEM • Flow direction • Flow Accumulation	 3 arc-second 3 arc-second 1 arc-second 12.5 m 3 arc-second 3 arc-second	 HydroSHEDS topographic data SRTM topographic data ASTER topographic data ALOS PALSAR topographic data Using ArcGIS (ESRI, USA) Hydro tools Using ArcGIS (ESRI, USA) Hydro tools
Gauged Rainfall Data	Hourly	Colombo station - Department of Meteorology Rathmalana station - Department of Meteorology Hanwella station - CUrW
AWS	Hourly	CUrW
Streamflow Data	Hourly	Hanwella Station – Irrigation Department Nagalagam Street Station – Irrigation Department
Maximum and Minimum Temperature	Daily	Colombo station – Department of Meteorology
Maximum and Minimum Relative Humidity	Daily	Colombo station – Department of Meteorology
Wind Speed	Monthly	Colombo Station – Department of Meteorology
Number of sunshine hours	Monthly	Colombo Station – Department of Meteorology
Manning's roughness in the river channel and on slope cells		Open Channel Hydraulics – Ven Te Chow, 1959 (Pakoksung, 2016)
Land use data	Yearly	MODIS yearly global land cover data

Soil Moisture Data	Daily	SMAP/ Sentinel-1 Radiometer/ Radar 30-second Scene 3 km EASE-Grid soil moisture version 2

3.4 Preparing input topographic data

The four products of DEM namely 3-arc (90 m grid) HydroSHEDS, 3-arc (90 m grid) SRTM, 1-arc (30 m grid) ASTER, and 12.5 m grid ALOS PALSAR were downloaded. The ASTER and ALOS PALSAR DEM have converted to 3-arc (90 m grid) DEM using nearest-neighbor and majority resampling techniques, respectively. The flow direction and flow accumulation raster files were prepared using each DEM product. The raster files of DEM, flow direction data, and flow accumulation was delineated using the ArcGIS (ESRI/USA) hydro tools. DEM, flow direction, and flow accumulation of 3-arc (90 m) resolution HydroSHEDS data are illustrated in Figure 3.2, Figure 3.3, and Figure 3.4, respectively.

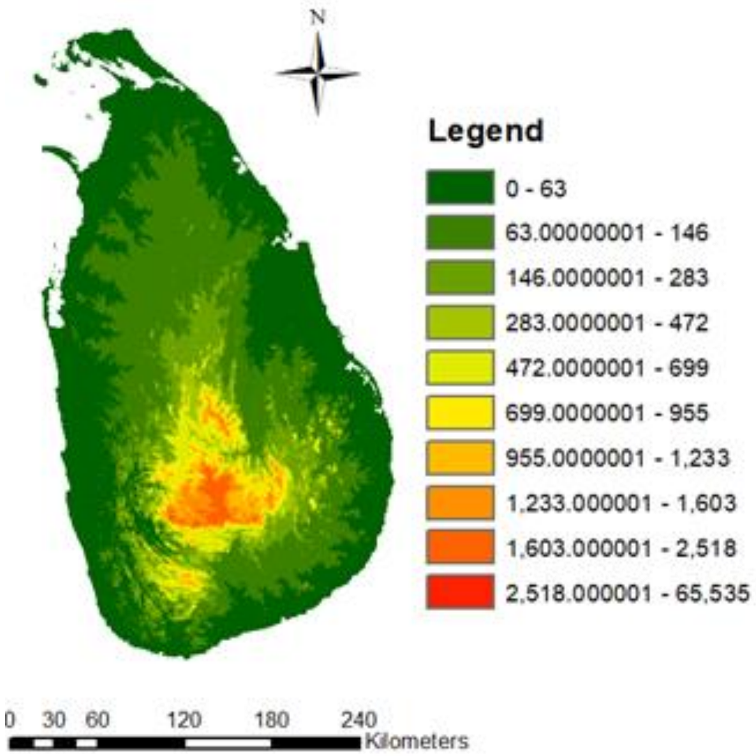

Figure 3.2: Delineation of DEM

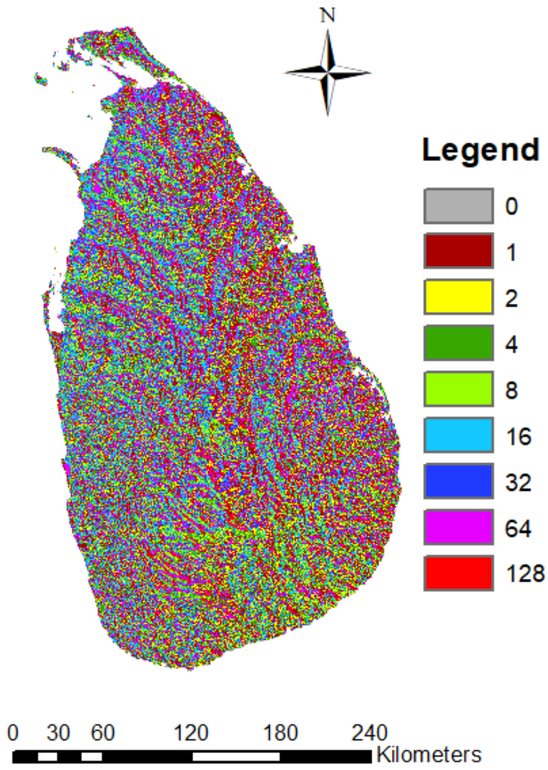

Figure 3.3: Delineation of flow direction data

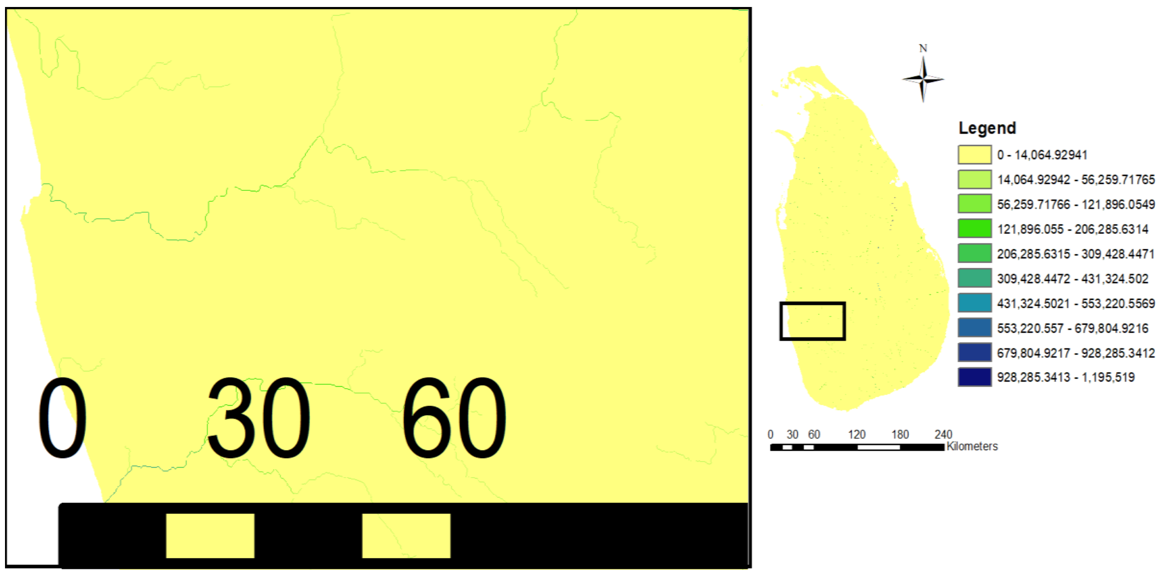

Figure 3.4: Delineation of Prepared flow accumulation data

The Lower Kelani River Basin boundary was created and defined boundaries for the Lower Kelani River Basin are,

- Outlet coordinates - 6.98º N, 79.87º E

- Value for the northern edge - 7.054º
- Value for the southern edge - 6.771º
- Value for the eastern edge - 80.077º
- Value for the western edge – 79.840º

The DEM, flow direction, and flow accumulation data of the Lower Kelani River Basin were prepared using HydroSHEDS, SRTM, ASTER, ALOS PALSAR DEM with 3-arc (90 m grid) resolution, and are illustrated in Figure 3.5, Figure 3.6, Figure 3.7, and Figure 3.8, respectively.

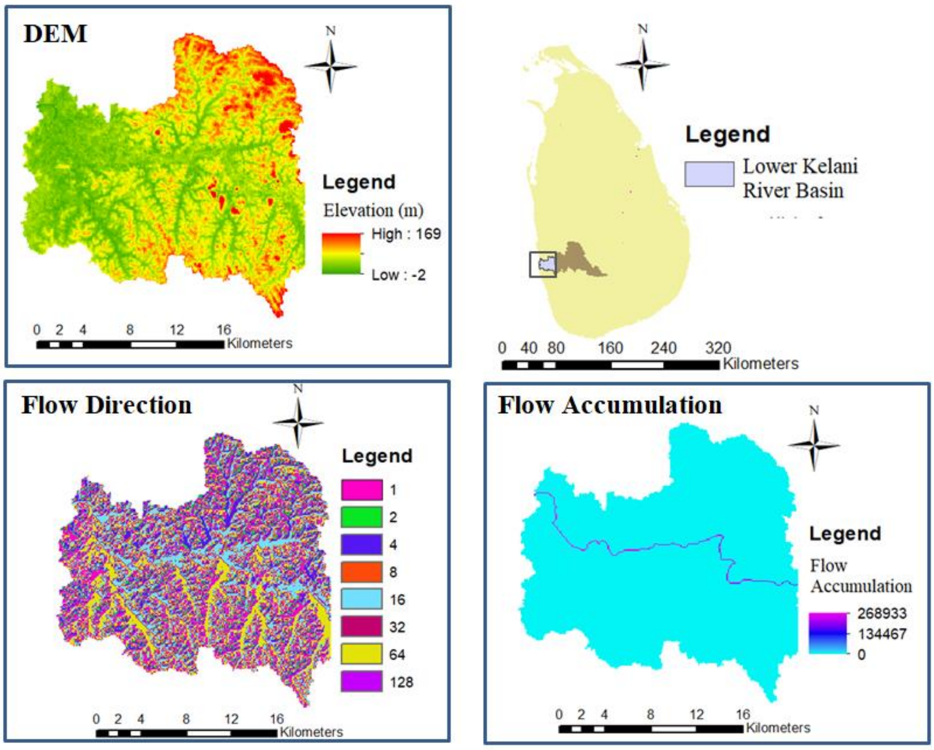

Figure 3.5: DEM, flow direction, and flow accumulation of the Lower Kelani River Basin using HydroSHEDS DEM

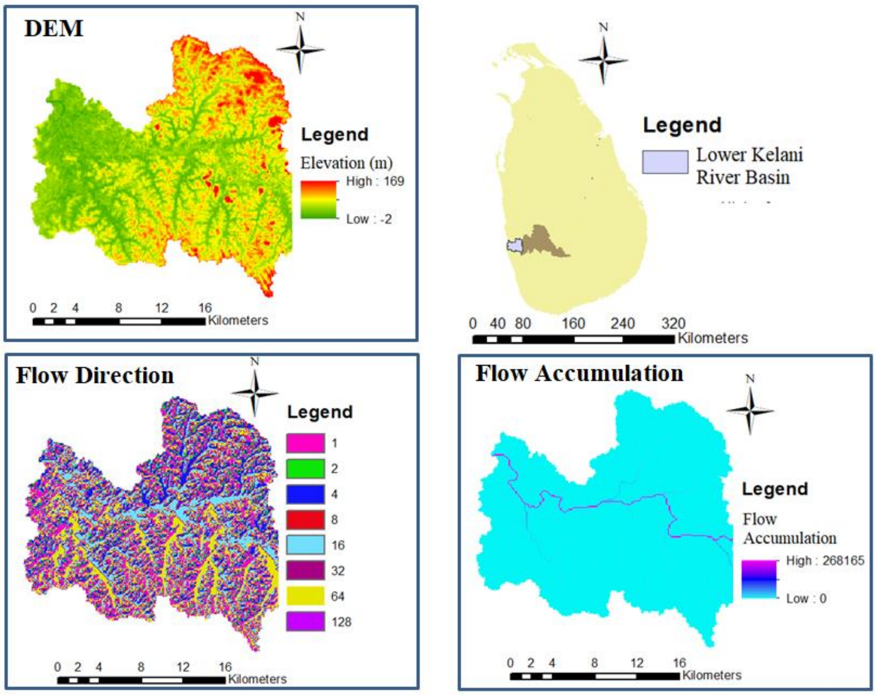

Figure 3.6: DEM, flow direction, and flow accumulation of the Lower Kelani River Basin using SRTM DEM

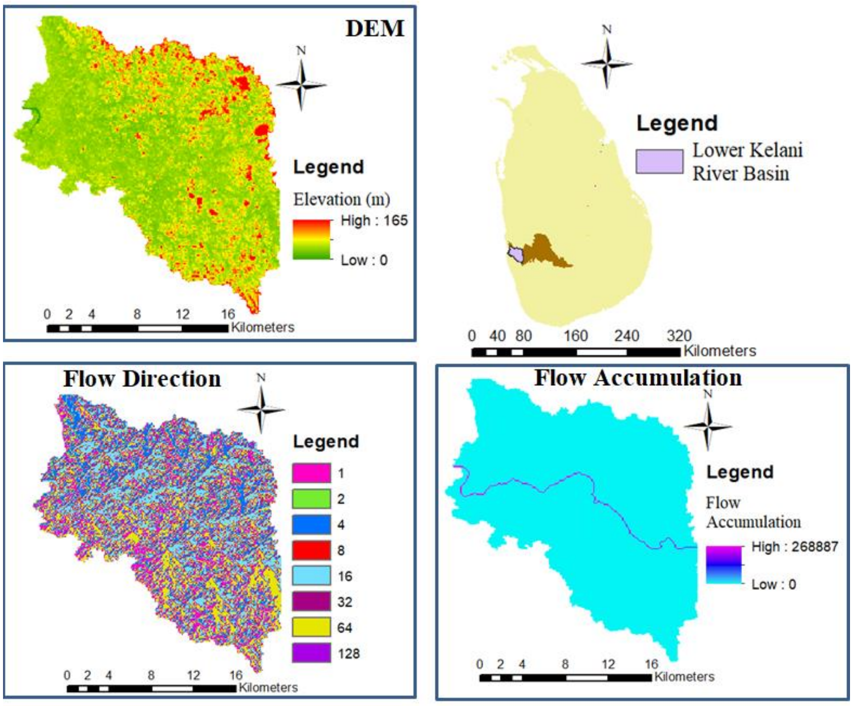

Figure 3.7: DEM, flow direction, and flow accumulation of the Lower Kelani River Basin using ASTER DEM

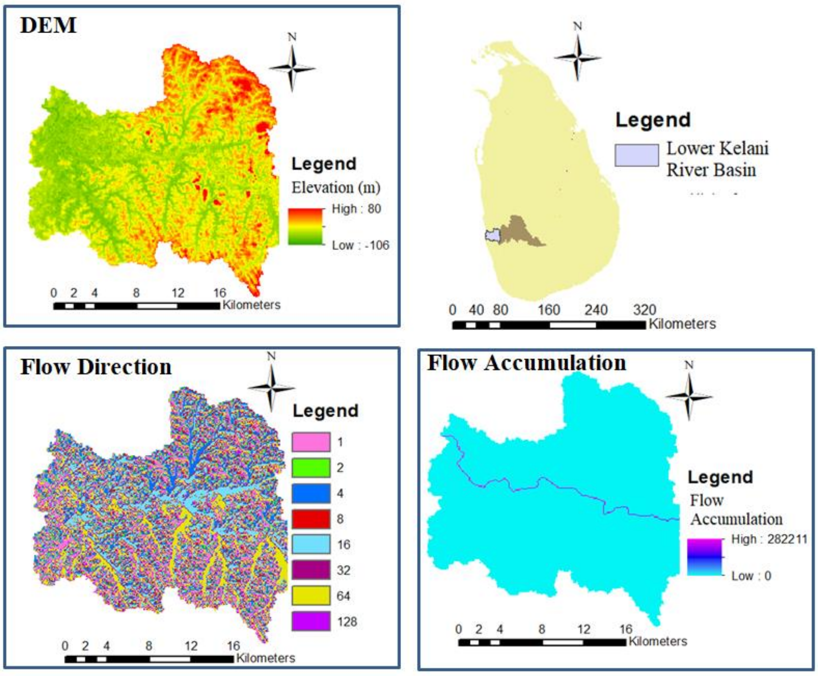

Figure 3.8: DEM, flow direction and flow accumulation of the Lower Kelani River Basin using ALOS PALSAR DEM

Then, three-layer data of DEM, flow direction, and flow accumulation in Raster format was converted to ESRI ASCII grid export format.

➢ DEM data Adjustment

The intrinsic characteristics and hollows of the original DEM shall be adjusted to avoid unrealistically. Therefore, the program called “demAdjust2” was used to remove negative slopes along the flow direction and elevation adjustments.

The algorithms of “demAdjust2” include,

1. Identify cells with no flows called upstream cells based on the direction of the flow.
2. Determine the order of the detected upstream cells in step 1.
3. Following the determined order in step 2, elevations are adjusted by making zero the negative elevation, replacing elevations of cells with extremely low elevation and sudden increment along the flow direction by its upstream elevation. The parameters “lift” and “carve” are used as a threshold to notice unexpected drops

and increments, respectively. The default values of "lift" and "carve" parameters are fixed to be 500 m and 5 m, respectively. In "Lifting" and "Carving", the point "L" which has higher downstream elevation is lifted and point "H" which has lower downstream elevation is carved.

The "demAdjust2.exe" program modifies DEM names as "adem" and DIR names as "adir" that sets flow direction to zero at the outlet cells. Adjusted DEM, and flow direction using HydroSHEDS, SRTM, ASTER, and ALOS PALSAR data are shown in Figure 3.9, Figure 3.10, Figure 3.11, and Figure 3.12.

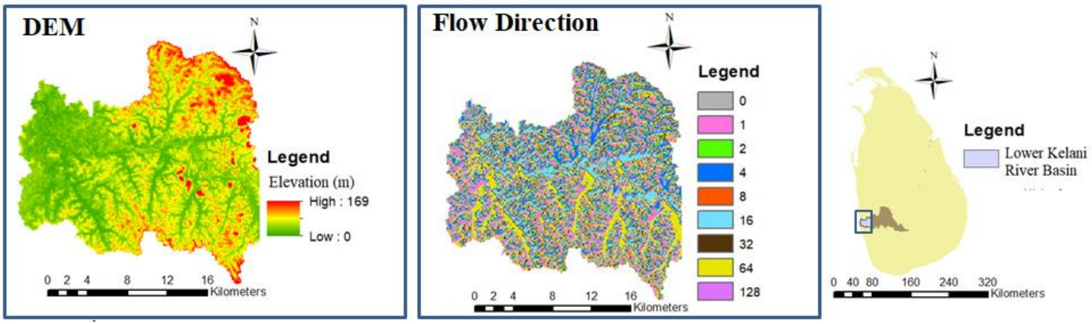

Figure 3.9: Adjusted DEM, and flow direction of the Lower Kelani River Basin using HydroSHEDS data

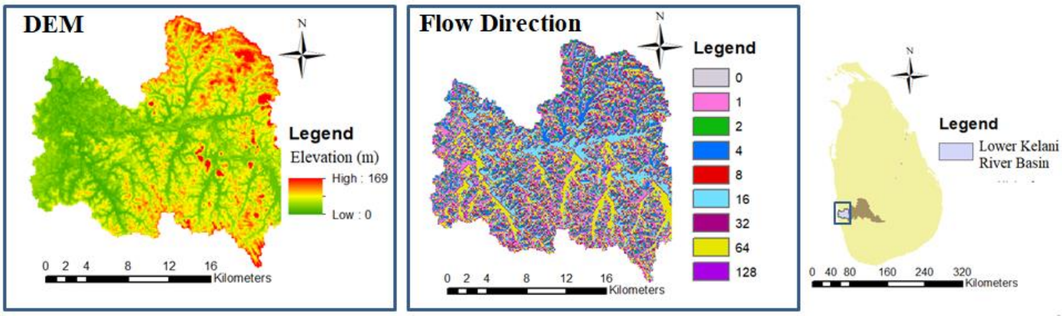

Figure 3.10: Adjusted DEM, and flow direction of the Lower Kelani River Basin using SRTM data

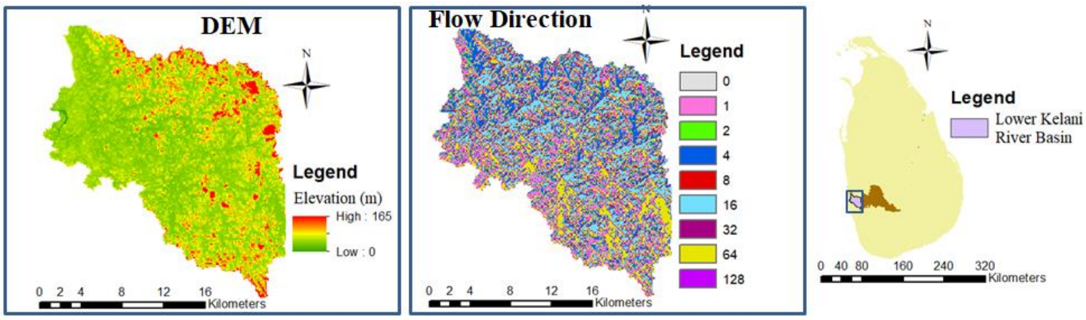

Figure 3.11: Adjusted DEM, flow direction of the Lower Kelani River Basin using ASTER data

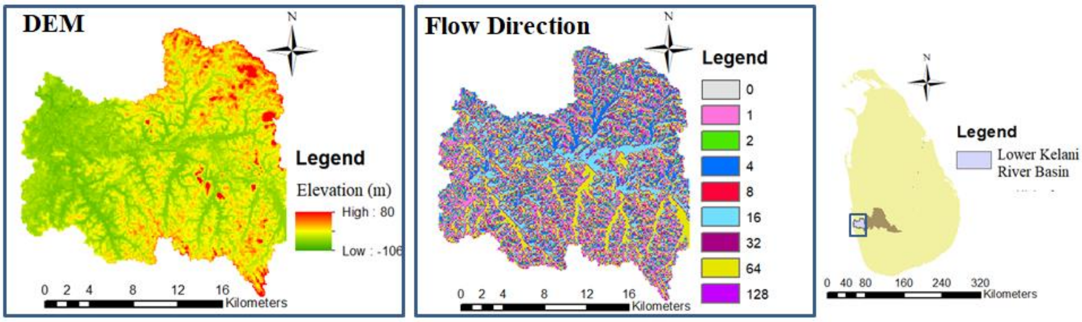

Figure 3.12: Adjusted DEM, flow direction of the Lower Kelani River Basin using ALOS PALSAR data

3.5 Preparing Rainfall data

3.5.1 Flood event selection for initial model

The period from 15th May 2016 to 23rd May 2016 was selected for initial RRI model development based on SCS triangular method as shown in Figure 3.13.

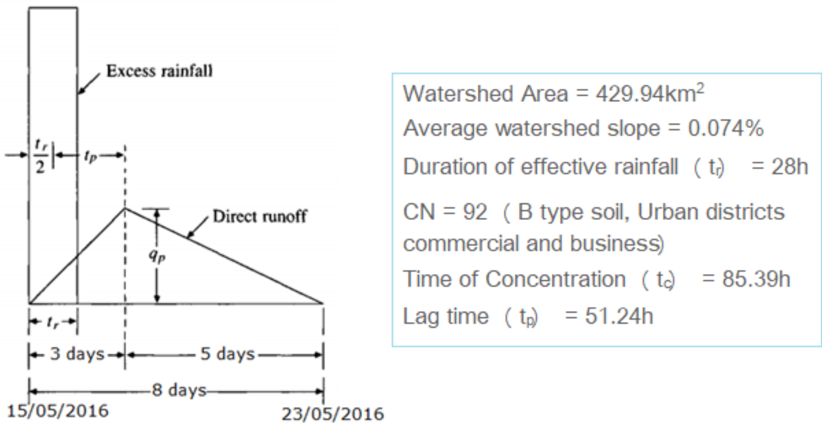

Figure 3.13: Simulation period selection for initial RRI model

The same method was followed to select flood events for the validation of the RRI model. The selected flood events for validation were the 2017 flood event from 25th May 2017 to 1st June 2017 and the 2018 flood event from 21st May 2018 to 29th May 2018.

3.5.2 Delineating rain gauge rainfall data for the study region

Hourly rainfall data at Colombo (6.9º N, 79.867º E), Rathmalana (6.817º N, 79.883º E) and Hanwella (6.911º N, 80.076º E) rain gauge stations shown in Figure 3.14 were obtained for the period from 15th May 2016 to 23rd May 2016 and prepared to input rainfall data in a format (Figure 3.15) for the RRI simulation using rainThiessen.exe program.

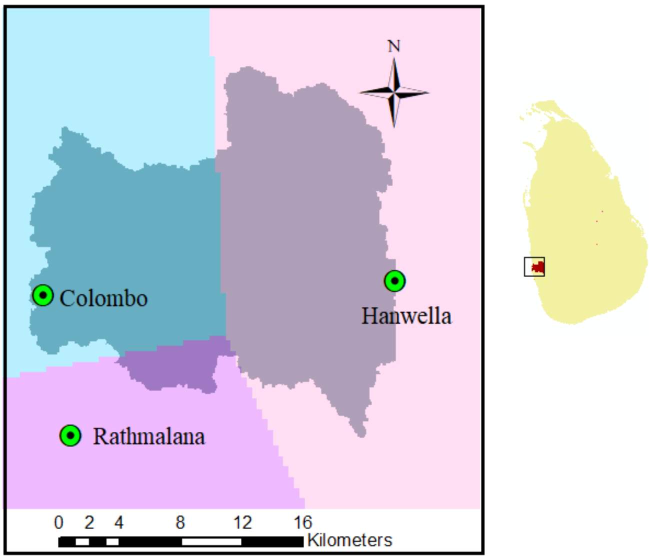

Figure 3.14: Rain gauge Map

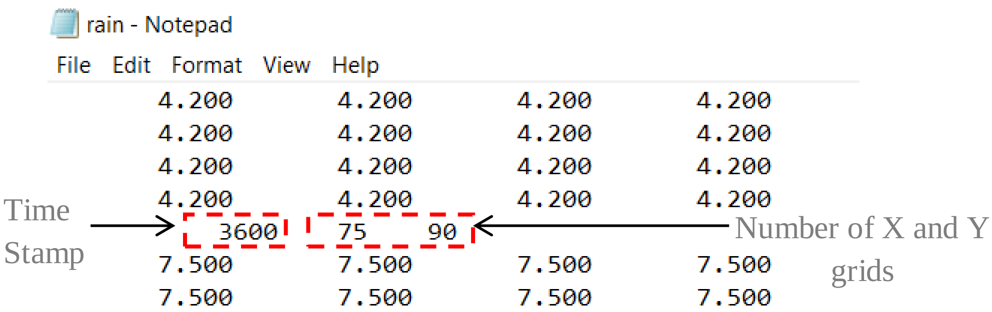

Figure 3.15: Input rainfall data format

3.5.3 Format of input Rainfall data for RRI Model

The details of cell size, xll_corner, and yll_corner of the rainfall data were defined in the RRI control file namely “RRI_Input.txt” shown in Figure 3.16 for covering rainfall distribution under the different ranges and resolution compared to topographic data and whole simulation extent.

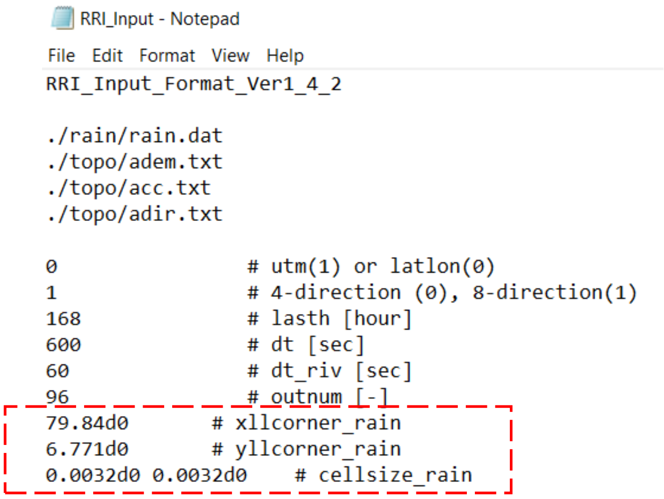

```
RRI_Input - Notepad
File  Edit  Format  View  Help
RRI_Input_Format_Ver1_4_2

./rain/rain.dat
./topo/adem.txt
./topo/acc.txt
./topo/adir.txt

0                 # utm(1) or latlon(0)
1                 # 4-direction (0), 8-direction(1)
168               # lasth [hour]
600               # dt [sec]
60                # dt_riv [sec]
96                # outnum [-]
79.84d0        # xllcorner_rain
6.771d0        # yllcorner_rain
0.0032d0 0.0032d0     # cellsize_rain
```

Figure 3.16: RRI control file

3.5.4 Calculation of watershed average rainfall

The hyetograph (mm/h), total rainfall distribution map (mm), and cumulative rainfall (mm) of the watershed for the period from 15th May 2016 to 23rd May 2016 were created. The total rainfall distribution map of the watershed during the 2016 flood event is illustrated in Figure 3.17.

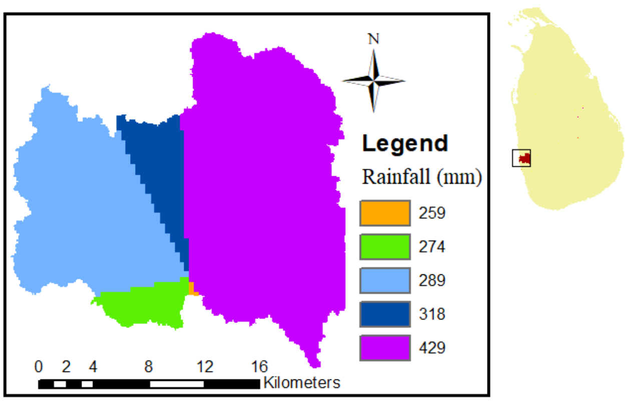

Figure 3.17: Total rainfall distribution in the study region

The hyetograph of the watershed during the 2016 flood event is shown in Figure 3.18.

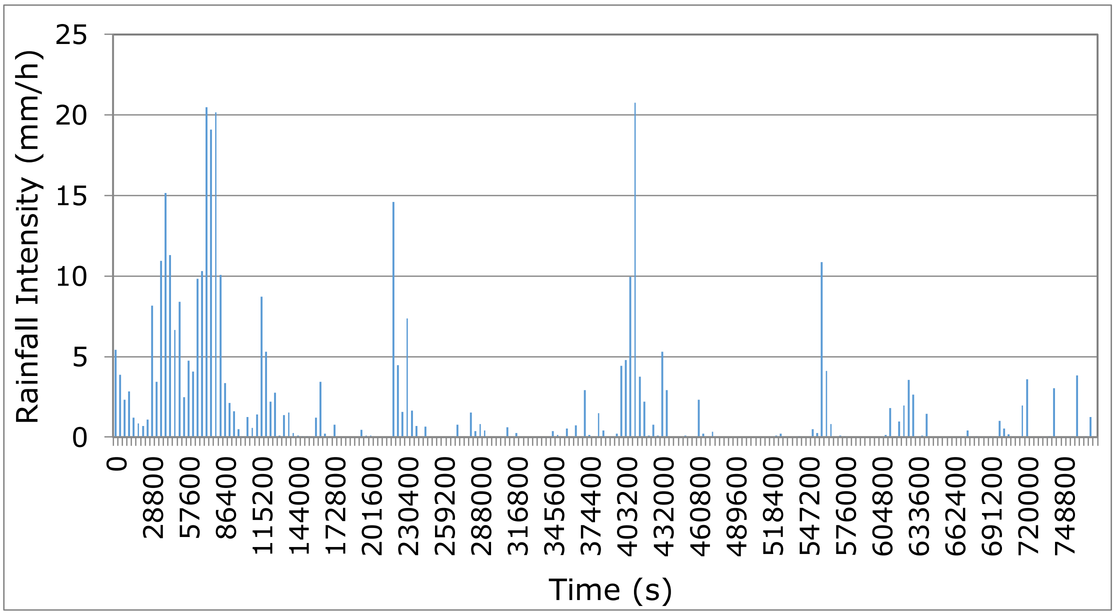

Figure 3.18: Hyetograph of the watershed during the 2016 flood event

The cumulative rainfall of the watershed during the 2016 flood event is shown in Figure 3.19.

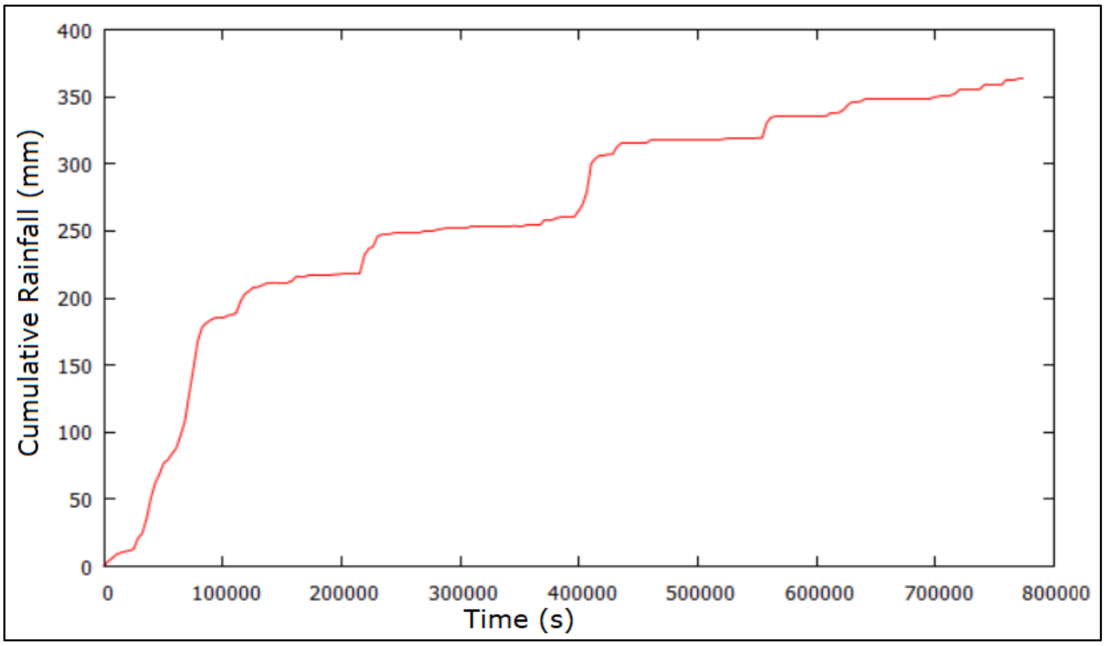

Figure 3.19: Cumulative Rainfall vs. Time

3.6 Conditions setting for Simulation

3.6.1 Input Evapotranspiration data

The daily potential evapotranspiration in mm/day for the study region was estimated using Penman's equation. For estimation of potential evapotranspiration, data on average monthly temperature, average relative humidity, average observed sunshine hours, and wind velocity at 2 m height at Colombo station (6.9^o N, 79.867^o E) for May 2016 were obtained from the Department of Meteorology and are listed in Table 3.3.

Table 3.3: Data for estimation of potential evapotranspiration

Observation Data	Value
Average Monthly Temperature	28.72 ^{o}C
Average Relative Humidity	84.48 %
Average Observed Sunshine Hours	4.7
Wind Velocity at 2 m height	141.6 km/day

The nature of the surface cover of the study region was considered as a water surface.

The input file of evapotranspiration data was set to a constant rate of evapotranspiration in which the rate of 5.33 mm/day corresponding to 0.222 mm/h.

The RRI control file was edited by changing the flag to 1, specifying the input evapotranspiration file, and defining the coordinates and cell sizes the same as the input rainfall data.

3.6.2 River Channel Geometry

The geometry of the river channel was assumed to be rectangular whose shape was defined using empirical equations (3.1) and (3.2) for river width and depth, respectively based on the Google Earth and DEM.

$$\text{River Width (m)} = 7A^{0.35} \tag{3.1}$$

$$\text{River Depth (m)} = 1.5\ A^{0.2} \tag{3.2}$$

where A is an upstream contributing area in km^2 (Sayama, 2017).

3.6.3 Land Class Settings

Manning's roughness of the river was taken as 0.06 for the natural major stream with irregular and rough sections (Chow, 1959).

According to Figure 3.20, almost all the area covers with homesteads. Therefore, parameters such as Manning's roughness of the slope, soil depth, and effective porosity were specified corresponding to one land-use. Manning's roughness of the slope cell was taken as 0.3 based on Manning's roughness estimating equation (Chow, 1959) for the earth, severe irregularities, alternating frequently cross-section, severe obstructions effects, low vegetation, and severe meandering. The study region mainly contains red-yellow podzolic soil associated with laterite soil (*Strategic Environmental Assessment*, 2018). The effective porosity and depth of the soil were taken as 0.453 (Sayama, 2017) and 175 cm (70-100 inch) (Moormann & Panabokke, 1961).

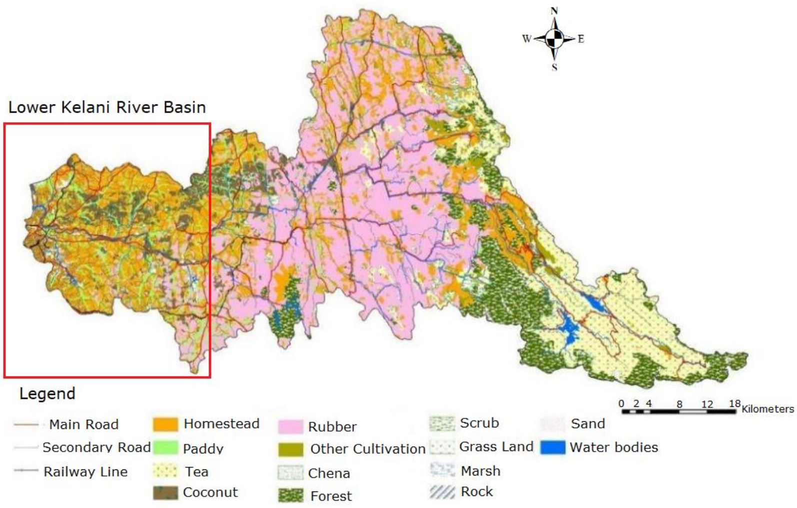

Figure 3.20: Land use variation in the Kelani river basin (*Natural Resource Profile of the Kelani River Basin*, 2016)

Since the watershed have been saturated before the torrential rainfall event on 15th May 2016 (Rogers et al., 2016), saturated subsurface and saturation excess overland flow conditions were considered. Therefore, k_v, unsaturated porosity, and lateral saturated hydraulic conductivity (k_a) were set to be zero, zero, and 7.2 x 10^{-6} ms^{-1}, respectively for sandy loam texture (Allen et al., 2010).

3.6.4 Boundary Conditions

The river discharge boundary conditions were defined for Hanwella station based on the observed water depths during Flood in 2016 from 15th May 2016 to 23rd May 2016 as shown in Figure 3.21.

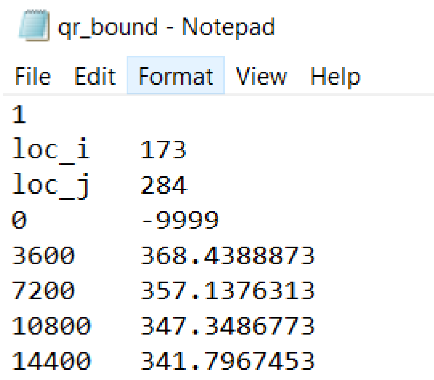
qr_bound - Notepad

File Edit Format View Help

```
1
loc_i    173
loc_j    284
0        -9999
3600     368.4388873
7200     357.1376313
10800    347.3486773
14400    341.7967453
```

Figure 3.21: Discharge boundary conditions input files

Then, the RRI Input file was edited to read the discharge boundary conditions input file by specifying input boundary files and setting flag 1.

3.7 Calibrate and Validate the RRI model

The RRI model parameters were calibrated for the 2016 flood event from 15th May 2016 to 23rd May 2016. Validation of the model was conducted for the 2017 flood event from 26th May 2017 to 1st June 2017 and the 2018 flood event from 21st May 2018 to 29th May 2018.

3.8 Visualize Output Data of the Model

The flood inundation depth distribution was illustrated using the GNUPLOT script named hs. plt as shown in Figure 3.22.

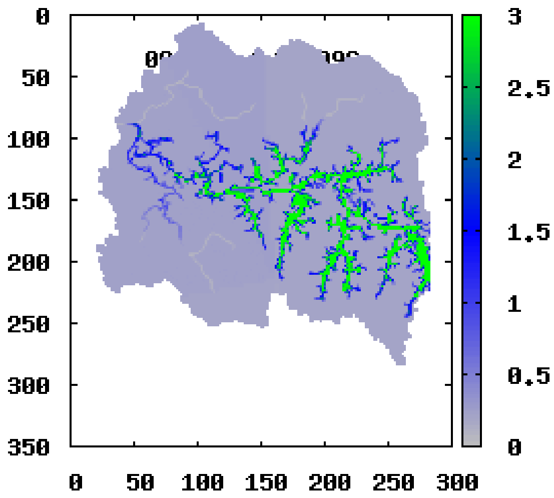

Figure 3.22: Flood inundation depth (m) on 15th May 2016 at 3.00 p.m.

Hydrographs at Hanwella (6.911º N, 80.076º E) station and Nagalagam Street (6.96º N, 79.882º E) were created as shown in Figure 3.23, and Figure 3.24, respectively using the calcHydro program for creating hydrographs at specific locations.

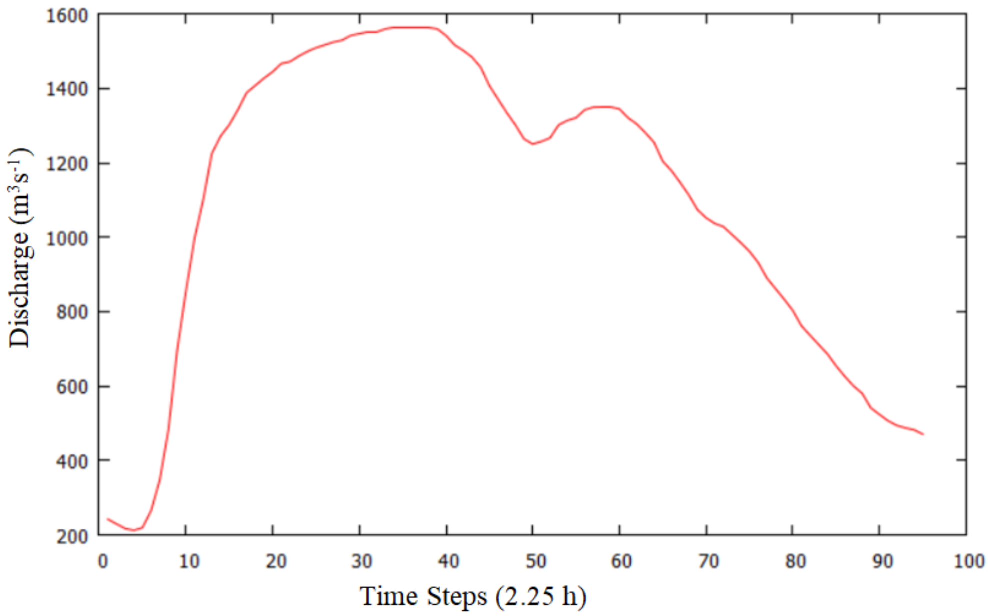

Figure 3.23: Hydrograph at Hanwella station

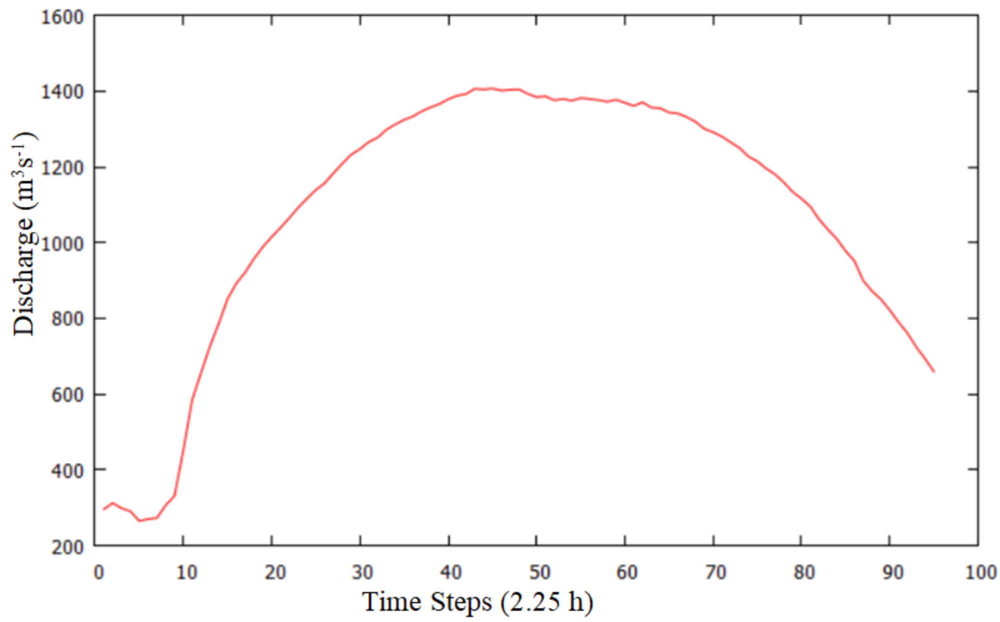

Figure 3.24: Hydrograph at Nagalagam Steet station

Water level variation during the simulation period at Nagalagam Street is shown in Figure 3.25.

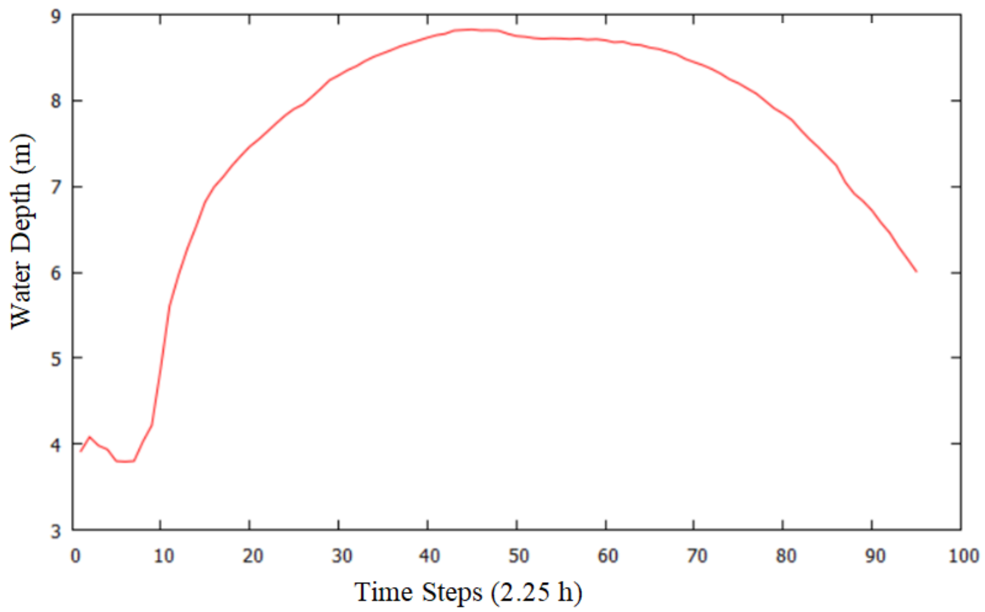

Figure 3.25: Water Depth at Nagalagam Street Station

The peak inundation depth was computed by executing the calcPeak.exe program and delineated using ArcGIS (ESRI/ USA) hydro tools as shown in Figure 3.26.

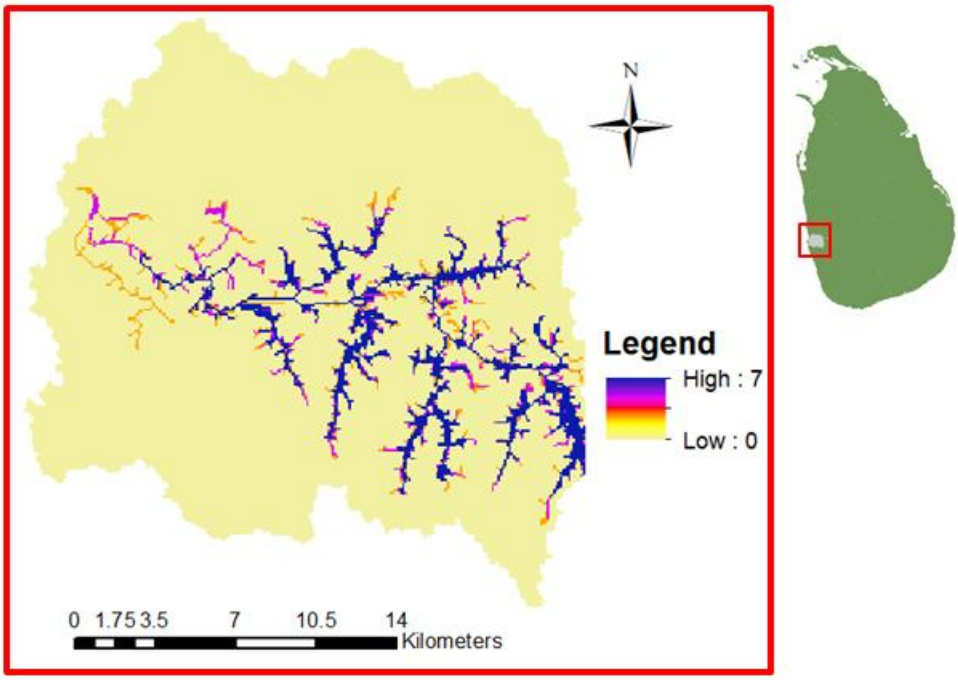

Figure 3.26: Peak inundation depths (m)

The runoff.kml file was created by executing the makeKml program. The gif files of inundation depths were created under the hs_kml folder using hs_kml.plt GNUPLOT file. The figures of inundation depths were animated with Google Earth as shown in Figure 3.27.

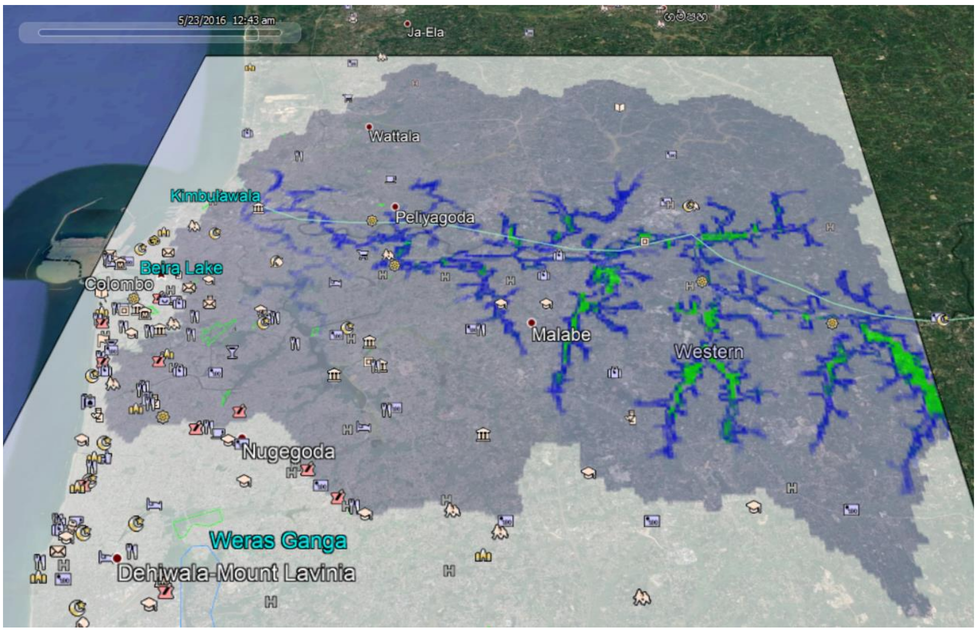

Figure 3.27: Visualize inundation depths

3.9 Evaluation of the performance of each RRI model

The performance of each RRI model was evaluated using Coefficient of Correlation (r^2), Root Mean Square Error (RMSE), Mean Error (ME) (Pakoksung, 2016), and Fit index (FIT) (Sayama et al., 2012) given by equations (3.3), (3.4), (3.5), and (3.6), respectively.

$$r^2 = \frac{\sum_{i=1}^{n}(O_i - \bar{O}).(S_i - \bar{S})}{\sqrt{\sum_{i=1}^{n}(O_i - \bar{O})^2}.\sqrt{\sum_{i=1}^{n}(S_i - \bar{S})^2}} \quad (3.3)$$

$$RMSE = \sqrt{\frac{\sum_{i=1}^{n}(O_i - S_i)^2}{n}} \quad (3.4)$$

$$ME = \frac{\sum_{i=1}^{n}(S_i - O_i)}{n} \quad (3.5)$$

$$FIT = \frac{I_{obs} \cap I_{sim}}{I_{obs} \cup I_{sim}} \quad (3.6)$$

where O_i is observed i^{th} water depth, $\bar{O}$ is mean observed water depth, S_i is simulated i^{th} water depth, $\bar{S}$ is mean simulated water depth, n is the total number of samples, O_{peak} is peak observed water depth, S_{peak} is peak simulated water depth, I_{obs} is observed flood inundation extent, and I_{sim} is simulated flood inundation extent.

Based on the performance of the RRI model, DEM was selected to further study.

3.10 Impacts of land-use change on RRI model using SRTM DEM

3.10.1 Sensitivity Analysis

The variation of river discharge with the RRI model parameters such as Manning's roughness, porosity, and saturated hydraulic conductivity of soil was studied. The most suitable parameter values were decided for Manning's roughness, effective porosity, and saturated hydraulic conductivity of each land-use type based on the sensitivity analysis results and literature. The used parameter values were given in Table 3.4.

Table 3.4: Manning's roughness, effective porosity, and saturated hydraulic conductivity for each land-use type

Land-use type	Manning's roughness	Porosity	Saturated hydraulic conductivity (ms^{-1})
Woody savannas	0.1	0.629	4.525×10^{-5}
Savannas	0.1	0.629	4.525×10^{-5}
Cropland	0.035	0.390	8.360×10^{-6}
Urban/ Built-up	0.4	0.001	6.470×10^{-6}
Unclassified	0.4	0.001	6.470×10^{-6}
Grassland	0.035	0.390	1.730×10^{-5}
Forest	0.15	0.629	4.020×10^{-5}

Source: Manning's roughness (Dorn et al., 2014), and saturated hydraulic conductivity (Dioniio & Costa, 2019).

3.10.2 Preparation of RRI models for 10 and 50 year return period flood

The RRI model developed using SRTM 3-arc (90 m gridded) DEM model was improved for input land-use maps. For land-use data, the Moderate Resolution Imagine Spectrometer (MODIS) yearly global land cover data version 6 was used. The land cover data were reclassified as per International Geosphere-Biosphere Programme (IGBP) global classification scheme.

This study was carried out for 2001, 2006, 2011, 2016, and 2019 years under 10 and 50 year return period flood events. The rainfall data at Colombo, and Hanwella stations, and streamflow data at Hanwella station were used for the 2016 flood event. The rainfall data for 2001, 2006, 2011, and 2019 was determined based on the 2016 flood event rainfall data with a -15.03 mm year^{-1} decreasing trend at Hanwella, and the 9.73 mm year^{-1} increasing trend at Colombo station (Jayasekara et al., 2020). For both 10 and 50 year return period flood events, the same rainfall data was used since the total 8-day rainfall of 2016 (15-year return period), and 1989 (50-year return period) were similar (Hettiarachchi, 2020). The streamflow data of 2001, 2006, 2011, and 2019 years at Hanwella station was determined based on the 2016 flood event streamflow data with a -766 $m^3s^{-1}year^{-1}$ decreasing trend (Jayasekara et al., 2020). For the streamflow data for the 50-year return period flood event, the streamflow data of the 2016 flood event were multiplied by 1.7896 to equivalent to the 50-year return period streamflow of 2,267 m^3s^{-1} (Hettiarachchi, 2020). The streamflow data for 2001, 2006, 2011, and 2019 were defined as previous by considering the -766 $m^3s^{-1}year^{-1}$ decreasing trend at Hanwella station.

The evapotranspiration for the year 2016 was determined using mean temperature, relative humidity, wind speed, and sunshine hours at Colombo agro-meteorological station for the 2016 flood event. For 2001, 2006, 2011, and 2019, evapotranspiration was determined in consideration of -0.005 ºC $year^{-1}$ decreasing trend for the temperature at Colombo station (Jayasekara et al., 2020).

3.11 Improve models with satellite land-use data and soil moisture data

For this study, only the 2017 flood event was selected since the satellite-based soil moisture data are not available for 2016, and 2018 flood events. The RRI model developed for the flood event in 2017 was improved for input land-use data and defining cross-sections at Nagalagam Street and Hanwella stations as per Appendix A.1. and A.2. (Gamini B Dodanwela Associates (Pvt) Ltd, 2007). For only the 2017 flood event, SMAP/ Sentinel-1 Radiometer/ Radar 30-second Scene 3 km EASE-Grid soil moisture version 2 soil moisture data are available and is shown in Figure 3.28.

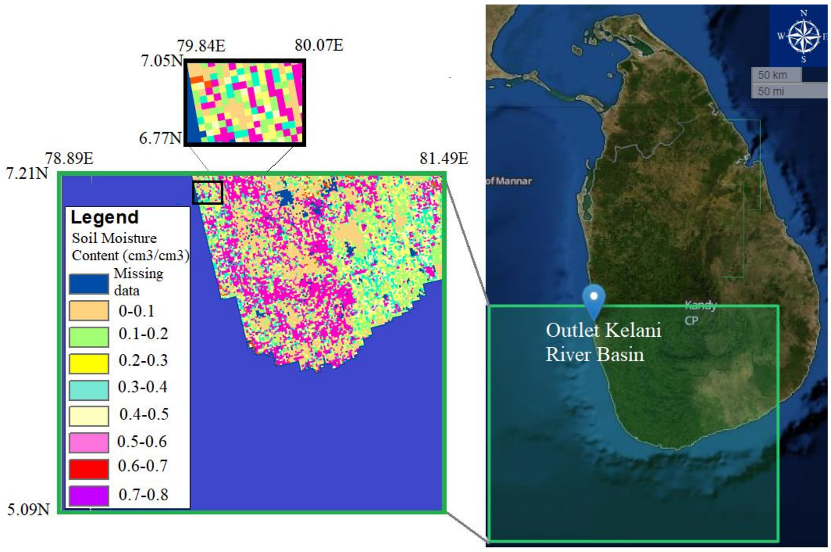

Figure 3.28: SMAP Soil Moisture Map on 25th September 2017

The soil moisture conditions of the 2017 flood event were determined by comparing the moisture content range in the SMAP soil moisture map and required minimum soil moisture content to saturate the soil in each land-use type. The soil moisture condition in the 2017 flood event is given in Table 3.5.

Table 3.5: Soil moisture condition in 2017 flood event

Land-use Type	Required minimum soil *MC* for saturation $(=\frac{1}{G}.\ e.S_r)$	25th September 2017	
		MC range	Soil condition
Woody Savannas	0.24	0.0 - 0.6	Unsaturated
Savannas	0.24	0.4 - 0.5	Saturated
Cropland	0.15	0.0 – 0.6	Unsaturated
Urban	0.0003	0.0 – 0.6	Saturated
Unclassified	0.0003	0.0 – 0.1	Saturated

where *MC* is Moisture Content, *G* is soil-specific gravity of 2.65, *e* is effective porosity and S_r is the degree of saturation.

3.12 Develop RRI model using AWS and satellite land-use data and soil moisture data

For this study, rainfall events during the periods from 12th September 2019 to 22nd September 2019 and 23rd September 2019 to 30th September 2019 were selected due to the recently introduced AWS in Sri Lanka. The rainfall data of 11 AWS were obtained. The locations of selected AWS are shown in Figure 3.29.

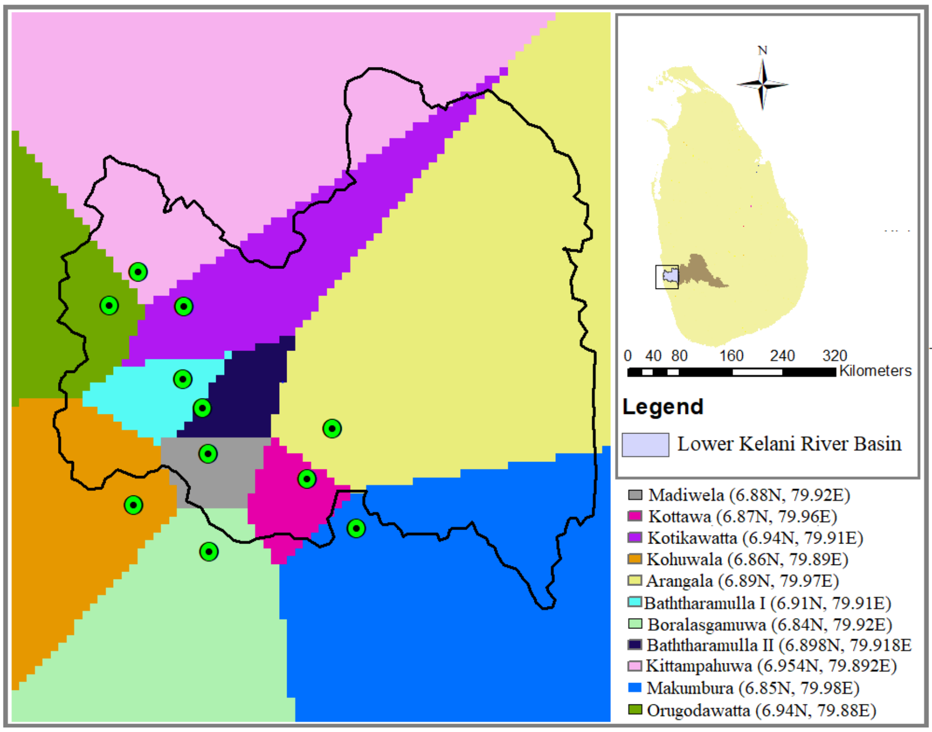

Figure 3.29: AWS locations

SRTM 3-arc DEM and MODIS yearly global land cover map for 2019 were used as described in section 3.10.2. The Soil condition of each period was determined using SMAP/ Sentinel-1 Radiometer/ Radar 30-second Scene 3 km EASE-Grid soil moisture version 2 data. The SMAP soil moisture map on 12th and 23rd September 2019 illustrates in Figure 3.30, and Figure 3.31, respectively.

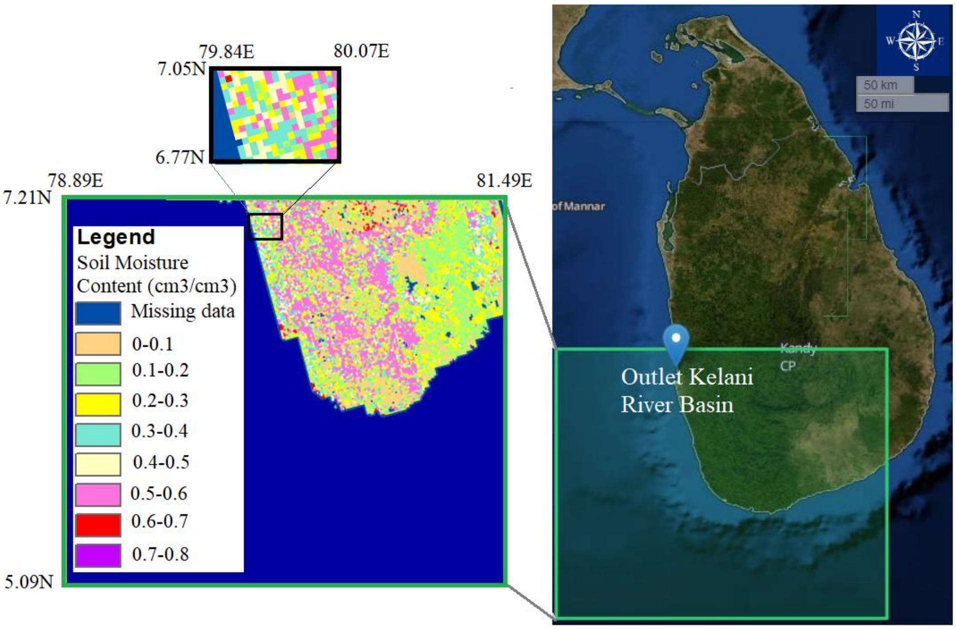

Figure 3.30: SMAP Soil Moisture Map on 12th September 2019

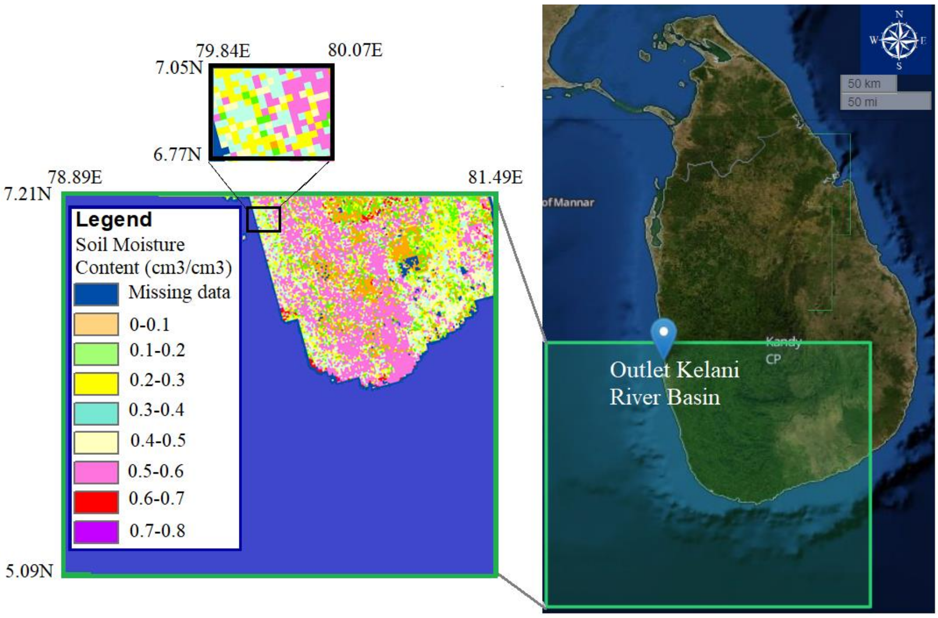

Figure 3.31: SMAP Soil Moisture on 23rd September 2019

The soil moisture condition of each land-use type is shown in Table 3.6.

Table 3.6: Soil moisture condition of each land-use type

Land-use Type	Required minimum soil *MC* for saturation ($= \frac{1}{G}. e.S_r$)	12th September 2019		23rd September 2019	
		MC range	Soil condition	*MC* range	Soil Condition
Woody Savannas	0.24	0.3 - 0.6	Saturated	0.5 – 0.6	Saturated
Savannas	0.24	0.3 - 0.6	Saturated	0.5 – 0.6	Saturated
Cropland	0.15	0.2 – 0.6	Saturated	0.2 – 0.6	Saturated
Urban	0.0003	0.1 – 0.6	Saturated	0.1 – 0.6	Saturated
Unclassified	0.0003	0.2 – 0.3	Saturated	0.3 – 0.4	Saturated
Forest	0.24	0.4 – 0.5	Saturated	0.4 – 0.5	Saturated

where *MC* is Moisture Content, *G* is soil-specific gravity of 2.65, *e* is effective porosity and S_r is the degree of saturation.

Before torrential rainfall events on 15th and 23rd September 2019, the catchment was completely saturated. Therefore, the soil condition of each land-use type was given as saturated condition, and parameters were defined for relevant to soil saturated conditions. The defines soil parameters such as Manning's roughness, porosity and saturated hydraulic conductivity of each land-use were similar to values given in Table 3.4.

Moreover, the cross-sections at Nagalagam street and Hanwella stations were defined with a section map. The details of cross-sections at the aforementioned locations are attached in Appendix A.1. and A.2. (Gamini B Dodanwela Associates (Pvt) Ltd, 2007). The other cross-sections of the river channel are assumed to be rectangles, and its width and depth were given by equations (3.1) and (3.2), respectively.

3.13 Evaluation of the adequacy of existing rain gauge/ AWS system

The required optimum number of rain gauges was determined as per IS 4987: 1994 specification (*IS 4987: 1994*, 1994).

$$\text{Optimum number of rain gauges } (N) = (C_v/\mathcal{E})^2 \tag{3.7}$$

where C_v is the coefficient of variation of the rainfall values of the existing rain gauge stations, and $\mathcal{E}$ is desired degree of percentage error in the estimate of basin mean rainfall.

$$C_v = 100\,\frac{S}{\bar{P}} \tag{3.8}$$

where S is standard deviation, and $\bar{P}$ is mean rainfall in the catchment.

$$S = \frac{1}{(m-1)}\left(\sum_{i=1}^{m} P_i^2 - \frac{\left|\sum P_i\right|^2}{m}\right)^{0.5} \tag{3.9}$$

where m is the number of rain gauges in the catchment, and P_i is total rainfall at i^{th} rain gauge or AWS.

$$\bar{P} = \frac{1}{m}\sum_{i=1}^{m} P_i \tag{3.10}$$

The adequacy of the rain gauges/ AWS was decided based on the required optimum number of rain gauges, and performance indices of RRI models. The number of rain gauges was assumed to be sufficient in the Lower Kelani River Basin where has at least an optimum number of rain gauges and better RRI model performance.

4. RESULTS AND DISCUSSION

4.1 Impact of DEM

The impacts of various DEM products such as HydroSHEDS, SRTM, ASTER, and ALOS PALSAR with a 3-arc (90 m grid) resolution on the Rainfall-Runoff-Inundation hydrological model are evaluates in this section.

4.1.1 Comparison between different DEM Products

Figure 4.1 illustrates the elevation of HydroSHEDS, SRTM, ASTER, and ALOS PALSAR with 3-arc (90 m grid) resolution DEM products, and original DEM products of 1-arc (30 m grid) resolution ASTER, and 12.5 m grid resolution ALOS PALSAR DEM at randomly selected 10 points in the lower catchment and 30 points in the upper catchment of Kelani river basin.

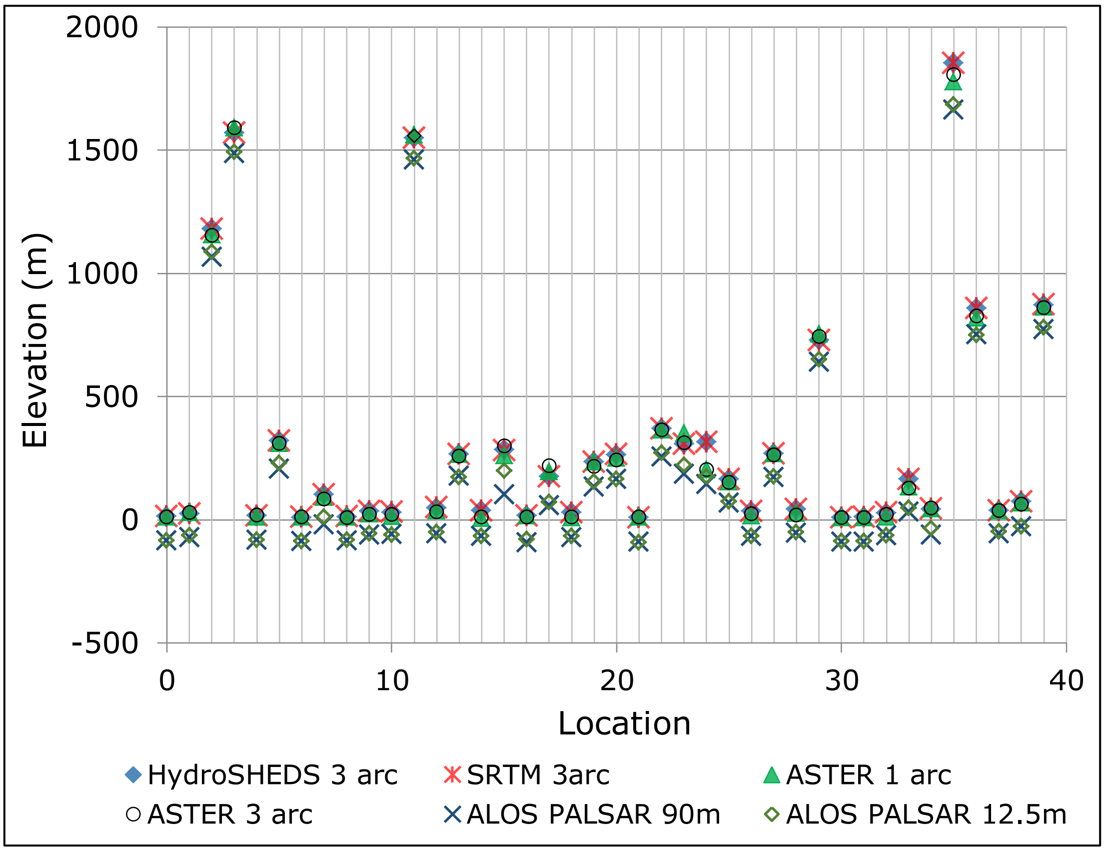

Figure 4.1: Comparison between different DEM products

The r^2, RMSE, and ME of elevation of each DEM product were estimated relative to 12.5 m gridded ALOS PALSAR DEM and are shown in Table 4.1.

Table 4.1: Statistical Coefficient of DEM products relative to 12.5 m gridded ALOS PALSAR DEM

DEM Product	**Resolution**	**Lower Kelani Basin**			**Upper Kelani Basin**		
		r^2	***RMSE***	***ME***	***r^2***	***RMSE***	***ME***
HydroSHEDS	3 arc (90m)	0.96	96.93	96.90	0.99	98.50	96.73
SRTM	3 arc (90m)	0.97	97.32	97.30	0.99	99.12	97.40
ASTER	1 arc (30m)	0.26	92.96	92.60	0.99	87.57	85.77
ASTER	3 arc (90m)	0.44	94.20	93.90	0.99	87.43	85.30
ALOS PALSAR	3 arc (90m)	0.88	4.94	-2.60	0.99	22.93	13.40

The elevation at the upper catchment is highly correlated with the 12.5 m gridded ALOS PALSAR DEM compared to elevations at the lower catchment since the upper catchment is mountainous and elevation differences are related to its elevation are noticeably low. The r^2 between SRTM (90 m gridded) and ALOS PALSAR (12.5 m gridded), and HydroSHEDS (90 m gridded) and ALOS PALSAR (12.5 m gridded) DEMs are higher compared to other DEM products as per Table 4.1. The values of ME and RMSE except for up-scaled ALOS PALSAR DEM are in the range of 85 m and 100 m. It may due to differences in the datum of the ALOS PALSAR DEM products from other DEM products. Moreover, there’s a significant effect when upscaling the DEM products, and the effect of upscaling DEM would be higher where the basin is in flat topography.

The elevation differences at the randomly selected points along the main Kelani river channel related to elevation at Hanwella station are shown in Figure 4.2. The elevation was estimated at the same point set for all studied DEM and when selected points are outside of the main river, the most nearby point on the main river was selected.

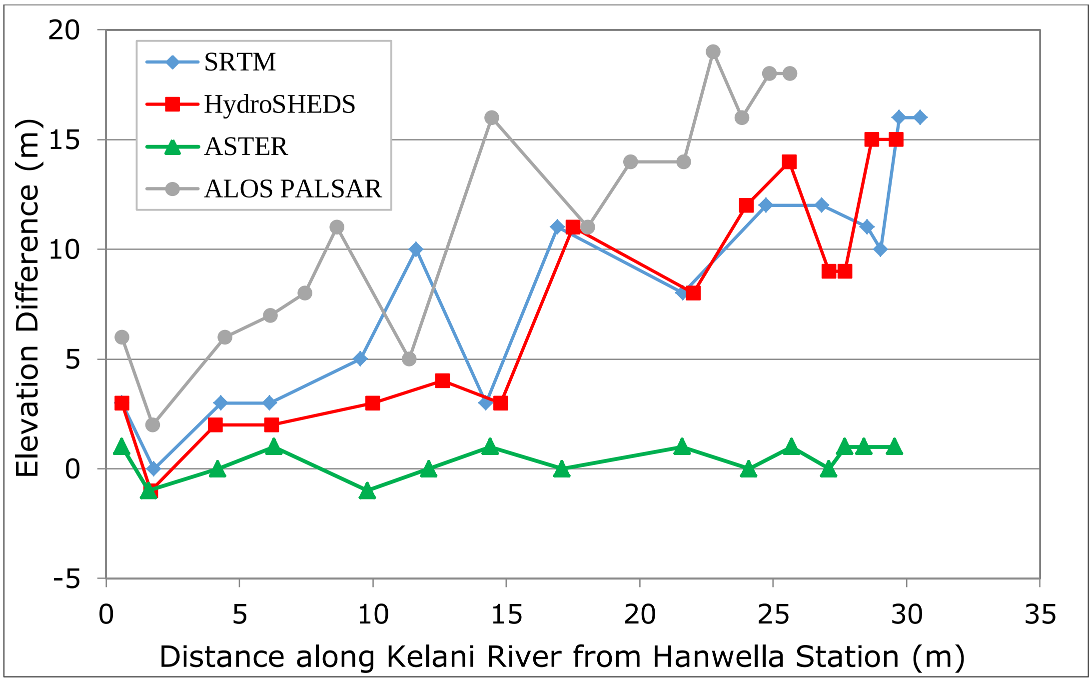

Figure 4.2: Elevation Difference along the Kelani river basin related to Hanwella Station

According to Figure 4.2, the elevation variation pattern of the HydroSHEDS, SRTM, and ALOS PALSAR are almost the same while the ASTER DEM shows a very low elevation variation along the main channel and contrasts to other DEM. The datasets of HydroSHEDS and ALOS PALSAR are highly correlated with the SRTM DEM about 0.95 and 0.94, respectively.

4.1.2 Delineation of Watershed from different DEM products

Watersheds of different DEM products with 3-arc (90 m) grid resolution was demarcated using ArcGIS (ESRI/USA) hydro tools and are illustrated in Figure 4.3. The area of each demarcated watershed is given in Table 4.2.

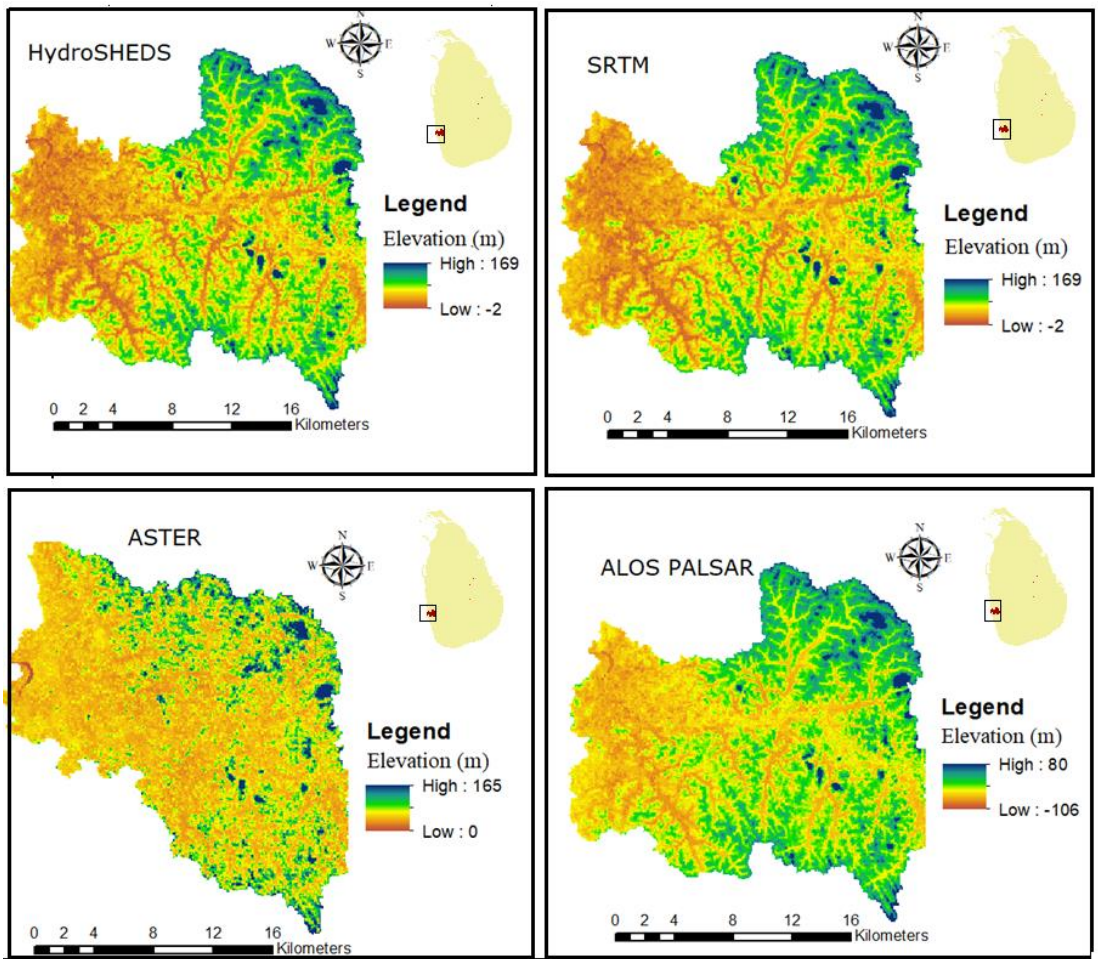

Figure 4.3: DEM of Lower Kelani River Basin

According to Figure 4.3, the shape of the watershed for the HydroSHEDS, SRTM, and ALOS PALSAR are almost the same, while the watershed delineating from ASTER DEM contracts from other watersheds. The elevation range of the watershed for HydroSHEDS, SRTM, and ASTER are identical.

Table 4.2: Area of the watershed for different DEM products

DEM Product	**HydroSHEDS**	**SRTM**	**ASTER**	**ALOS PALSAR**
Area (km^2)	381.3	374.9	362.7	380.7

However, the areas of watersheds for HydroSHEDS, SRTM, and ALOS PALSAR DEMs have slightly varied despite the shapes of watersheds are almost the same. The lowest area was obtained from the watershed demarcating from ASTER DEM.

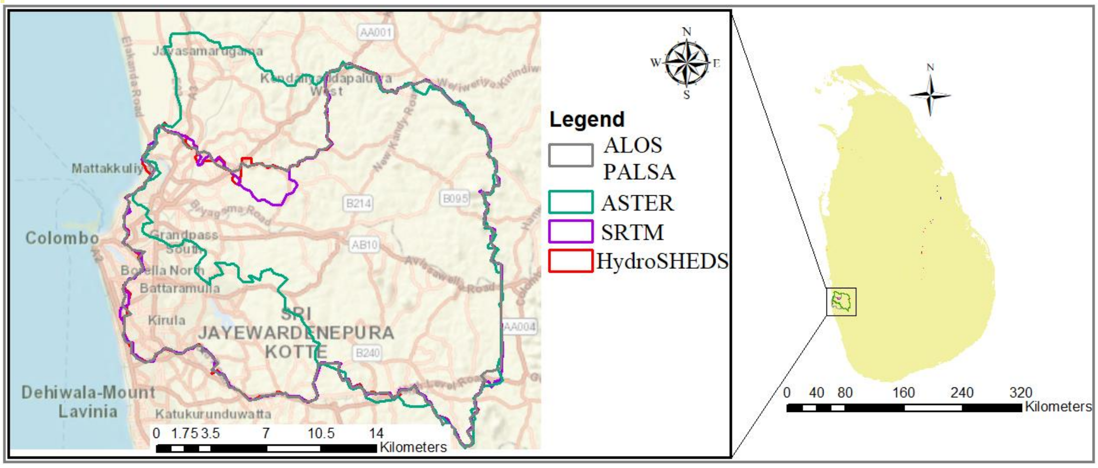

Figure 4.4: Lower Kelani River Basin boundaries of different DEM

According to Figure 4.4, the watershed boundaries delineated from HydroSHEDS, SRTM, and ALOS PALSAR DEMs are almost equal. The union of all demarcated watersheds is similar to the Kelani watershed attached in the manual of watersheds of Sri Lanka (*Watersheds of Sri Lanka*, 2011). The watershed from ASTER DEM has followed the upper part correctly, and the watersheds from HydroSHEDS, SRTM, and ALOS PALSAR DEMs have followed the lowest part of the watershed correctly.

4.1.3 Impacts of land-use variation on DEM

For evaluation of impacts of land-use change on DEM, 1-arc resolution ASTER GDEM version 2 and version 3, 3-arc resolution SRTM version 4.1 and 1-arc resolution SRTM version 3.0 released in the year 2011, 2019, 2008, and 2015, respectively were utilized. The MODIS yearly global land cover data were retrieved from the internet for the released year of each aforementioned DEM. The land-use and cover types were categorized in the manner of the IGBP Global vegetation classification scheme. The elevation deviation between ASTER version 2 and 3, and SRTM version 4.1 and 3.0 related to different land-use types, and land-use change with the time are illustrated in Figure 4.5, and Figure 4.6, respectively.

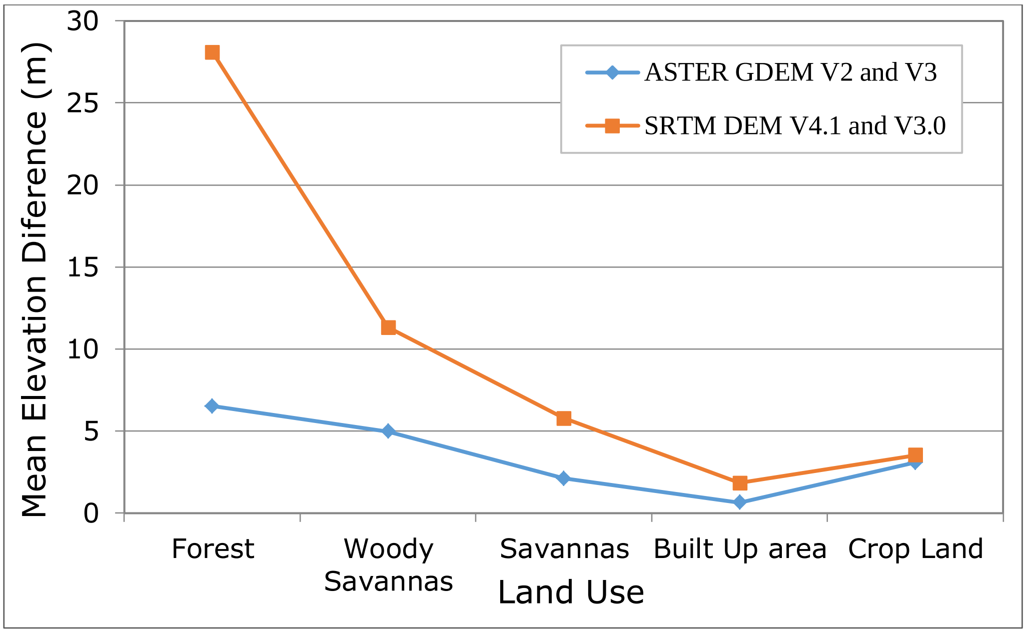

Figure 4.5: Elevation difference in a different version of DEM related to land-use

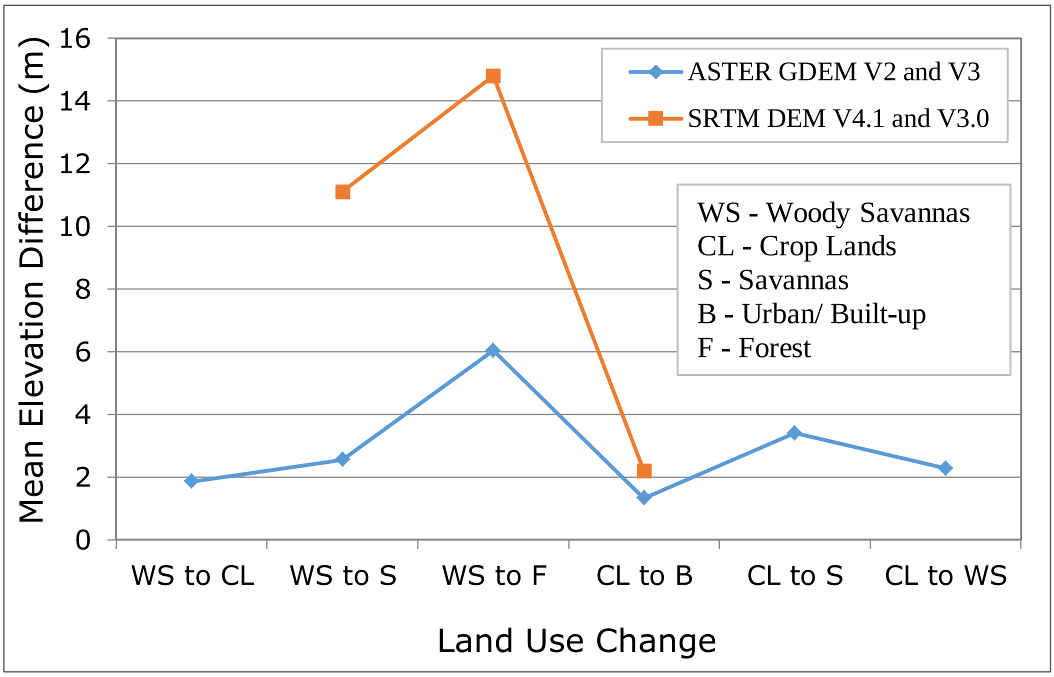

Figure 4.6: Elevation difference in different versions of DEM related to land-use change

The elevation variations for 7-8 years are higher in the region with forest while the lowest elevation variations are obtained in the urban/ built-up regions. When considering the land-use change with time, the elevations are highly varied in regions where the land-use change from savannas to the forest while elevation variations are low when the land-use change from croplands to urban/ built-up areas. The elevation variations are higher in the SRTM DEM data sets since the resolutions of the selected two versions of SRTM DEM are different while the resolution of ASTER GDEM V2 and V3 are 1-arc (30 m gridded) DEMs.

4.1.4 Effect of DEM product on RRI simulation

The simulated discharge at Hanwella station and Nagalagam street for the period from 15th May 2016 to 23rd May 2016 are illustrated in Figure 4.7. For all RRI models, hydrographs at Hanwella stations are equal due to define it as a boundary condition based on the observed discharges during the simulated period at Hanwella station.

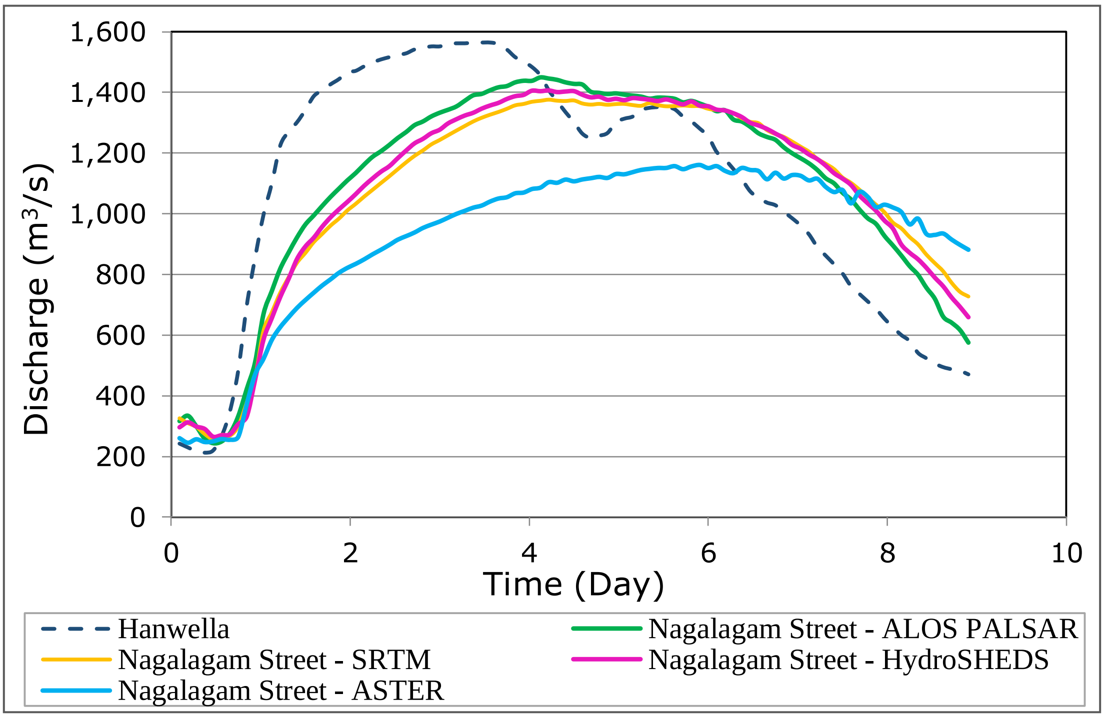

Figure 4.7: Simulated discharge at Hanwella and Nagalagam Street using different DEM

According to Figure 4.7, hydrograph at Nagalagam Street from RRI model using ASTER DEM contrasts to hydrographs from RRI model using HydroSHEDS, SRTM, and ALOS PALSAR. The lowest peak discharge was obtained from the RRI model using ASTER GDEM about 1160 m^3s^{-1} while the other models result in a peak discharge of nearly 1400 m^3s^{-1}. The simulated discharge at Nagalagam Street using HydroSHEDS, SRTM, and ALOS PALSAR DEM has represented a good agreement with the derivation of hydrograph at Nagalagam Street by Irrigation Department (Hettiarachchi, 2020).

The observed and simulated water depth at Nagalagam Street for the period from 15th May 2016 to 23rd May 2016 is illustrated in Figure 4.8.

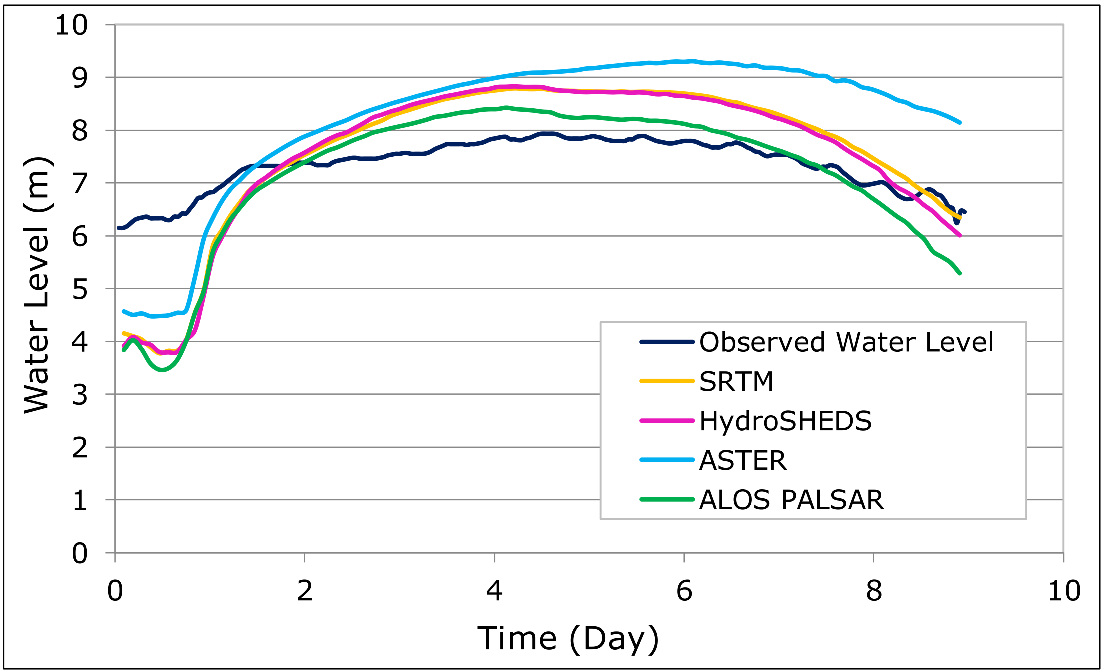

Figure 4.8: Simulated water level at Nagalagam Street using different DEM

According to Figure 4.8, all models overestimate the water depth at Nagalagam Street. The highest peak water level of 9.30 m was obtained from the RRI model using ASTER DEM while the lowest peak water level of 8.42 m was in the RRI model using ALOS PALSAR DEM. Both RRI models using HydroSHEDS and SRTM are shown almost the same variation in water depths during the simulation period.

The performance indices for the RRI model using HydroSHEDS, SRTM, ASTER, and ALOS PALSAR are given in Table 4.3.

Table 4.3: Performance Indices for RRI model using different DEM

Performance Index	HydroSHEDS	SRTM	ASTER	ALOS PALSAR
R^2	0.95	0.94	0.83	0.96
ME	0.27	0.30	0.90	-0.14
RMSE	1.00	1.00	1.35	0.90

According to performance indices, the RRI model using ASTER data performed weakly compared to other RRI models while the best performance was shown in the RRI model using ALOS PALSAR DEM with the highest R^2 of 0.96, lowest ME of -0.14 m, and lowest RMSE of 0.9 m.

The simulated inundation extent by each RRI model using HydroSHEDS, SRTM, ASTER, and ALOS PALSAR with the flood map for the 2016 flood by Survey Department is represented in Figure 4.9, Figure 4.10, Figure 4.11, and Figure 4.12, respectively.

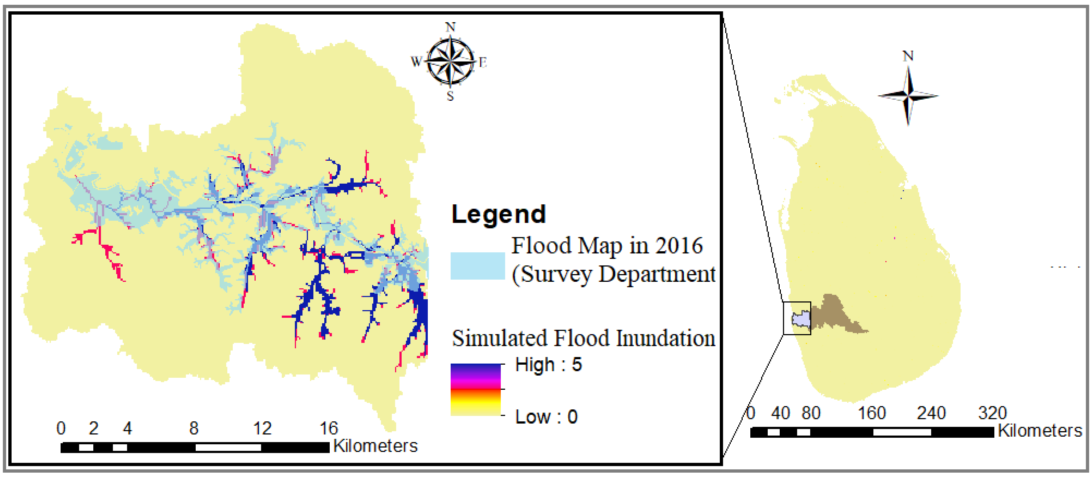

Figure 4.9: Flood Inundation from RRI model using HydroSHEDS DEM

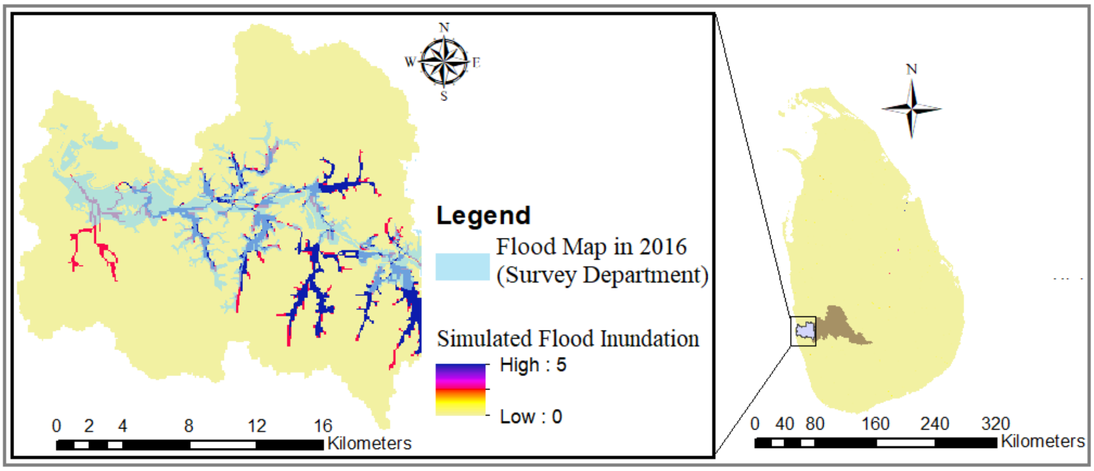

Figure 4.10: Flood Inundation from RRI model using SRTM DEM

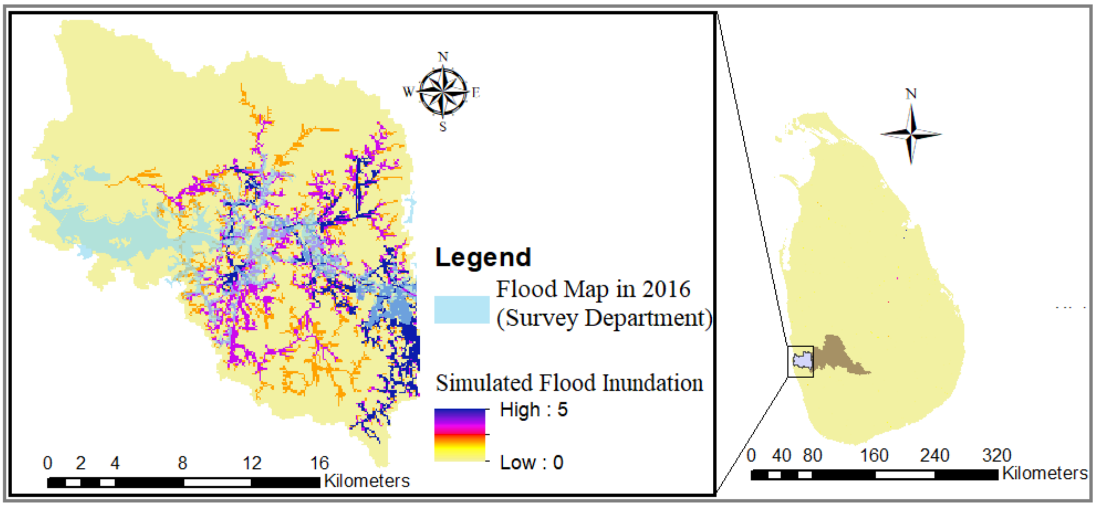

Figure 4.11: Flood Inundation from RRI model using ASTER DEM

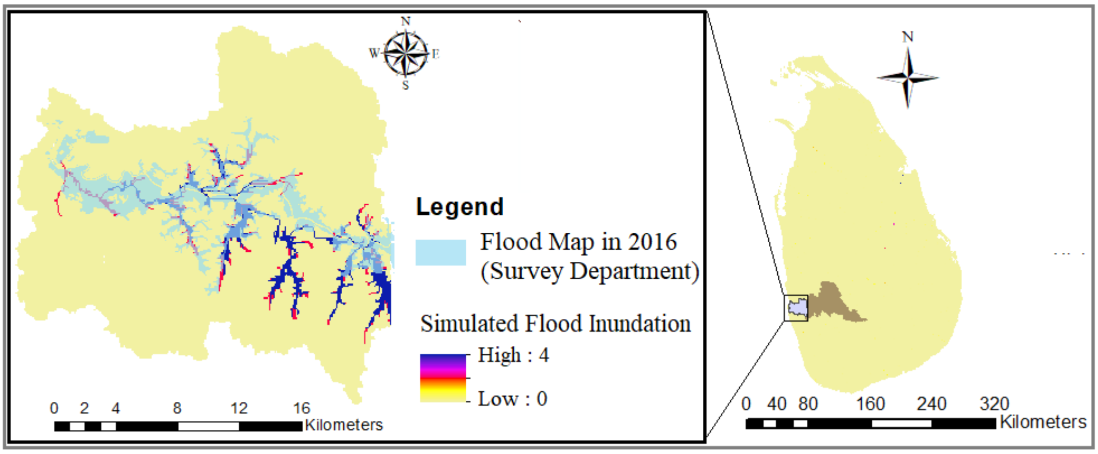

Figure 4.12: Flood Inundation from RRI model using ALOS PALSAR DEM

The FIT index for each RRI model is given in Table 4.4.

Table 4.4: FIT indices of RRI models using different DEM

DEM	**SRTM**	**ALOS PALSAR**	**HydroSHEDS**	**ASTER**
FIT index	0.60	0.55	0.43	0.23

According to Table 4.4, the RRI model using SRTM DEM has the highest fit index of about 0.6 and shows the best performance related to flood inundation simulation. The value of the FIT index is acceptable since it has identified the majority of the inundated area. The FIT indices of past researches on flood modelling with RRI models are similar to the FIT indices range of this study. For instance, the FIT index for the Pakistan flood in 2010 was about 0.61 (Sayama et al., 2012), and the FIT indices for the Thailand flood in 2010 were in the range of 0.18 and 0.47 (Sayama et al., 2017).

4.2 Validation of RRI model

The RRI model was validated for 2017 and 2018 flood events. Simulated hydrographs at Hanwella and Nagalagam Street and water depths at Nagalagam Street for the 2017 flood event are shown in Figure 4.13, and Figure 4.14.

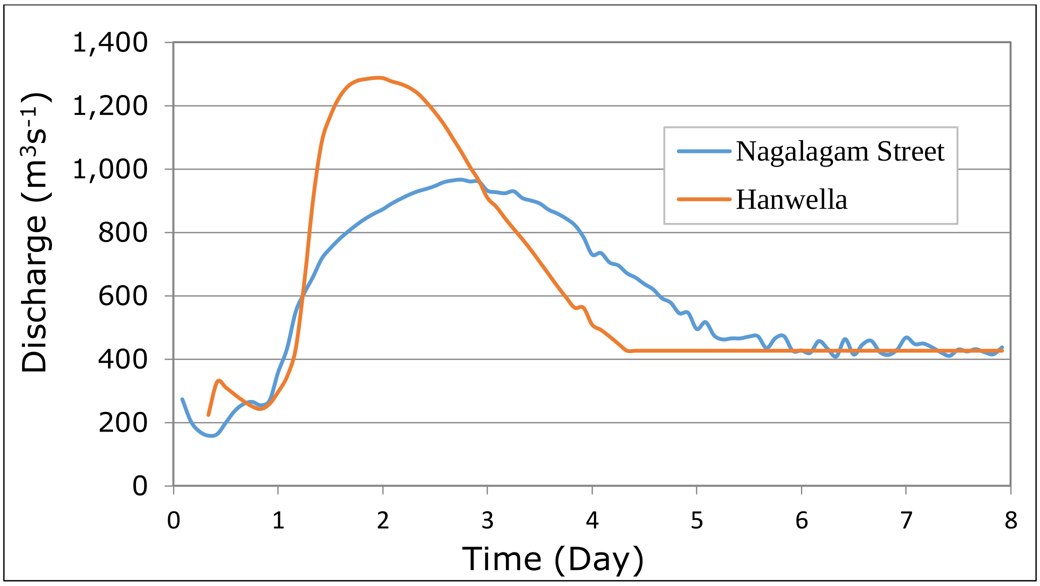

Figure 4.13: Simulated Hydrographs at Hanwella and Nagalagam Street for 2017 flood event

According to Figure 4.13, the peak discharge values at Hanwella and Nagalagam Street were 1,290 m^3s^{-1}, and 966 m^3s^{-1}, respectively.

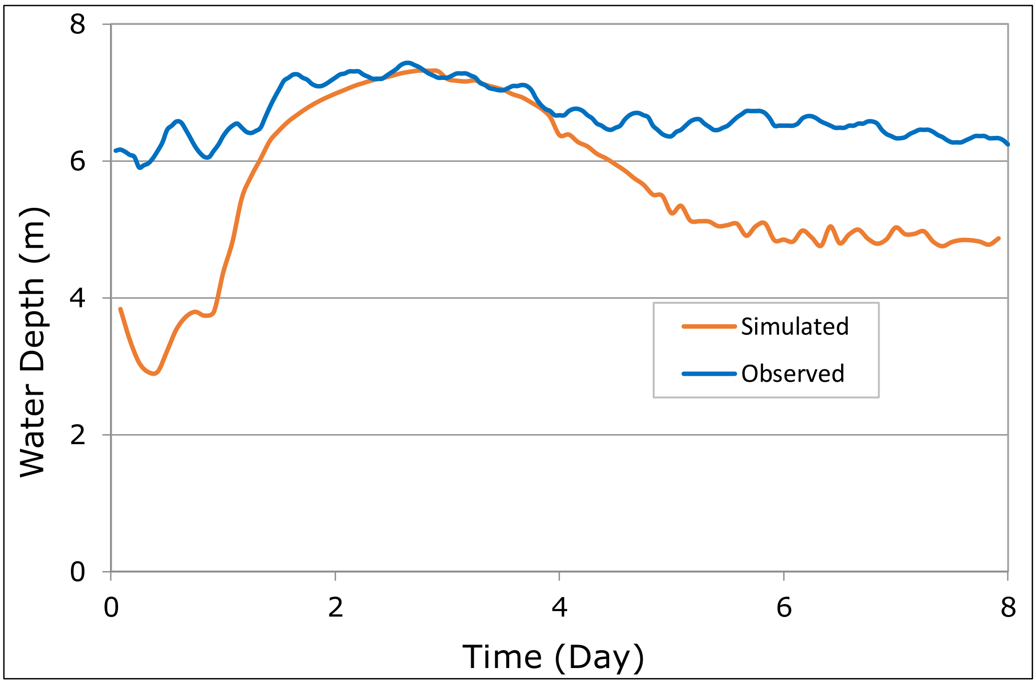

Figure 4.14: Water depth at Nagalagam Street for 2017 flood event

According to Figure 4.14, the simulated and observed peak water depth at Nagalagam Street deviates only 11 cm.

Simulated flood inundation for the 2017 flood event is illustrated in Figure 4.15.

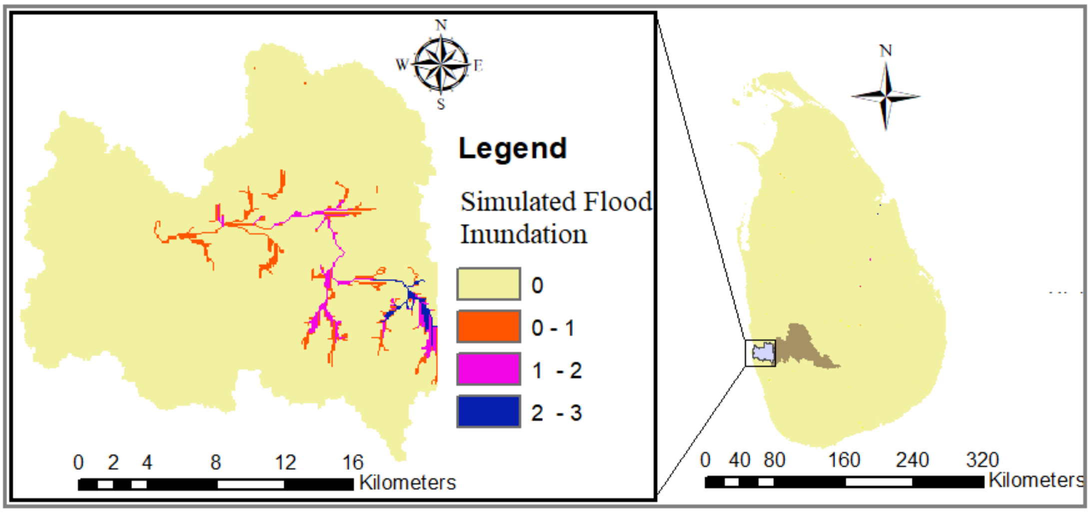

Figure 4.15: Flood Inundation for 2017 flood event

The simulated hydrographs at Hanwella and Nagalagam Street and water depth at Nagalagam Street for the 2018 flood event are shown in Figure 4.16, and Figure 4.17.

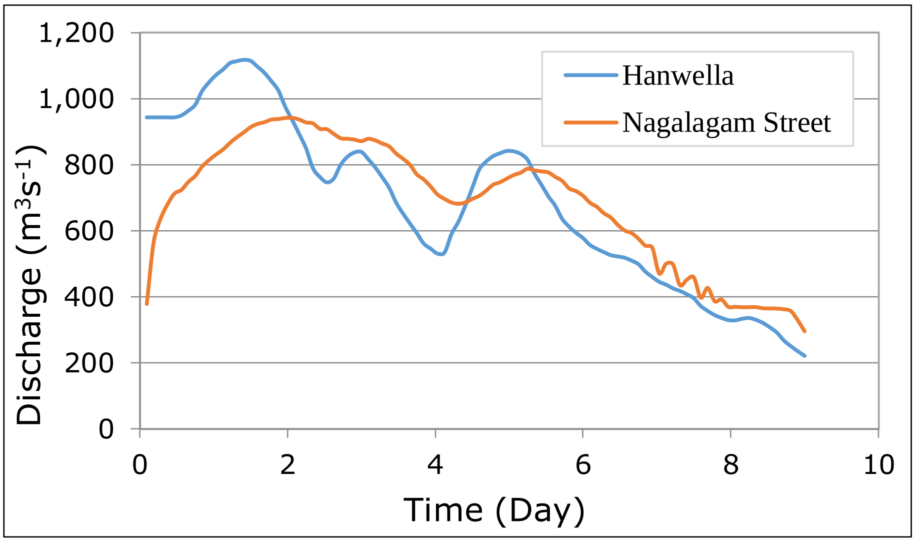

Figure 4.16: Simulated Hydrographs at Hanwella and Nagalagam Street for 2018 flood event

The peak discharge values at Hanwella and Naglagam Street for the 2018 flood event were 1,120 m^3s^{-1} and 942 m^3s^{-1}, respectively.

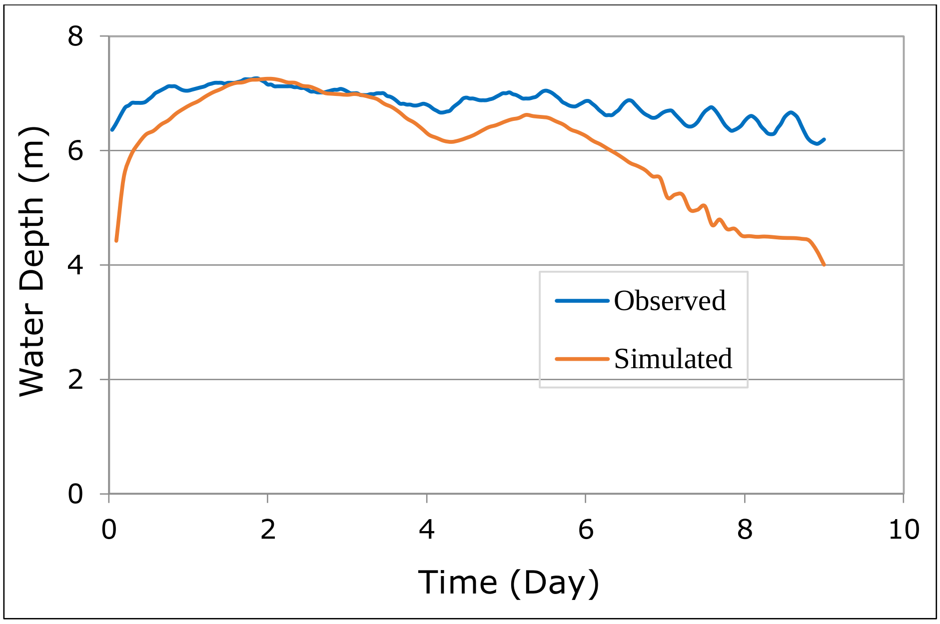

Figure 4.17: Water depth at Nagalagam Street for 2018 flood event

The difference between observed and simulated peak discharge at Nagalagam Street was only 1 cm.

The comparison between simulated flood inundation and flood map by Survey Department is shown in Figure 4.18.

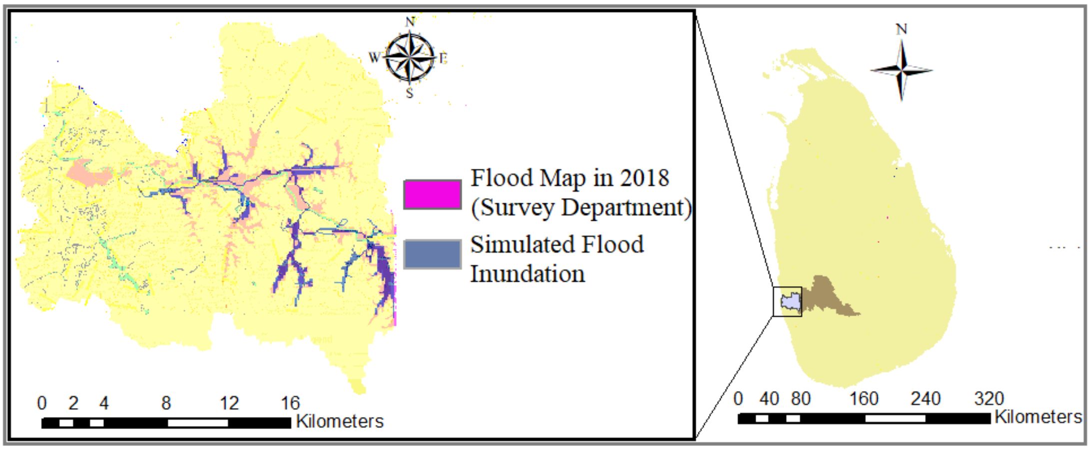

Figure 4.18: Flood Inundation for 2018 flood event

The flood inundation extents are underestimated by the RRI model. However, most of the flooded areas have been identified.

The performance indices of the RRI model for each simulated flood event are given in Table 4.5.

Table 4.5: Performance indices of RRI model for 2016, 2017, and 2018 flood event

Flood Event	**2016**	**2017**	**2018**
R^2	0.94	0.90	0.93
ME	0.3	-0.55	-0.73
RMSE	1.00	0.99	1.01
FIT index	0.6	-	0.4

The RRI model performed well for 2016, 2017, and 2018 flood events. The obtained all r^2 were above 0.9 for simulated water depth at Nagalagam Street. The model shows an approximately 1 m RMSE for water depth at Nagalagam Street for these selected flood events. The model has underestimated the water depths at Nagalagam Street for flood event 2017, and 2018, while the water depths for the 2016 flood event has been overestimated. The FIT indices for 2016 and 2018 are acceptable since most of the flood inundated areas have been identified and these values are in the range of FIT indices for previous RRI models (e.g. FIT index for 2010 Pakistan flood was around 0.61 (Sayama et al., 2012) and FIT indices range for 2011 Thailand flood was 0.18 to 0.47 (Sayama et al., 2017)).

4.3 Impact of land-use data

4.3.1 Sensitivity analysis

The river runoff variation with the Manning's roughness, effective porosity of the soil, and saturated hydraulic conductivity are graphically represented in Figure 4.19, Figure 4.20, and Figure 4.21.

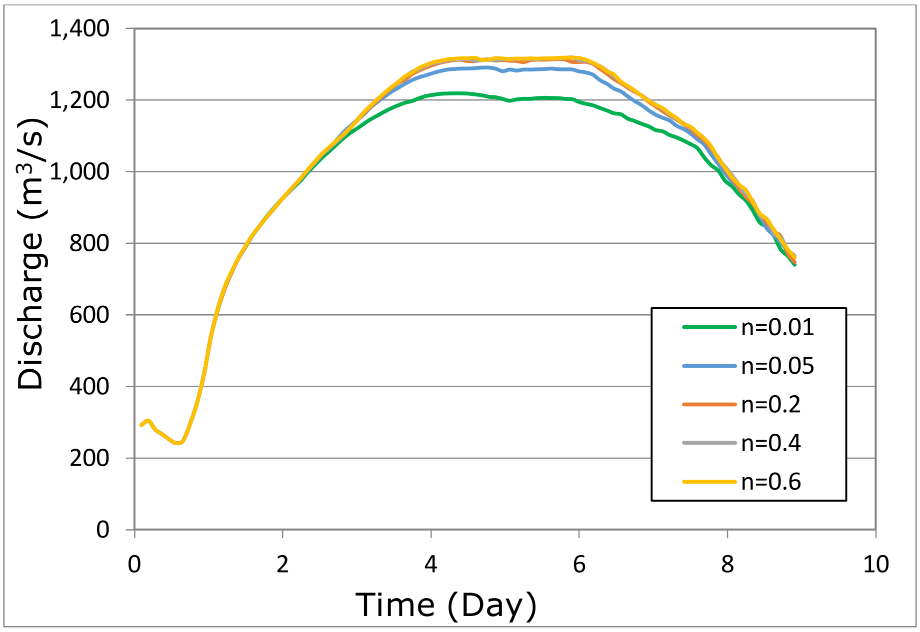

Figure 4.19: River runoff variation with Manning's roughness

According to Figure 4.20, the peak runoff was higher for higher Manning's roughness values.

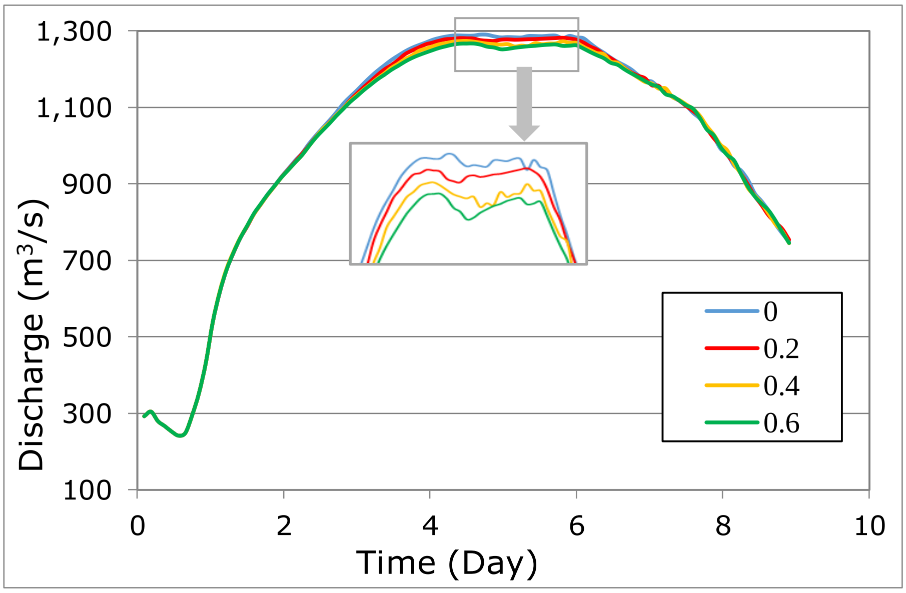

Figure 4.20: River runoff variation with effective porosity of the soil

According to Figure 4.20, the peak runoff was higher for lower soil effective porosity values.

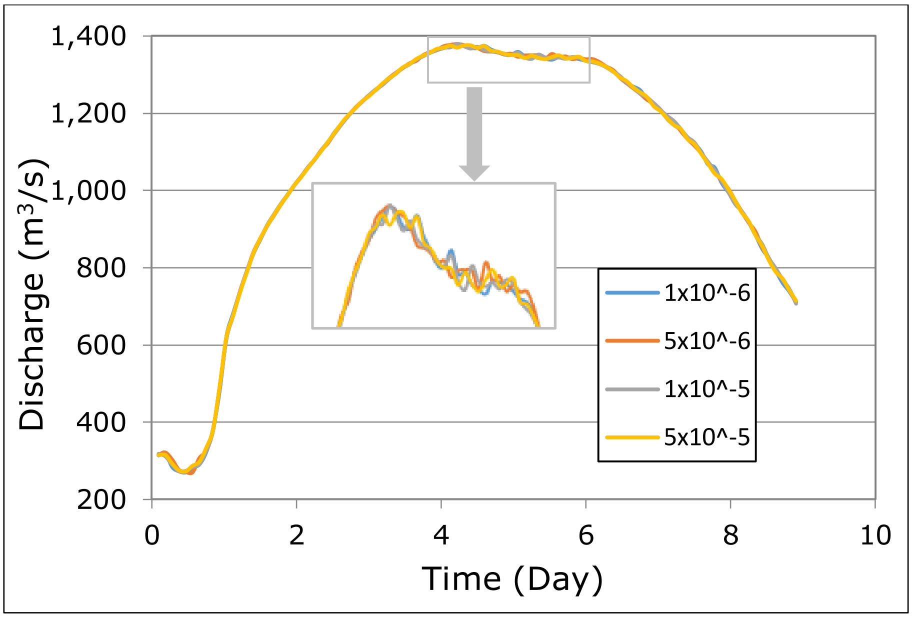

Figure 4.21: River runoff variation with saturated hydraulic conductivity

According to Figure 4.21, runoff variation was almost the same for the selected range of saturated hydraulic conductivity values.

4.3.2 Effect of land-use data on RRI Simulation

The MODIS land-use/ land cover maps of the study region for 2001, 2006, 2011, 2016, and 2019 years were given in Figure 4.22, Figure 4.23, Figure 4.24, Figure 4.25, and Figure 4.26, respectively.

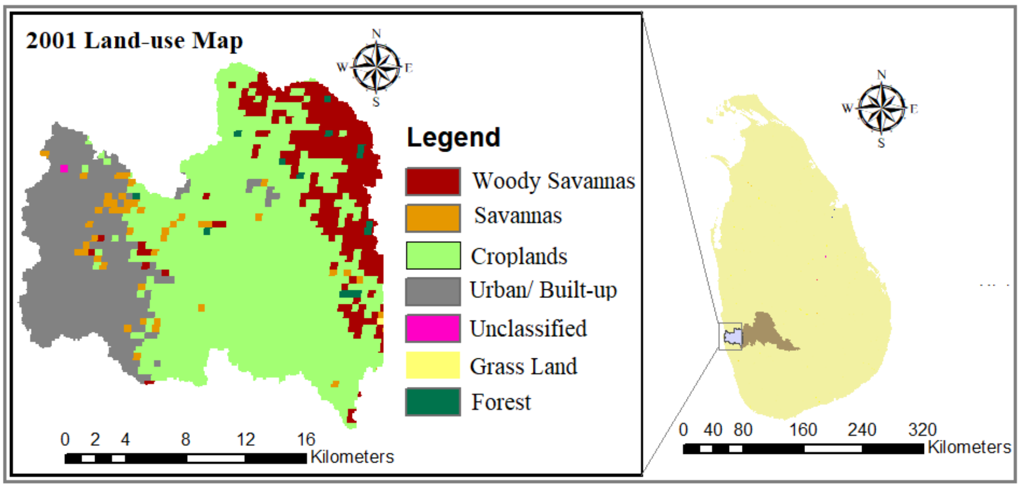

Figure 4.22: Land-use map for the year 2001

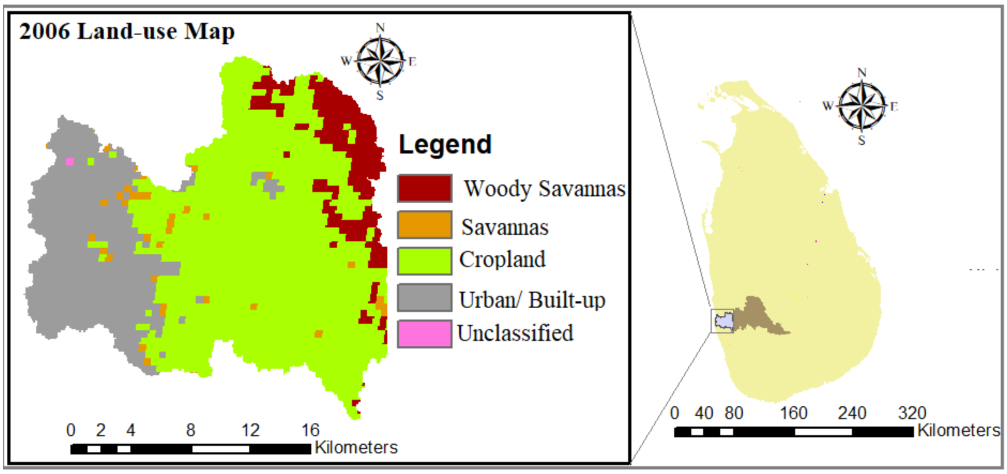

Figure 4.23: Land use map for the year 2006

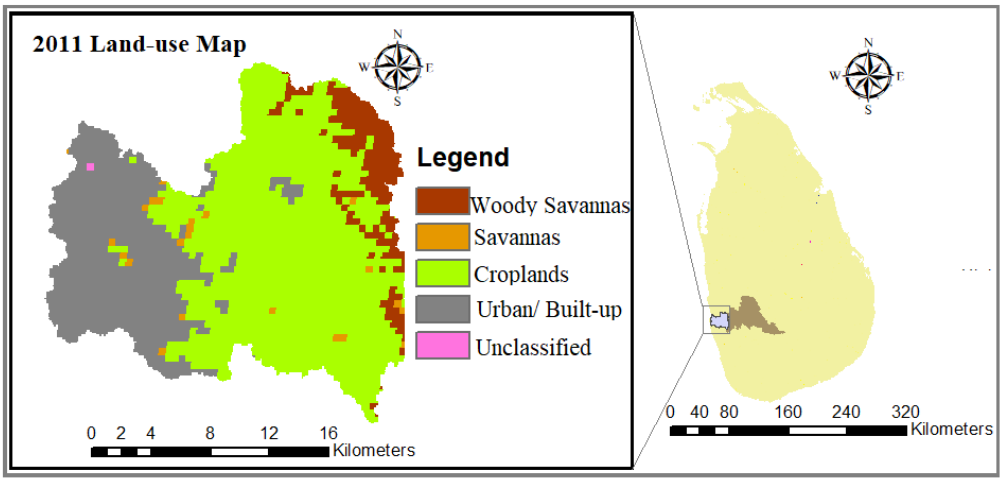

Figure 4.24: Land-use map for the year 2011

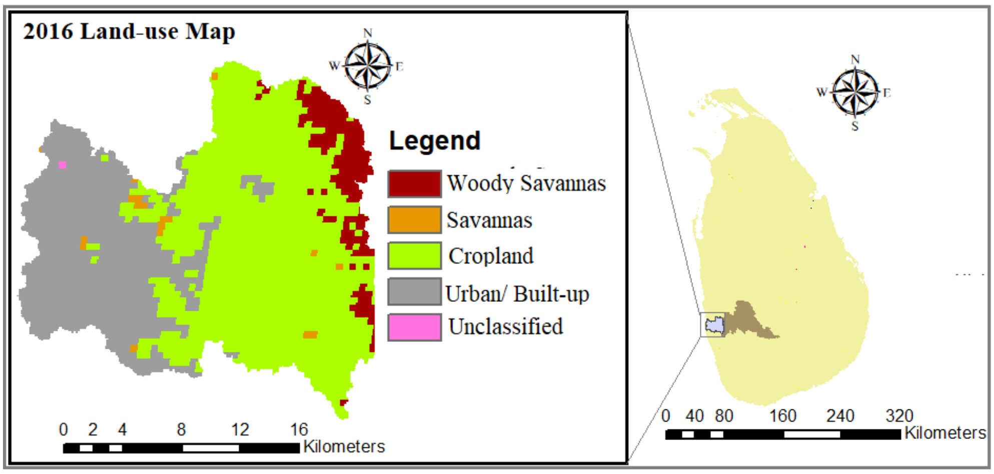

Figure 4.25: Land-use map for the year 2016

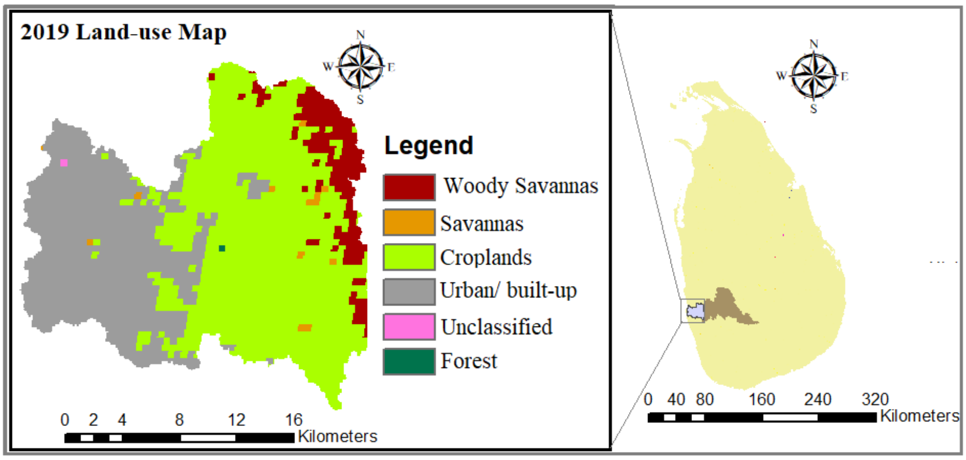

Figure 4.26: Land-use map for 2019

Woody Savannas, Croplands, and Urbal/ built-up areas can be identified as the main land-use types of the Lower Kelani River Basin. The total area of each land-use type for each year is given in Table 4.6.

Table 4.6: Total area of each land-use type for 2001, 2006, 2011, 2016, and 2019

Land-use type	**Total area of each land-use type (km^2)**				
	2001	***2006***	***2011***	***2016***	***2019***
Woody Savannas	51.49	34.67	31.61	27.75	28.94
Savannas	9.17	6.89	4.31	3.40	2.49
Croplands	206.11	221.88	213.85	207.17	196.13
Urban/ built-up	87.87	94.26	107.94	119.38	129.93
Unclassified	0.20	0.20	0.20	0.20	0.20
Grasslands	0.20	0.00	0.00	0.00	0.00
Forest	2.86	0.00	0.00	0.00	0.20

According to Table 4.6, urban/ built-up areas have increased by 12% of the total river basin extent, while all other land-use types have shown a decreasing trend for the selected period. The net area change in each land-use type for the period from 2001 to 2019 illustrates in Figure 4.27.

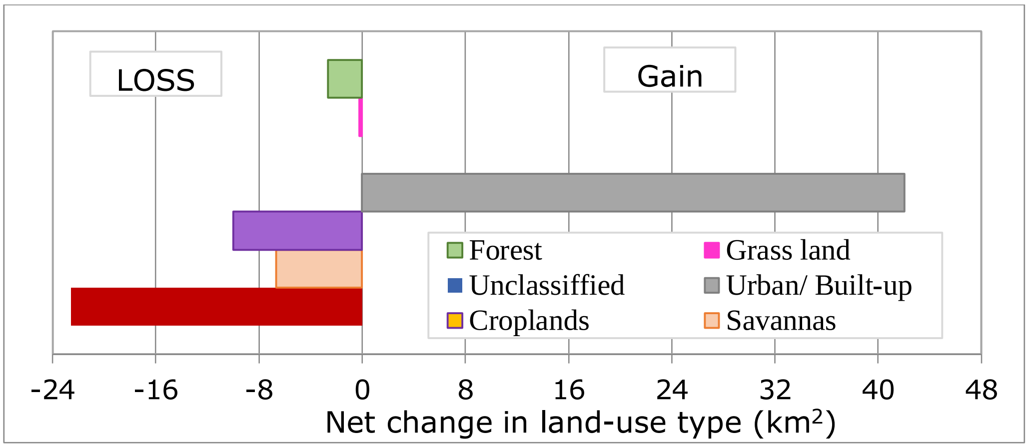

Figure 4.27: Net area change in each land-use type

The land extent has gained only in the urban/ built-up land-use type and it was the highest net area change about 42.1 km^2. The land extent has losses in other land-use types and the land extent of woody savannas shows the highest variation about -22.6 km^2.

The RRI model results for the 10-year return period flood illustrates in Figure 4.28, Figure 4.29, and Figure 4.30.

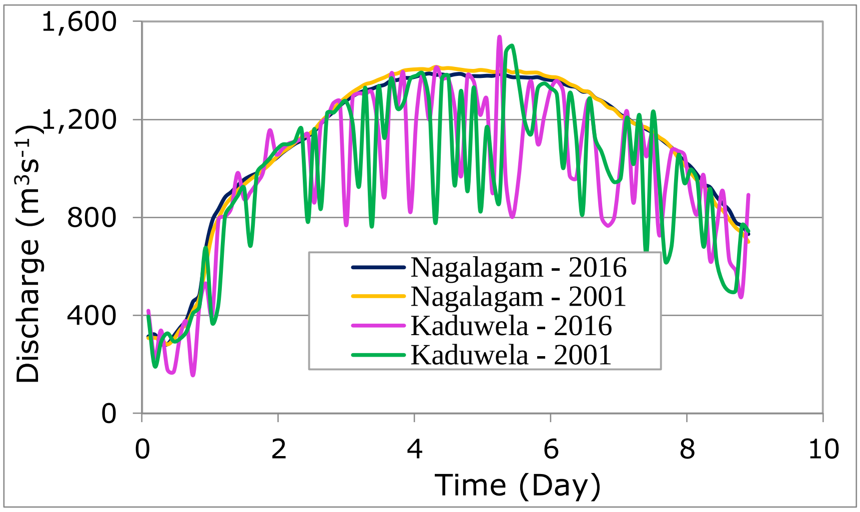

Figure 4.28: Simulated discharge for the 10-year flood

According to Figure 4.28, the peak runoff of the 2016 year at Nagalagam street was lower by 20 m^{3}s^{-1} while at Kaduwela was higher by 40 m^{3}s^{-1} than the year 2001.

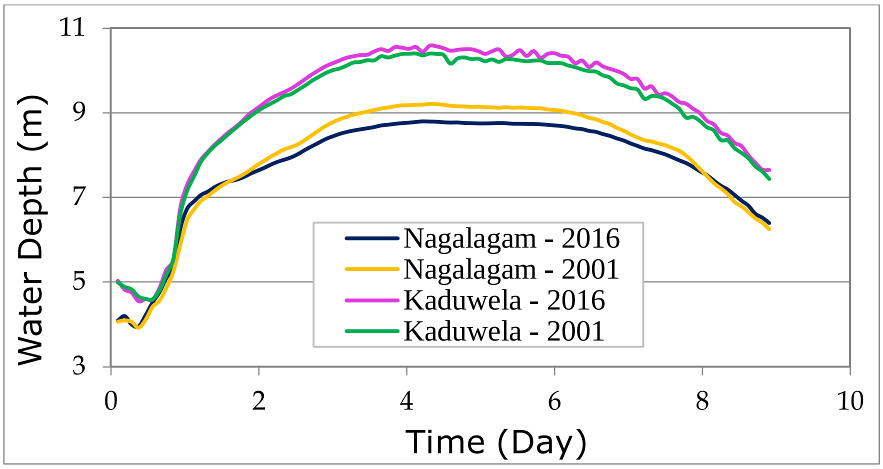

Figure 4.29: Simulated water depth for the 10-year flood

According to Figure 4.29, the peak water depth of the 2016 year at Nagalagam street was lower by 0.41 m while at Kaduwela was higher by 0.20 m than in the year 2001.

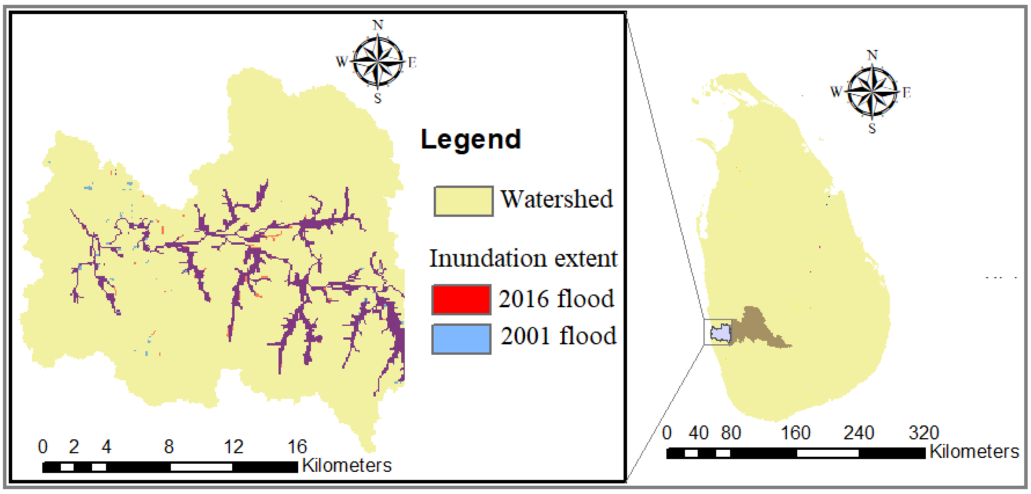

Figure 4.30: Flood inundation for the 10-year flood

According to Figure 4.30, flood inundation extent in the upper region of the catchment for the 2016 year was higher compared to 2001. The lower part of the catchment shows a lesser inundation extent in 2016 than in 2001.

The RRI model results for the 50-year return period flood illustrates in Figure 4.31, Figure 4.32, Figure 4.33, Figure 4.34, Table 4.7, and Figure 4.35.

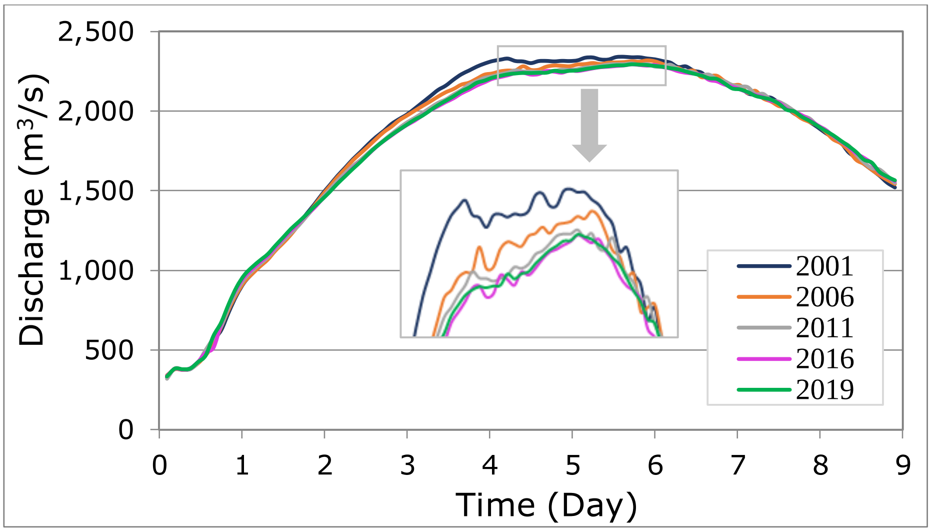

Figure 4.31: Simulated discharge at Nagalagam street for the 50-year flood

According to Figure 4.31, discharge at Nagalagam street was lower by 50 m^3s^{-1} in 2019 than in 2001.

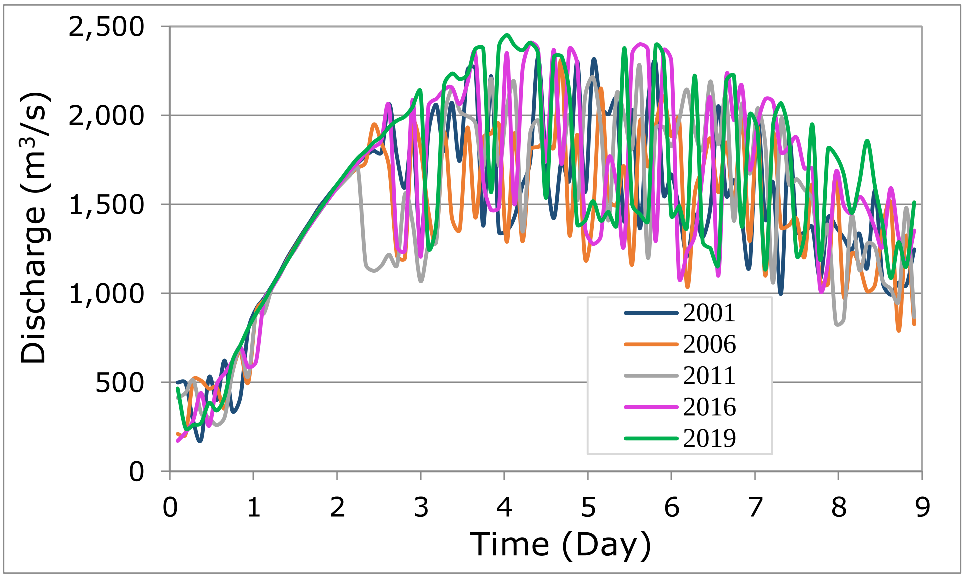

Figure 4.32: Simulate discharge at Kaduwela station for the 50-year flood

According to Figure 4.32, discharge at Kaduwela station was higher by 120 m^3s^{-1} in 2019 than in 2001.

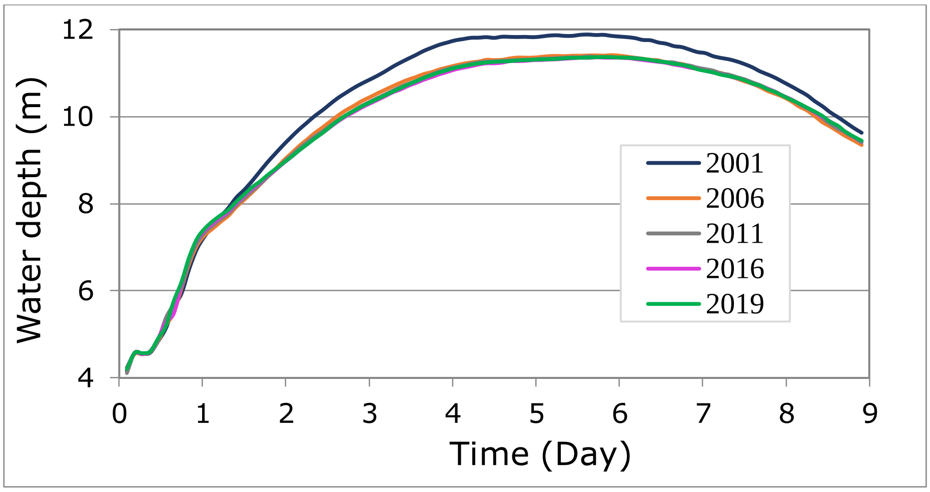

Figure 4.33: Simulated water depth at Nagalagam Street for the 50-year flood

According to Figure 4.33, the water depth at Nagalagam Street was lower by 0.51 m in 2019 compared to the 2001 year.

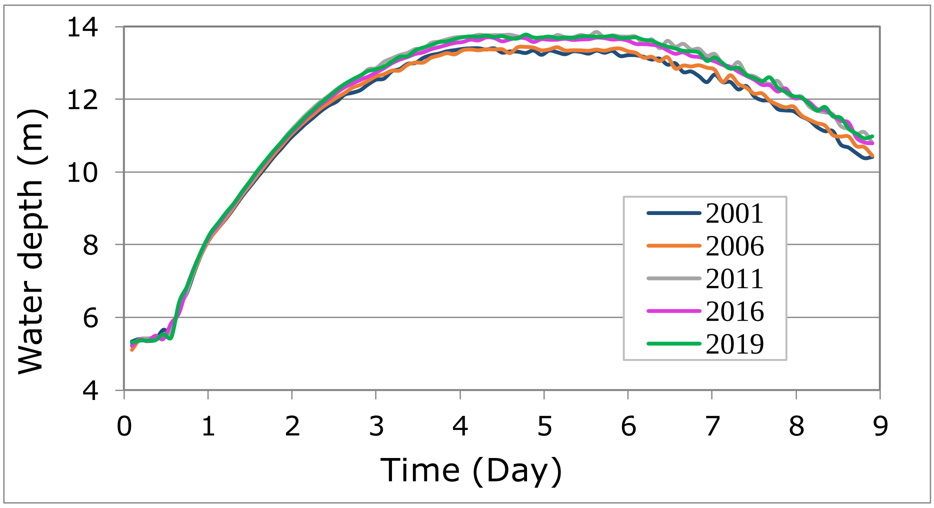

Figure 4.34: Simulated water depth at Kaduwela for the 50-year flood

According to Figure 4.34, the water depth at Kaduwela was higher by 0.37 m in 2019 compared to the year 2001.

The total area of the classified flood inundation for each year has given in Table 4.7.

Table 4.7: Total area of each classified inundation depth for the 50-year flood

Inundation depth (m)	**Total area of each classified inundation depth (km^2)**				
	2001	**2006**	**2011**	**2006**	**2019**
0	296.87	296.31	296.41	296.83	296.18
1	11.62	11.66	11.49	11.40	11.28
2	11.05	10.77	10.73	11.09	10.80
3	11.01	11.54	10.91	10.48	10.77
4	7.91	7.82	7.40	7.23	7.44
5	8.24	7.88	7.48	7.61	7.33
6	9.72	9.34	8.47	7.95	7.78
7	1.49	2.56	4.92	5.31	6.20
8	0.00	0.02	0.09	0.00	0.11

According to Table 4.7, the flood inundation extent was greater by 0.69 km^2 in 2019 than in 2016. Moreover, flood depths in 2019 have increased compared to previous years.

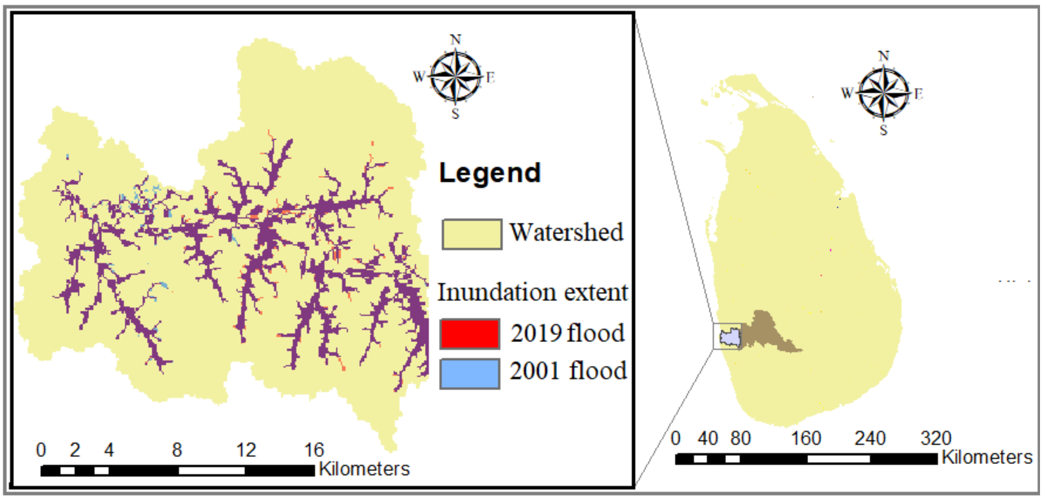

Figure 4.35: Flood inundation for the 50-year flood

According to Figure 4.35, flood inundation extent in the upper region of the catchment for the year 2019 was greater than in 2001. However, in the lower part of the catchment flood inundation has decreased in comparison to the year 2001.

Table 4.8 shows estimated aggregate values of Manning's roughness, effective porosity, and saturated hydraulic conductivity based on the land-use area fraction of each year.

Table 4.8: Aggregate Manning's roughness, effective porosity, and saturated hydraulic conductivity for each year

Aggregate Value	**Year**				
	2001	***2006***	***2011***	***2016***	***2019***
Manning's roughness	0.137	0.139	0.152	0.162	0.173
Effective porosity	0.337	0.315	0.296	0.281	0.269
Saturated hydraulic conductivity $\times 10^{-5}$ (ms^{-1})	1.441	1.214	1.149	1.094	1.093

The higher Manning's roughness and lower effective porosity in 2019 cause higher flood inundation than previous years.

4.4 Improved RRI Models using satellite-based data for 2017 flood events

The comparison between discharge, water depth, and flood inundation from typical RRI model and improved RRI model using MODIS yearly global land cover data and SMAP/ Sentinel-1 soil moisture data for the 2017 flood event are shown in Figure 4.36, Figure 4.37, and Figure 4.38.

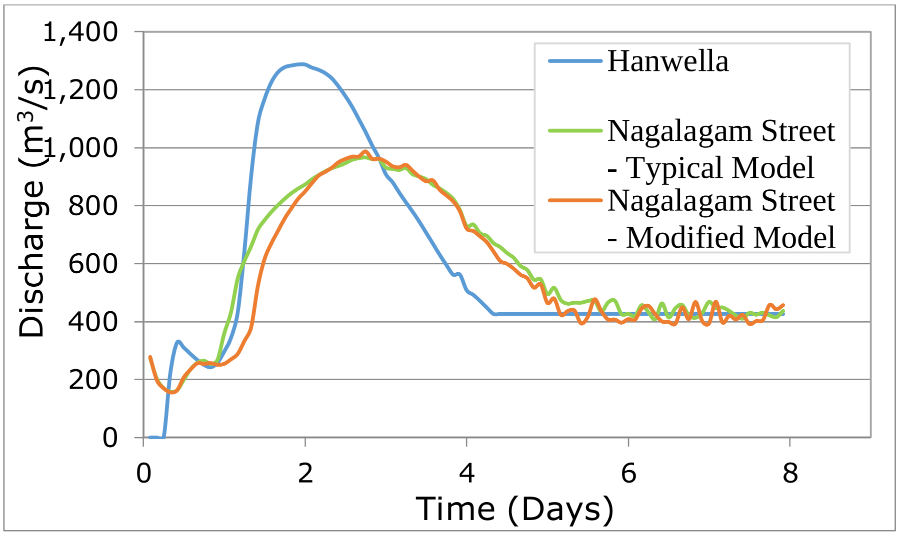

Figure 4.36: Simulated discharge at Hanwella and Nagalagam street for 2017 flood event

The simulated discharge variation at Hanwella is similar for both improved and typical RRI models. The simulated discharge variation at Nagalagam Street has changed slightly without changing the peak discharge and time lag. The area under the discharge curve was slightly lower in the simulated discharge curve from the modified RRI model than the typical RRI model. It may be due to assigning arbitrary cross-sections at Nagalagam Street and Hanwella station for the modified RRI model.

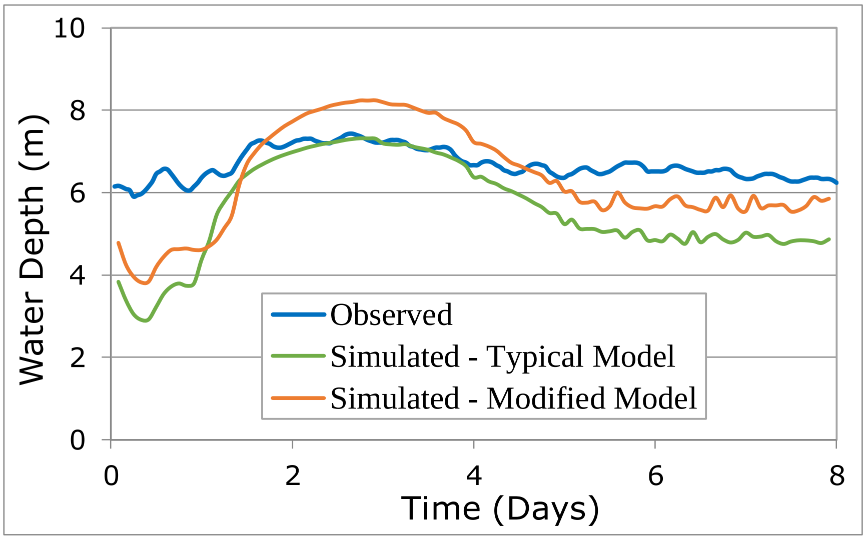

Figure 4.37: Simulated and observed water depth at Nagalagam street for 2017 flood event

The water depth variation in the modified RRI model has shown a considerable increment compared to the typical RRI model. The peak water depth at Nagalagam Street in the modified RRI model has increased by 0.92 m. It may occur due to assign arbitrary cross-sections at Nagalagam Street and Hanwella and consider some locations which were already saturated before the torrential rainfall event according to satellite-based soil moisture data as an unsaturated condition in the typical model.

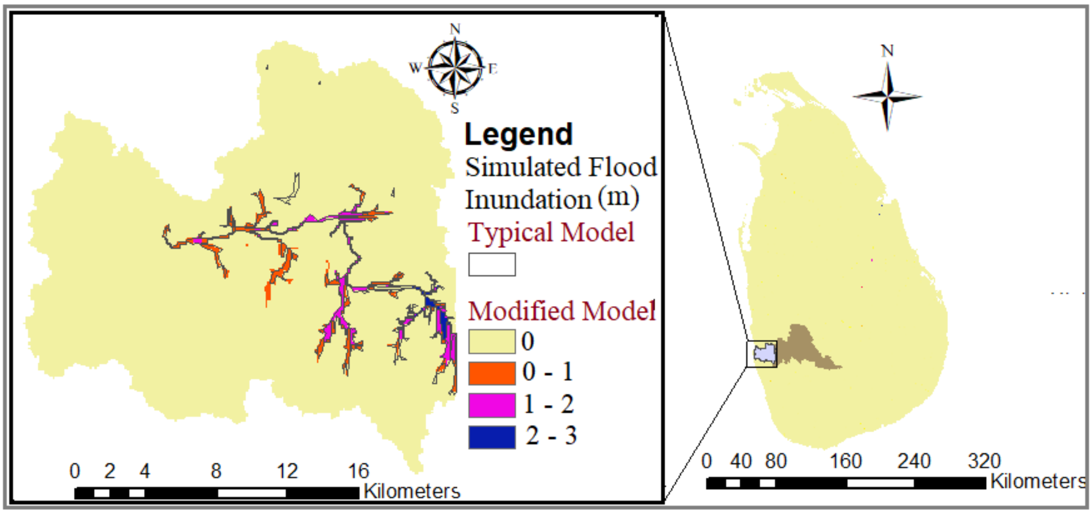

Figure 4.38: Simulated flood inundation for 2017 flood event

The downstream flood inundation of the modified RRI model has slightly increased compared to the typical RRI model while the upstream flood inundation extent has decreased in the modified RRI model. The ME, RMSE, and R^2 for simulated water depth using the modified RRI model for the 2017 flood event were 0.18 m, 0.69 m, and 0.9, respectively. The performance indices have been improved compared to the performance indices of the typical RRI model.

4.5 RRI Models using AWS, and satellite-based data

The discharge, water depth, and flood inundation for the period from 12th September 2019 to 22nd September 2019 are shown in Figure 4.39, Figure 4.40, and Figure 4.41, respectively.

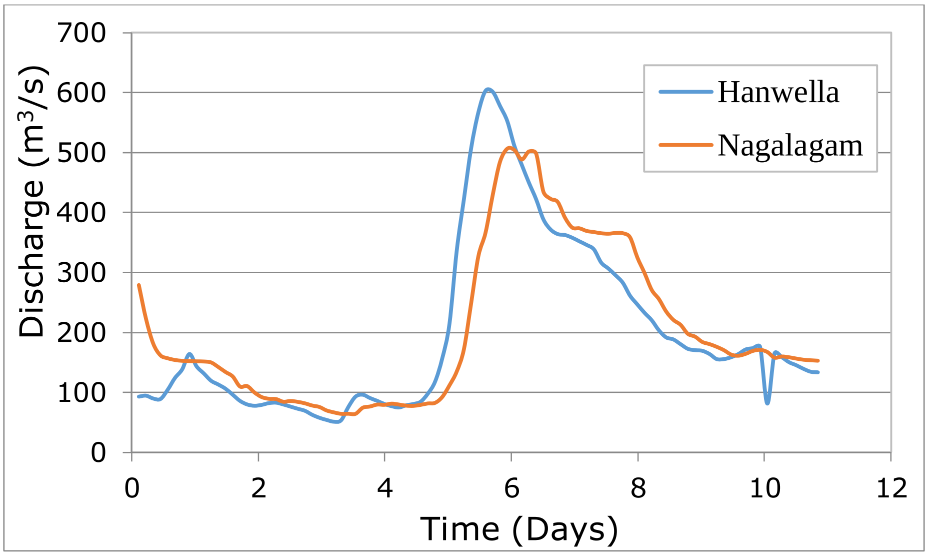

Figure 4.39: Simulated discharge at Hanwella and Nagalagam Street for rainfall event from 12th to 22nd September 2019

According to Figure 4.39, The peak discharge at Hanwella and Nagalagam Street were about 603 m^3s^{-1} and 507 m^3s^{-1}, respectively. The peak streamflow at Hanwella and Nagalagam Street has not variated highly as the flood events in 2016, 2017, and 2018 since the water levels at Hanwella and Nagalagam Street have not achieved flood level during this rainfall event. The time lag between peak discharge at these locations was about half of the day.

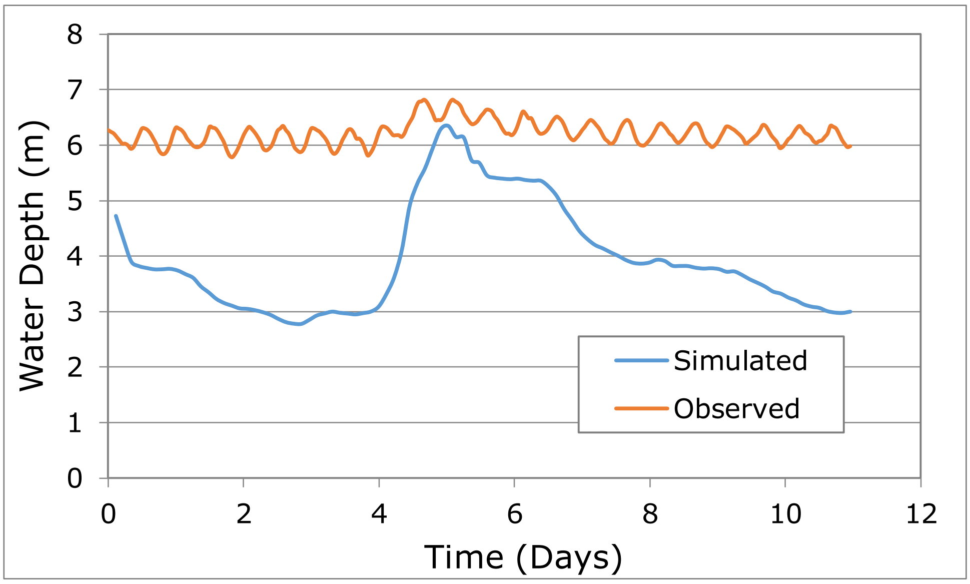

Figure 4.40: Simulated and observed water depths at Nagalagam Street for rainfall event from 12th to 22nd September 2019

According to Figure 4.40, the observed and simulated peak water depths at Naglagam Street were about 6.16 m and 6.81 m, respectively. The actual water depth has not shown a considerable fluctuation during this rainfall event. However, the simulated water depth has started from 4.79 m and decreased gradually in the next three days since torrential rainfall occurred on the 3rd day of the simulation period (15th May 2019).

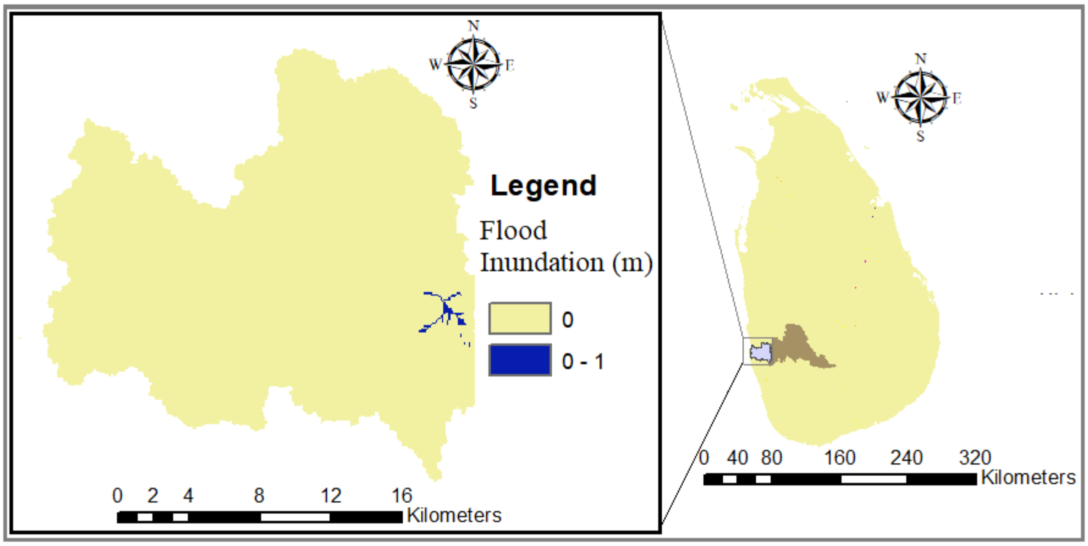

Figure 4.41: Simulated flood inundation for rainfall event from 12th to 22nd September 2019

The model shows a very low flood inundation in Hanwella despite the water level in the Lower Kelani River Basin has not achieved flood level during this period.

The discharge, water depth, and flood inundation for the period from 23rd September 2019 to 30th September 2019 are shown in Figure 4.42, Figure 4.43, and Figure 4.44, respectively.

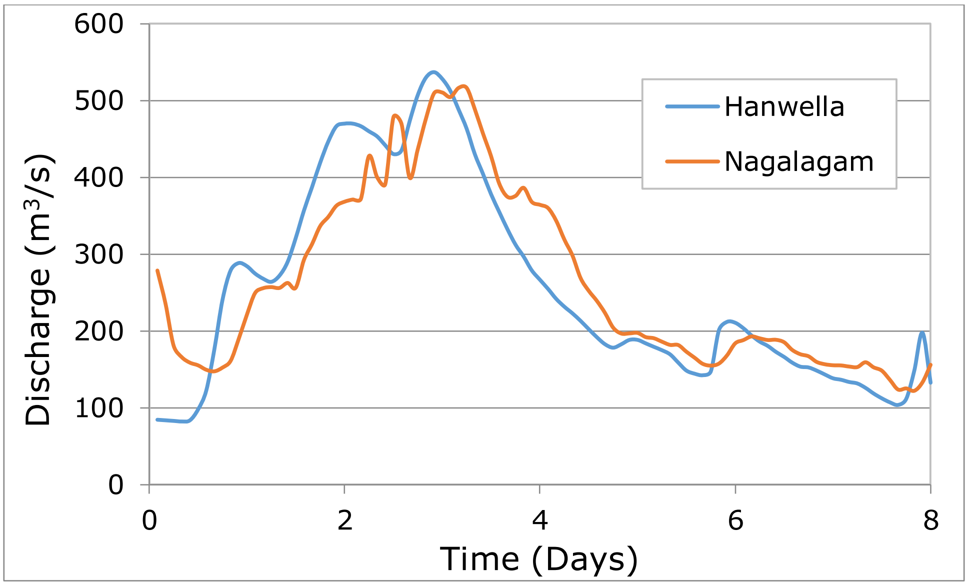

Figure 4.42: Simulated discharge at Nagalagam street and Hanwella for rainfall event from 23rd September 2019 to 30th September 2019

According to Figure 4.42, the peak discharge values at Nagalagam Street and Hanwella station were about 522 ms^{-3} and 537 ms^{-3}, respectively. The time lag between hydrographs at the aforementioned locations was very close since the rainfall event occurred only in the Lower Kelani River Basin.

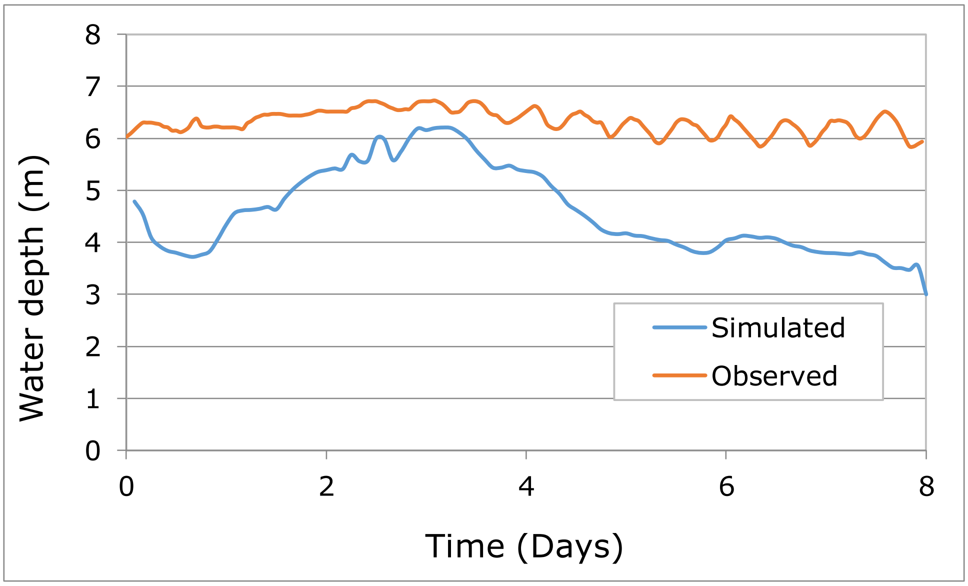

Figure 4.43: Simulated and observed water depth at Nagalagam Street from 23rd September 2019 to 30th September 2019

According to Figure 4.43, water depths were underestimated, however, the simulated peak water depth at Nagalagam Street was lower by 0.46 m than the actual water depth.

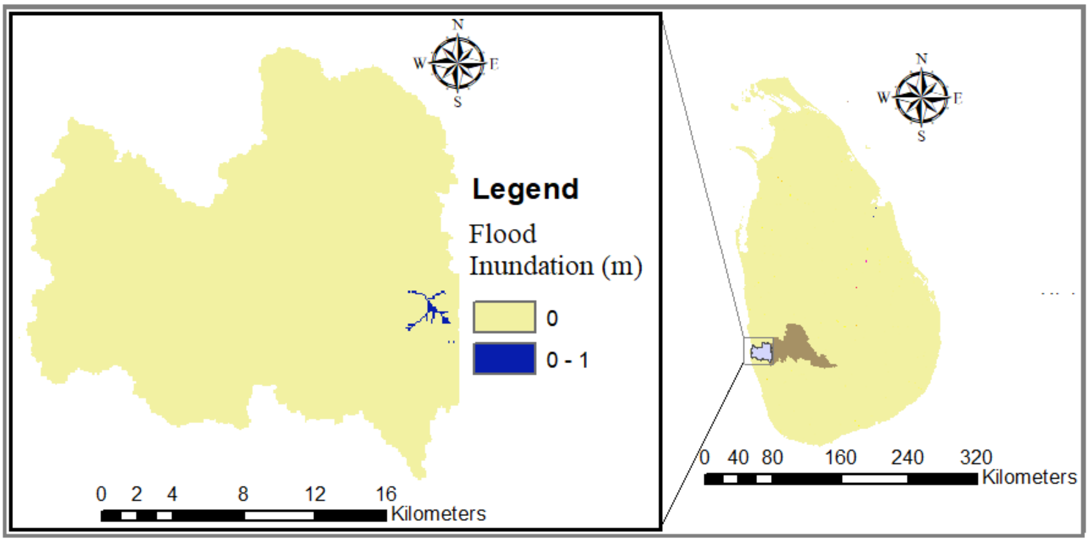

Figure 4.44: Simulated flood inundation for rainfall event from 23rd to 30th September 2019

During this period, Colombo areas have flooded due to torrential rainfall on 23rd September 2019. However, the river water depth was not reached even the flood alert level. According to Figure 4.44, the very low flood inundation extent can be identified near the Hanwella. It may be due to receive significant rainfall at Hanwella during this torrential rainfall. Hanwella station has recorded heavy rainfall above 150 mm for the past 24 hours as of 9.00 a. m. 25th September 2019 (Disaster Management Centre, 2019). The performance indices for each RRI model developed using AWS are given in Table 4.9.

Table 4.9: Performance indices for RRI model using real-time and satellite data

Rainfall Event	**12th – 22nd September 2019**	**23rd – 30th September 2019**
R^2	0.65	0.77
ME	-2.28	-0.87
RMSE	2.4	1.32

According to Table 4.9, the RRI model performed well for the rainfall event started on 23rd September 2019 with the highest R^2 of 0.77, lowest ME of 0.87 and, lowest RMSE of 1.32. The high ME and RMSE values of approximately 2 m show for the rainfall event from 12th to 22nd September 2019. The higher number of missing rainfall data may cause poor performance in the RRI model using AWS rainfall data.

4.6 Comparison between typical and modified RRI models

The summary of all developed typical and modified RRI models is given in Table 4.10.

Table 4.10: Comparison between typical and modified RRI models

Input data	**Typical Model**			**Improved Model**		
Flood event	2016	2017	2018	2017	2019- 12th September	2019- 23rd September
Rainfall data	Rain gauges	Rain gauges	Rain gauges	Rain gauges	AWS	AWS
DEM	SRTM-90m	SRTM-90m	SRTM-90m	SRTM-90m	SRTM-90m	SRTM-90m

Satellite-based data	-	-	-	MODIS yearly land cover data, SMAP/ Sentinel-1 Soil Moisture data	MODIS yearly land cover data, SMAP/ Sentinel-1 Soil Moisture data	MODIS yearly land cover data, SMAP/ Sentinel-1 Soil Moisture data
Arbitrary Cross Sections	-	-	-	Assigned at Nagalagam Street and Hanwella	Assigned at Nagalagam Street and Hanwella	Assigned at Nagalagam Street and Hanwella
Performance Indices						
R^2	0.94	0.9	0.93	0.9	0.65	0.77
ME	0.3	-0.55	-0.73	0.18	-2.28	-0.87
RMSE	1.00	0.99	1.01	0.69	2.4	1.32
FIT index	0.6	-	0.4	-	-	-

The modified RRI model for the 2017 flood event performed well compared to the typical RRI model for this event. The modified RRI model has overestimated water depth at Nagalagam Street while the typical RRI model underestimates the water depth at Nagalagam Street for the 2017 flood event.

The modified RRI models using AWS show the lowest performance compared to all developed RRI models and underestimate the water levels at Nagalagam Street. It may occur due to include a higher number of missing data in the rainfall data set even the 11 AWSs were considered. Moreover, the rainfall at Hanwella wasn’t considered for the 2019 rainfall event despite Hanwella has received heavy rainfall above 150 mm (Disaster Management Centre, 2019). Because all 11 AWS are located downstream and no AWS at Hanwella.

4.7 Adequacy of rain gauges/ AWS

The optimum number of rain gauges was determined based on rainfall values of each rain gauge in the Lower Kelani River Basin for 2016, 2017, and 2018 flood events and are given in Table 4.11.

Table 4.11: Optimum Number of Rain gauges for each flood event

Event	**Precipitation (mm/day)**			$\overline{P}$ **(mm)**	**S (mm)**	C_v	**Ɛ (%)**	**N**
	Hanwella	***Colombo***	***Rathmalana***					
2016	125.5	83.9	124	111.1	16.69	15.01	10	2.25
2017	38.41	28.7	37.4	34.8	3.77	10.84	10	1.17
2018	35.84	35.2	34.6	35.2	0.44	1.25	10	0.02

Since the number of existing rain gauges is greater than the optimum number of rain gauges of the catchment, the existing rain gauge network is adequate to obtain average rainfall with a percentage error of less than or equal to 10%.

According to performance indices of the RRI model shown in Table 4.5, the model performed well for 2016, 2017, and 2018 floods. Since the accuracy of rainfall data directly affect the performance of the RRI model, the better performance of the RRI model implies that the existing rain gauge network is adequate.

The optimum number of AWS of the catchment is given in Table 4.12.

11 AWSs are located in the Lower Kelani River Basin. Since the missing rainfall data of Kohuwala and Orugodawatta AWS during the 2019 flood event were higher, only 9 AWS were considered for estimating the optimum number of AWS in the catchment.

Table 4.12: Optimum Number of AWS for each flood event

Event	**Precipitation**		$\bar{P}$	S	C_v	n	N
12th September 2019 to 22nd September 2019	Madiwela	26.6	23.5	3.5	14.7	10	2.17
	Kottawa	25.8					
	Kotikawatta	13.8					
	Arangala	29.0					
	Baththaramulla I	14.0					
	Boralasgamuwa	44.0					
	Baththaramulla II	14.0					
	Kittampahuwa	25.4					
	Makumbura	18.8					
23rd September 2019 to 30th September 2019	Madiwela	304.4	310.3	12.7	4.1	10	0.17
	Kottawa	325.0					
	Kotikawatta	300.0					
	Arangala	325.4					
	Baththaramulla I	294.2					
	Boralasgamuwa	314.0					
	Baththaramulla II	369.3					
	Kittampahuwa	234.2					
	Makumbura	326.0					

Since the existing number of AWS is greater than the optimum number of AWS, the existing AWS are adequate to obtain average rainfall with a percentage error of less than or equal to 10%. However, the accuracy of the rainfall data of the AWS is not sufficient as per the performance indices of RRI models using AWS.

5. CONCLUSIONS AND RECOMMENDATIONS

5.1 Conclusions

1. The research concluded that the performance of the RRI model can be improved using surveyed cross-section data and satellite-based data such as MODIS yearly global land cover and SMAP/Sentinel-1 soil moisture data.
2. The RRI model using surveyed cross-section data and satellite-based data for the 2017 flood event shows the best performance with the r^2 of 0.9, the lowest ME of 0.18 m, and the lowest RMSE of 0.69 m. The RRI models using AWS show the weakest performance with the lowest r^2 of 0.65, the highest ME of -2.28 m, and the highest RMSE of 2.4 m due to less accuracy in the AWS rainfall data set resulting from the high number of missing data.
3. The SRTM and ALOS PASAR 90-m DEMs fit best for flood modelling in the Lower Kelani River Basin among SRTM, HydroSHEDS, ASTER, and ALOS PALSAR DEMs. The performance of ASTER DEM contrasts to SRTM, HydroSHEDS, and ALOS PALSAR even all DEMs have an equal resolution of 3-arc. The accuracy of the RRI model depends on the DEM product. The elevations of different DEM products highly variate for flat terrain basins and show considerably low variation in steep terrain basins. Furthermore, the elevation variation of DEM is higher in forest areas and the transition from woody savannas to a forest, and lesser in urban/ built-up areas and transition from croplands to urban/ built-up areas.
4. The main land-use types of the Lower Kelani River Basin are urban/ built-up areas, woody savannas, and croplands. The catchment has urbanized by 12% of the total area. However, other land-use types are in a decreasing trend for the 2001 to 2019 period.
5. According to the study on the impact of land-use and climate change on the 10 and 50 year return period flood for the 2001 to 2019 period in the Lower Kelani River Basin, the downstream runoff, water depth, and flood inundation are in a decreasing trend. However, the upstream runoff, water depth, and flood inundation are in an incremental tendency. The total flood inundation extent is increasing as a result of land-use and climate change. The

effects of land-use and climate change on rainfall-runoff-inundation processes are increasing when increasing the return period of the flood.

6. According to sensitivity analysis of the RRI model, the peak runoff of the catchment is higher for higher Manning's roughness and lower soil effective porosity and no considerable effect on runoff by saturated hydraulic conductivity.
7. The existing number of rain gauges and AWS are adequate to obtain average rainfall in the Lower Kelani River Basin with a percentage error of less than or equal to 10%.

5.2 Recommendations

1. The RRI model can be improved by using validated AWS and rain gauge rainfall data, especially data from the Hanwella rain gauge station.
2. Furthermore, the performance of the RRI model can be enhanced by using surveyed river cross-sections for river channels rather than the use of empirical equations for defining river width and depth based on the assumption of the river channel to be rectangular.
3. The study on the impact of DEM products on the RRI model can be extended with high-resolution elevation data set such as Lidar data.
4. This study can be extended to flood predictions in the Lower Kelani River Basin for risk mitigation and flood management.
5. Further studies can be carried out to identify the impacts of tidal effects at Nagalagam Street on flood modelling in order to improve the performance of the RRI model.

6. REFERENCES

Abdelkhalek, A. M., Awadallah, A. G., & Awadallah, N. (2018). Optimal selection of rainfall gauges for safe extreme events estimation using a geostatistical approach. *Saudi Society for Geosciences 2018*, 438. https://doi.org/10.1007/s12517-018-3765-2

Allen, D. M., Cannon, A., Toews, M. W., & Scibek, J. (2010). *Variability in simulated recharge using different gcms*. *46*.

Amorocho, J., Brandstetter, A., & Morgan, D. (1968). *The effects of density of recording rain gauge networks on the description of precipitation patterns*. IAHS-AISH.

Andiego, G., Waseem, M., Usman, M., & Mani, N. (2018). *The Influence of Rain Gauge Network Density on the Performance of a Hydrological Model*. *7*, 27–50.

Area and climate—Department of census and statistic- Sri Lanka. (n.d.). Www.Statistic.Gov.Lk.

Baboo, S. S., & Devi, M. R. (2010). An analysis of different resampling methods in Coimbatore, District. *Global Journal of Computer Science and Technology*.

Bahremand, A., Smedt, F. D., Corluy, J., Liu, Y. B., Poorova, J., Velcicka, L., & Kunikova, E. (2006). Wetspa Model Application for Assessing Reforestation Impacts on Floods in Margecany–Hornad Watershed, Slovakia |. *Spriger*, *21*, 1373–1391.

Beven, K. (2012). *Rainfall-Runoff Modelling The Primer* (second). John Wiley & Sons, Ltd.

Bhagabati, S. S., & Kawasaki, A. (2017). *Consideration of the rainfall-runoff-inundation (RRI) model for flood mapping in a deltaic area of Myanmar*. *11*(3), 155–160. https://doi.org/10.3178/hrl.11.155

Brocca, L., Moramarco, T., Melone, F., Wagner, W., Hasenauer, S., & Hahn, S. (2012). Assimilation of surface- and rootzone ASCAT soil moisture products into rainfall–runoff modeling. *IEEE Transactions on Geoscience and Remote Sensing*, *50*(7), 2542–2555.

Brunsdon, C., mcclatchey, J., & Unwin, D. J. (2001). Spatial variations in the average rainfall-altitude relationship in Great Britain: An approach using geographically weighted regression. *Wiley Online Library*, *21*(4), 455–466.

Chow, V. T. (1959). *Open channel hydraulics*.

Chow, V. T., Maidment, D. R., & Mays, L. W. (1988). *Applied hydrology*. Mcgraw-Hill, Inc.

Coz, M., François, D., Genthon, P., & Favreau, G. (2009). Assessment of Digital Elevation Model (DEM) aggregation methods for hydrological modeling: Lake Chad basin, Africa. *Computers & Geosciences*, *35*, 1661–1670. https://doi.org/10.1016/j.cageo.2008.07.009

Curw Center for Urban Water. (2019). Curw Weather Stations. Www.curwsl.org

De Silva, M. M. G. T., Weerakoon, S. B., Herath, S., Ratnayake, U. R., & Mahanama, S. (2012). Flood Inundation Mapping along the Lower Reach of Kelani River Basin under the Impact of Climatic Change. In *ENGINEER: Vol. XXXXV* (pp. 23–29). The Institution of Engineers, Sri Lanka.

Devia, G. K., Ganasri, B. P., & Dwarakish, G. S. (2015). *A review on hydrological models*. *4*, 1001–1007.

Diamond, H., Washington, D. C., & Wilbur, S. H. (1942). *Automatic weather stations* (United States Patent office Patent No. 2,287,786).

Dioniio, E. A., & Costa, M. H. (2019). Influence of Land Use and Land Cover on Hydraulic and Physical Soil Properties at the Cerrado Agricultural Frontier. *MDPI*, *9*(24). https://doi.org/doi:10.3390/agriculture9010024

Disaster Management Centre. (2019). *Sri Lanka summary situation update*.

Dissanayaka, K. D. C. R., & Rajapakse, R. L. H. L. (2019). Long-term precipitation trends and climate extremes in the Kelani River basin, Sri Lanka, and their impact on streamflow variability under climate change. *Paddy and Water Environment*, *17*(2), 281–289. https://doi.org/10.1007/s10333-019-00721-6

Donigian, A. S., & Imhoff, J. C. (2006). *History and Evolution of watershed modeling derived from the Stanford Watershed Model*.

Dorn, H., Vetter, M., & Hofle, B. (2014). *GIS-Based Roughness Derivation for Flood Simulations: A Comparison of Orthophotos, lidar and Crowdsourced Geodata*. *6*, 1739–1759.

Fewtrell, T. J., Bates, P. D., Horritt, M., & Hunter, N. M. (2008). Evaluating the effect of scale in flood inundation modelling in urban environments. *Hydrological Processes*, *22*(26), 5107–5118. https://doi.org/10.1002/hyp.7148

Gamini B Dodanwela Associates (Pvt) Ltd. (2007). *River cross section survey or comprehensive study on disaster management in Sri Lanka*.

Gann, D. (2019). *Quantitative spatial upscaling of categorical information: The multi-dimensional grid-point scaling algorithm—Gann—2019—Methods in Ecology and Evolution—Wiley Online Library*. *10*(12). https://besjournals.onlinelibrary.wiley.com/doi/full/10.1111/2041-210X.13301

Goovaerts, P. (1997). *Geostatistics for Natural Resources Evaluation*. Oxford University Press.

Grimes, D. I. F., Pardo-Iguzquiza, & Bonifacio, R. (1999). Optimal areal rainfall estimation using raingauges and satellite data. *Elsevier*, *222*, 93–108.

Hawker, L., Bates, P., Neal, J., & Rougier, J. (2018). *Perspectives on Digital Elevation Model (DEM) Simulation for Flood Modeling in the Absence of a High-Accuracy Open Access Global DEM | Earth Science*.

Hawker, L., Rougier, J., Neal, J., Bates, P., Archer, L., & Yamazaki, D. (2018). *Implications of Simulating Global Digital Elevation Models for Flood Inundation Studies*.

Hema, N., & Kant, K. (2016). Hourly real-time rainfall estimation for improved smart irrigation system using nearby automated weather station. *Sciencedomain International*, *18*(5), 1–13. https://doi.org/10.9734/BJAST/2016/30934

Hettiarachchi, P. (2018). *Flood frequency analysis for the Kelani River and the Design flood for Kelani flood bund*.

Hettiarachchi, P. (2020). *Hydrological Report on the Kelani River Flood in May 2016*.

Hoggan, D. H. (1989). *Computer-Assisted floodplain hydrology and hydraulics*. Mcgraw-Hill.

Hu, Q., Li, Z., Wang, L., Huang, Y., Wang, Y., & Li, L. (2019). *Rainfall Spatial Estimations: A Review from Spatial Interpolation to Multi-Source Data Merging. 11*.

Huffman, G. J., Adle, R. F., Arkin, P., & Chang, A. (1997). *The Global Precipitation Climatology Project (GPCP) Combined Precipitation Dataset*.

IS 4987: Recommendations for establishing network of rain gauge stations: Bureau of Indian Standards. (1994). https://archive.org/details/gov.in.is.4987.1994

Jayasekara, S. M., Abeysingha, N. S., & Meegastenna, T. J. (2020). Streamflow trends of Kelani river basin in Sri Lanka (1983-2013). *National Science of Sri Lanka*, *48*(4).

Kokkonen, T., Koivusalo, H., & Karvonen, T. (2001). *A semi-distributed approach to rainfall-runoff modelling—A case study in a snow affected catchment*. *16*(5), 481–493.

Komolafe, A. A., Herath, S., & Avtar, R. (2017). Development of generalized loss functions for rapid estimation of flood damages: A case study in Kelani River basin, Sri Lanka. *Società Italiana Di Fotogrammetria e Topografia (SIFET)*, *10*, 13–30.

Lakshmi, S., & Yarrakula, K. (2019). Review and critical analysis on digital elevation models. *Geofizika*, *35*, 129–157. https://doi.org/10.15233/gfz.2018.35.7

Lee, J., Kim, S., & Jun, H. (2018). A study of the influence of the spatial distribution of Rain Gauge Networks on areal average rainfall calculation. *MDPI*, *10*(1635). https://doi.org/doi:10.3390/w10111635

Lopez, M. G., Wennerstom, H., Norden, L.-A., & Seibert, J. (2015). Location and density of rain gauges for the estimation of spatial varying precipitation. *© 2015 Swedish*

Society for Anthropology and Geography, *97*, 167–179. https://doi.org/DOI:10.1111/geoa.12094

Maleika, W. (2020). Inverse distance weighting method optimization in the process of digital terrain model creation based on data collected from a multibeam echosounder. *Springer*, *12*, 397–407.

Mallawatantri, A. (Ed.). (2016). *Natural resource profile of the Kelani river basin* (Medium to Long-Term Multi-Stakeholder Strategy and Action Plan for Management and Conservation of the Kelani River Basin 2016-2020, p. 39).

Mesa-Mingorance, J. L., & Ariza-López, F. J. (2020). Accuracy Assessment of Digital Elevation Models (dems): A Critical Review of Practices of the Past Three Decades. *Remote Sensing*, *12*(16), 2630. https://doi.org/10.3390/rs12162630

METI/ERSDAC, NASA/LPDAAC, & USGS/EROS. (2009). *ASTER global DEM validation.*

Miller, S. N., Kepner, W. G., Mehaffey, M. H., Hernandez, M., Miller, R. C., Goodrich, D. C., Devonald, K., Heggem, D. T., & Miller, W. P. (2002). Integrating landscape assessment and hydrologic modeling for land cover change analysis. *Journal of the American Water Resources Association*, *38*(4), 915–929. https://doi.org/10.1111/j.1752-1688.2002.tb05534.x

Montanari, A. (2016). *Rainfall-Runoff modelling*. University of Bologna Home Page.

Moormann, F. R., & Panabokke, C. R. (1961). *A new approach to the identification and classification of the most important soil groups of Ceylon*.

Moradkhani, H., & Sorooshian, S. (2009). *General review of rainfall-runoff modelling: Model calibration, data assimilation and uncertainty analysis*. 1–24.

Nastiti, K. D., Kim, Y., Jung, K., & An, H. (2015). The application of Rainfall-Runoff-Inundation (RRI) model for inundation case in upper Citarum Watershed, West Java-Indonesia. *Procedia Engineering*, *125*, 166–172.

Pakoksung, K. (2016). *Runoff Analysis using Satellite Data for Regional Flood Assessment—Spatial and Time Series Bias Correction of Satellite Data* [Thesis, Kochi University of Technology]. https://ci.nii.ac.jp/naid/500000997617

Pakoksung, K., & Takagi, M. (2016). *Effect of satellite based rainfall products on river basin responses of runoff simulation on flood event*. https://doi.org/DOI 10.1007/s40808-016-0200-0

Patabendige, C. S., Kazama, S., & Kondage, Y. S. (2019). Spatial and Temporal Variation of Runoff Trend in Sri Lanka During the Past Decades. *2019 Moratuwa Engineering Research Conference (mercon)*, 751–756. https://doi.org/10.1109/mercon.2019.8818782

Paula, S. C. D., Tassi, R., Piccilli, D. G. A., & Neto, F. L. (2018). Influence of the rain gauge network on the performance of a hydrological lumped model applied at different basin scales. *RBRH*, *23*(45).

Pechlivanidis, I. G., Jackson, B. M., Mcintyre, N. R., & Wheater, H. S. (2011). *Catchment scale hydrological modelling: A review of model types, calibration approaches and uncertainty analysis methods in the context of recent developments in technology*. *13*(3), 193–214.

Rainbird, A. F. (2007). *Precipitation basic principles of network design*.

Rasmy, M., Iwami, Y., Sayama, T., Lawford, P., & Koike, T. (2016). *Preliminary Investigation of Water and Energy based Rainfall-Runoff Inundation (WEB-RRI) Model in the Lower Kinu River Basin, Japan.*

Rasmy, M., Sayama, T., & Koike, T. (2019). Development of water and energy Budget-based Rainfall-Runoff-Inundation model (WEB-RRI) and its verification in the Kalu and Mundeni River Basins, Sri Lanka. *Elsevier*, *579*.

Remson, I., Hornberger, G. M., & Molz, F. J. (1971). Numerical Methods in Subsurface Hydrology. *John Wiley & Sons*, *36*(4), 389.

Rigol, J. P., Jarvis, C. H., & Stuart, N. (2001). *Artificial neural networks as a tool for spatial interpolation*. *15*(4), 323–343.

Rinsema, J. G. (2014). *Comparison of rainfall runoff models for the florentine catchment*. University of Twente.

Rogers, D., Love, G., & Bruce, S. (2016). *Meteorological and hydrological services in Sri Lanka—Review*.

Saksena, S., & Merwade, V. (2015). *Incorporating the effect of DEM resolution and accuracy for improved flood inundation mapping*.

Santillan, J. R., & Makinano-Santillan, M. (2016). *Vertical accuracy assessment of 30 m resolution ALOS, ASTER, and SRTM global dems over Northeastern Mindanao, Philippines*.

Savage, J. T. S., Bates, P., Freer, J., Neal, J., & Aronica, G. (2016). When does spatial resolution become spurious in probabilistic flood inundation predictions? *Hydrological Processes*, *30*(13), 2014–2032. https://doi.org/10.1002/hyp.10749

Sayama, T. (2017). *Rainfall-Runoff-Inundation (RRI) Model* (ver. 1.4.2).

Sayama, T., Ozawa, G., Kawakami, T., Nabesaka, S., & Fukami, K. (2012). Rainfall–runoff–inundation analysis of the 2010 Pakistan flood in the Kabul River basin. *IAHS Press*, *57*(2).

Sayama, T., Tatebe, Y., & Tanaka, S. (2017). An emergency response-type rainfall-runoff-inundation simulation for 2011 Thailand floods. *015 the chartered institution of water and environmental management(CIWEM) and john wiley & sons ltd*, *10*, 65–78. https://doi.org/10.1111/jfr3.12147

Schumann, A. H. (1998). Thiessen Polygon. In *Encyclopedia of Earth Science* (pp. 648–649). Springer.

Shahrban, M., Walker, J. P., Wang, Q. J., & Robertson, D. E. (2018). On the importance of soil moisture in calibration of rainfall–runoff models: Two case studies. *Taylor & Francis*, *63*(9), 1292–1312. https://doi.org/10.1080/02626667.2018.1487560

Shrestha, B. B. (2019). Approach for Analysis of Land-Cover Changes and Their Impact on Flooding Regime. *MDPI*, *2*(27). https://www.mdpi.com/2571-550X/2/3/27

Shustikova, I., Domeneghetti, A., Neal, J. C., Bates, P., & Castellarin, A. (2019). Comparing 2D capabilities of HEC-RAS and LISFLOOD-FP on complex topography. *Taylor & Francis*, *64*(14), 1769–1782.

Sikka, A. K., Samra, J. S., Sharda, V. N., Samraj, P., & Lakshmanan, V. (2003). Low flow and high flow responses to converting natural grassland into bluegum (Eucalyptus globulus) in Nilgiris watersheds of South India. *Journal of Hydrology*, *270*(1), 12–26. https://doi.org/10.1016/S0022-1694(02)00172-5

Singh, V. P. (1995). *Computer models of watershed hydrology Rev. Ed.*

Singh, V. P. (2018). Hydrologic modeling: Progress and future directions. *Spriger*.

Sitterson, J., Knightes, C., Parmar, R., Wolfe, K., Muche, M., & Avant, B. (2017). *An Overview of Rainfall-Runoff Model Types*. Environmental Protection Agency (EPA).

Smith, M. B., Koren, V., Zhang, Z., Reed, Z. S. M., Cui, Z., & Zhang, Y. (2012). *Results of the DMIP 2 oklahoma experiments*. 17–48.

Sorooshian, S., Hsu, K. I., Coppola, E., Tomassetti, B., Verdecchia, M., & Visconti, G. (2008). *Hydrological modelling and the water cycle*.

Strategic Environmental Assessment (Strategic Environmental Assessment of Development of River Basin Level Flood and Drought Mitigation Investment Plans-Kelani River Basin, p. 278). (2018). Consulting Engineers and Architecs Associated(pvt) Ltd.

Subramanya, K. (2008). *Engineering hydrology third edition*. Tata mcgraw-Hill Publishing Company Limited.

Suwanwerakamtorn, R. (1994). *GIS and hydrologic modelling for the management of small watersheds*. *1994*, 343–348.

Tan, M. L., Ficklin, D. L., Dixon, B., Ibrahim, A. L., Yusop, Z., & Chaplot, V. (2015). Impacts of DEM resolution, source, and resampling technique on SWAT simulated streamflow. *Elsevier*, *63*, 357–368.

Tapiador, F. J., Turk, F. J., Petersen, W., Hou, A. Y., Garcia-Ortega, E., & Machado, L. A. T. (2012). Global precipitation measurement: Methods, datasets and applications. *Elsevier*, 70–97.

Tilford, K. A., Sene, K., & Collier, C. G. (2003). *Flood Forecasting – Rainfall Measurement and Forecasting*.

Usery, E. L., Finn, M. P., Scheidt, D. J., Ruhl, S., Beard, T., & Bearden, M. (2004). Geospatial data resampling and resolution effects on watershed modeling: A case study using the agricultural non-point source pollution model. *Journal of Geographical Systems*, *6*(3), 289–306. https://doi.org/10.1007/s10109-004-0138-z

Vaze, J., Jordan, P., Beecham, R., Frost, A., & Summerell, G. (2012). *Guidelines for rainfall-runoff modelling*. Australian government department of innovation, industry, science and research.

Wagener, T., Wheater, H. S., & Gupta, H. V. (2003). *Rainfall-Runoff Modelling in Gauged and Ungauged Catchments*. Imperial College Press.

Watersheds of Sri Lanka (first). (2011). [Map]. Department of Agrarian development of Sri Lanka.

Wolff, D. B., Marks, D. A., Amitai, E., & Silberstein, D. S. (2005). *Ground validation for the tropical rainfall measuring mission (TRMM)*. *4*(22).

Wu, S., Li, J., & Huang, G. H. (2008). A study on DEM-derived primary topographic attributes for hydrologic applications: Sensitivity to elevation data resolution. *Applied Geography*, *28*(3), 210–223. https://doi.org/10.1016/j.apgeog.2008.02.006

Yue, T. X. (2011). *Surface Modeling: High Accuracy and High Speed Methods* (1st ed.). CRC Press.

Zandbergen, P. A. (2010). Methodologic Issues in Using Land Cover Data to Characterize Living Environments of Geocoded Addresses. *Environmental Health Perspectives*, *118*(3), A108. https://doi.org/10.1289/ehp.0901863

Zeng, Q., Chen, H., Xu, C.-Y., Jie, M.-X., Chen, J., & Guo, S.-L. (2018). The effect of rain gauge density and distribution on runoff simulation using a lumped hydrological modelling approach. *Elesvier*, *563*, 106–122.

APPENDIX – A

A.1. Cross-section at Hanwella

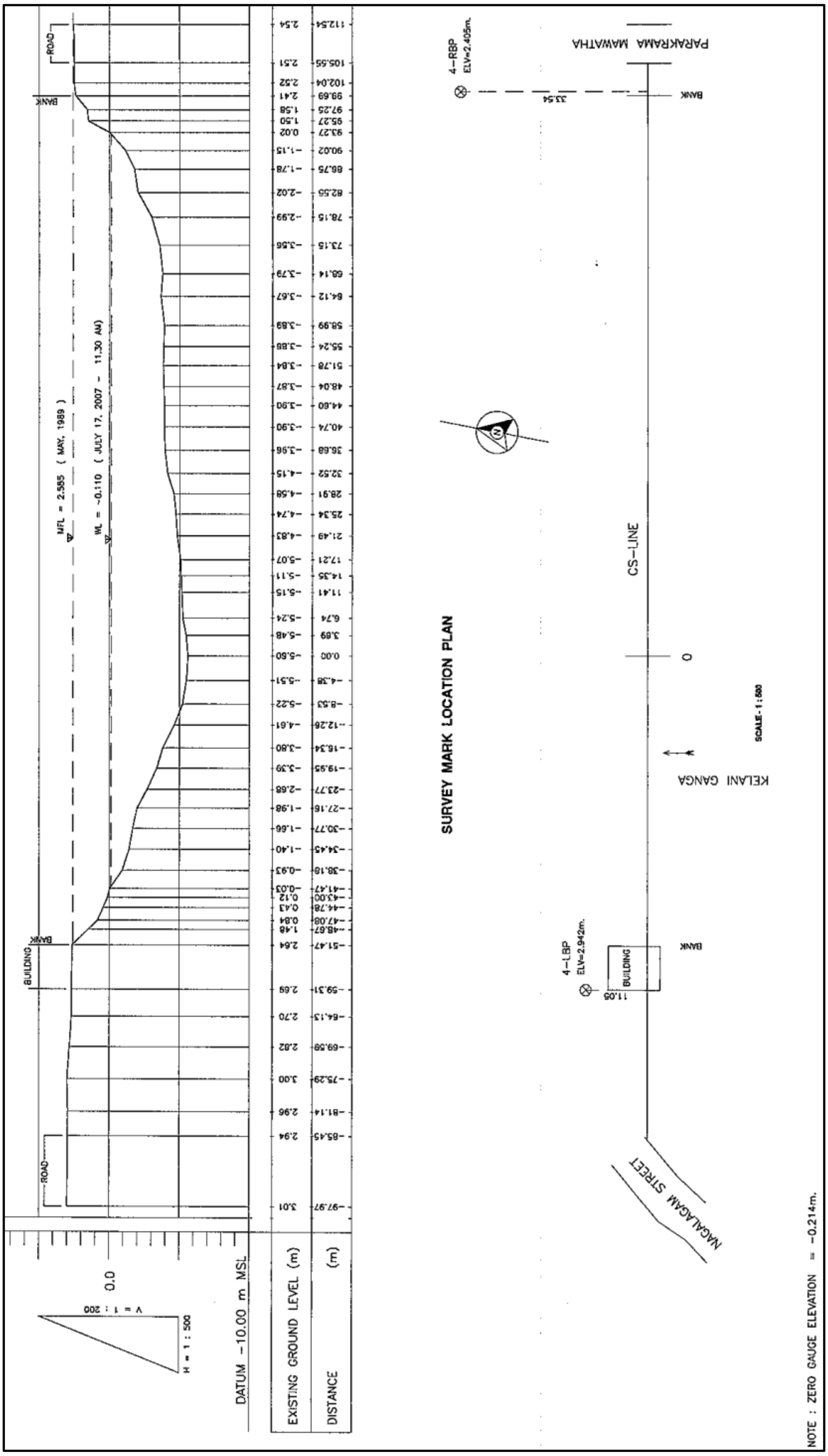

A.2. Cross-section at Nagalagam Street